COMPUTATIONAL ANALYSIS OF GENE EXPRESSION IN COMPLEX DISEASE

A Thesis
Presented to
The Academic Faculty

by

Andrew Douglas Huang

In Partial Fulfillment
of the Requirements for the Degree
Doctor of Philosophy in Bioinformatics in the
School of Biology

Georgia Institute of Technology
December 2014

COMPUTATIONAL ANALYSIS OF GENE EXPRESSION IN COMPLEX DISEASE

Approved by:

Dr. John F. McDonald, Advisor
School of Biology
Georgia Institute of Technology

Dr. Kathyrn M. Momary
Department of Pharmacy Practice
Mercer University

Dr. Nathan Bowen
Department of Biological Science
Clark Atlanta University

Dr. Jung H. Choi
School of Biology
Georgia Institute of Technology

Dr. George W. Daneker
School of Biology
Georgia Institute of Technology

Date Approved: August 5th, 2014

For my parents, who share my dream.

ACKNOWLEDGEMENTS

The work described herein would have been impossible without significant efforts in the wet side of the McDonald lab from L. DeEtte Walker, Lilya Matyunina, Lijuan Wang, Laura Kapa, Jing Chen, GT Wagner, Ken Scarberry, and Shubin Shahab, as well as their scientific insights. I would also like to thank my friends on the dry (and sometimes wet) side of the McDonald lab: Roman Mezencev, Neda Jabbari, Chris Hill, Vinay Mittal, Loukia Lili, and Gaurav Arora for their ongoing discussions and motivation. The support of all in the McDonald lab, especially from John F. McDonald, helped propel me through this convoluted pathway to my doctorate.

The work on firefighter coronary health and drug-eluting stents would not have been possible without the hard work of our collaborators at St. Joseph's Hospital. In particular I'd like to thank Radhika Gadesam, Cathy Skrifvars, Lakshmana Pendyala, Angela Stoppar, Dongming Hou, Kumar Natarajan, as well as Kathryn Momary of Mercer University, for their work gathering and interpreting data. Particular recognition goes to Robert Superko and Jaipal Singh for spearheading these projects and providing insights into the nature of collaboration.

For their support in my as part of Stephen Harvey's lab, I'd like to thank Tom Caulfield, Batsal Devkota, M. Burak Boz, Anton Petrov, Amanda McCook, Marcella Aliste, Geoff Rollins, Minmin Pan, Yingying Zeng, and Piyush Ranjan.

The support, friendship, and last minute paperwork filings of a number of Georgia Tech staff and faculty, including Todd Streelman, I King Jordan, Marc Pline, Kevin

Roman, Lisa Redding, Nael McCarty, Inga Schmidt-Krey, Soojin Yi, Steve Harvey, Steven Kudravi, Rupal Cutting, Jennifer Leavey, Angie Lessard, Francesca Storici, Rob Butera, Laura Cook, Al Merrill, Chong Shin, Mirjana Brockett, Yuhong Fan, Roger Wartell, and Verene Lancaster, kept me going through these years.

I also wanted to recognize the fine fellowship of many from around Georgia Tech, some of whom I'd met my first year and others gathered along the way, including Nick Parnell, Jon Sylvester, Sara Delavan, Karla Vincent, Ahsan Huda, Lee Katz, Daudi Jjingo, Andrey Kislyuk, Jen Kovacs, Rachel Lasley, Sam Parks, Amin Momin, Elizabeth Padilla, Randi Wilson, Jason Landrum, Taylor Updegrove, Wenhan Zhu, Jittima Piriyapongsa, Vardges Ter-Hovhannisyan, Adam Offenbacher, Eric Dammer, Aarti Urs, Jan Davidson-Drexel, Jianrong Wang, Wendy Morrison, Diya Mohan, Chiao Hsiao, Christine Fennessy, Brandy Jones, Astrid Layton, Andrew Farmer, Sean Kolk, Austin Ward, Ikay Okafor, Joan Fernandez, Vanessa Smet, Marissa Meier, Mariel Frieberg, Steve Heitner, Beth Kelly, Chris Kelly, Rhadika Dhingra, Miller Templeton, David Knobbe, Matt Marcus, Will Reeves, Bartek Ilkowski, Brandon Strellis, Heather Holmes, Zach Marion, Nikolai Curtis, Luke Beardslee, Henrik Muhe, Edouard De Watteville, Giuseppe Trianiti, and many others.

Outside Georgia Tech, I'd also like to recognize Paige Leitman, Ben Heisler, Erik Hofmeister, David Brainard, Gillen Heisler, Ron Franke, Joe Streaky, Mike Hanftt, Alex Medina, Sarah Peck, Ken Blumreich, Amanda Loftis, Chris Russell, Ignacio Portabella, and Jessica Halpin for keeping me grounded.

TABLE OF CONTENTS

LIST OF TABLES

LIST OF FIGURES

SUMMARY

Cardiovascular disease (CVD) causes 45% of on-duty firefighter fatalities, a high fraction even when compared to the risk of CVD found in other first-responder professions like police work and emergency medical services. Monitoring and managing firefighter cardiac health is important for both individual health and public safety. In our study, we are interested in assessing the utility of the most commonly used risk assessment scoring, known as the Framingham Risk Score, in evaluating the atherosclerotic risk in asymptomatic firefighters. To this end we determined FRS for 159 male firefighters from Gwinnett County, Georgia, and compared their risk categorization against their known atherosclerotic burden as determined by CIMT and CAC. While the 20% FRS threshold, corresponding to medium risk, had a high specificity for both CAC and CIMT, it also had a low sensitivity (17% and 40%, respectively), indicating that a large percentage of individuals with clinically significant atherosclerosis are being misclassified. By adjusting the FRS threshold downward, we were able to raise the sensitivity greatly with only a modest loss of specificity.

Following percutaneous transluminal coronary angioplasty for the treatment of coronary artery disease, stents are commonly implanted at the treatment site to prevent recoil and negative remodeling. To combat in-stent restenosis, an arterial healing response that results in luminal loss in stented arteries, anti-restenotic drugs like sirolimus (SES) and zotarolimus (ZES) are commonly eluted by stents to suppress cell proliferation at the treatment site. While comparative studies have revealed significant difference

between bare metal stents (BMS), SES, and ZES in both clinical and histological arterial response, the molecular basis of these differences remains poorly understood. We conducted a comparative gene expression profiling study using microarrays to examine differences in gene expression and pathway function in coronary arteries exposed to ZES, SES, and BMS in a porcine animal model. These molecular profiles suggest a model of delayed restenosis, resulting from a drug-induced suppression of inflammatory responses and proliferative processes, rather than an elimination of restenosis.

microRNAs play a regulatory role in metastasis-related epithelial to mesenchymal transitions and mesenchymal to epithelial transitions in ovarian cancer cells. We previously showed that over-expression of miR-429 in ovarian cancer cells drove a transition from mesenchymal phenotypes to epithelial phenotypes both in morphology and expression of markers like ZEB1, ZEB2, and E-cadherin. Our study represents the first time course analysis of miR-429-induced MET in ovarian cancer cells. We transfected Hey cells with miR-429 and assayed gene expression over the course of 144 hours at regular intervals. The cell morphology and gene expression of our transfected cells changed to become more epithelial-like at 24 and 48 hours and then became more mesenchymal-like by 144 hours. By 144 hours the average gene expression levels for 98.6% of our genes were not significantly different from the levels they started from at 0 hours when we adjusted for baseline expression changes observed in our negative control treated cells. This suggests the use of microRNAs as cancer therapies and driving cancer cells to a more drug susceptible state.

CHAPTER 1

INTRODUCTION

1.1 Gene expression

Transcriptional regulation and the post-transcriptional processing of messenger RNAs (mRNA) are early steps in the regulation of gene expression, controlling the types and amounts of proteins produced by cells via control of mRNA content and quantity. Transcriptional regulation through the direct action of activators, repressors, enhancers, and transcription factors alter transcription rates and have a large influence on transcript abundance. Post-transcriptional regulation and processing also influences the abundance and content of transcripts. Capping and polyadenylation protect mRNA from degradation, extending their expressive life spans. Splicing both removes intronic material from transcripts and can generate alternative transcripts, where different proteins can be generated from one complex transcription unit, altering the balance of content in mRNAs. RNA interference and microRNAs can also drive the silencing and degradation of mRNA signals post-transcriptionally. The ensemble of mRNA molecules in a cell is described as the transcriptome. Although changes in the amounts of specific mRNAs are not always directly related to the amount of the protein product encoded by the message, ensemble changes in mRNAs can be linked to ensemble changes in protein abundance and shifts in metabolic pathway component expression and phenotypic

changes. Thus the abundance of transcripts is a quantitative trait that connects DNA sequence variation with phenotype.

Transcriptomic analysis with expression microarrays, RT-PCR and RNA-Seq makes it possible to link the state of a cell to a high-resolution signature of mRNA abundances. Genes linked to particular mRNAs whose abundances change in response to a stimulus can be grouped together by their expression changes using covariance analysis, ontologically-driven pathway analyses, or network analyses using no *a priori* knowledge. Moreover, the ability of mRNAs to be sequenced or assayed with microarrays, generating "linear" data for many mRNAs in parallel, render them more convenient to measure than the proteins of the same genes, which are unstable, have detailed 3D conformations, and form multi-protein complexes. This ability to quantify tens of thousands of mRNAs at once is the primary advantage that new transcriptomic assays provide over the classic Northern blot. It permits sampling of expression across the genome, allowing for the unsupervised determination of differentially expressed genes rather than relying on a pre-determined set of genes or pathways that would limit the scope of analysis, facilitating their use in hypothesis-generation. It also allows for the detection of differential expression in complex pathways and systems containing many genes, particularly in those cases where small expression differences and network effects may drive changes.

The Affymetrix GeneChip expression analysis platform used both in our time-course work in tracking the mesenchymal-epithelial transition in ovarian cancer cells as well as our analysis of coronary artery changes in response to different

drug-eluting coronary stents is one of the most commonly used gene expression microarrays used in gene expression studies. Affymetrix arrays are produced by *in situ* synthesis of 24mer oligonucleotides probes at high densities where individual feature sizes can be as small as 8 μm (Lockhart et al. 1996). Typically 11 perfect match probes complementary to different positions along each mRNA transcript measure relative expression while a set of mismatch probes that are identical to the perfect match probes except for a single base modification in the middle position detect non-specific hybridizations (Dalma-Weiszhausz et al. 2006). The GeneChip Human Genome U133 Plus 2.0 Array is comprised of 1.3 million oligonucleotide features to assay the relative expression levels of 54,000 transcripts. These types of oligonucleotide arrays have the advantage of being relatively high density, have good reproducibility compared to spotted arrays, and ease of preparation. However compared to RNA-Seq approaches made possible by next-generation sequencing, these microarrays are expensive and limited to known gene targets (Baginsky et al. 2010).

1.1.1 Interpretation

To extract useful information from normalized gene expression data, we must apply the appropriate statistical tests to determine if expression levels are significantly different between treatments. Here the large number of gene transcripts measured at once for each sample presents a challenge where a large number of variables are measured for relatively few samples per treatment as well as an advantage where greater insight can be had into more complex biological systems. Whatever the level of detail desired, successful gene expression studies must be carefully planned so

that the experimental design is capable of answering the questions posed with appropriate sample sizes across groups, and well-chosen controls. Given the high cost of gene expression studies, failure to consider statistical analyses during the planning stage can lead to results with low discriminatory power and a poor ability to support strong conclusions.

In the past, fold change values were used to describe differences between two treatment groups, typically a case and control group, using a chosen threshold for determining significant differences or a ranked fold change list to describe expression patterns found between the two groups. This approach suffered from fold-change thresholds that were subjective choices, as well as a lack of accounting for within-system variance, where genes can have large fold-changes that may actually be insignificant when considered in the context of highly variable data. A more sound approach utilizes statistical tests like t-tests that describe the difference in estimated means of each group relative to the amount of variance found in both groups. Although the traditional t-test does not perform optimally in cases with small sample sizes, as are often found in microarray studies, variations of the t-test such as penalized t-tests and moderated t-tests as well as likelihood ratio tests can be more suited to these designs (Tusher et al. 2001; Smyth 2004; Zhang and Cao 2009). In those cases where we wish to find genes that have significantly different estimated average expressions across more than two groups, a multi-group analog of the t-test, analysis of variance (ANOVA), can be used that asks if variance among groups is significantly large compared to within-group variance (Kerr et al. 2000). By using a statistical approach to determining which genes are significantly

differentially expressed, we can rest our premise on p-values for rejecting null hypotheses and confidence intervals for describing modeled distributions of test statistics.

Single gene expression analysis techniques offer a very limited view of the overall gene expression profile, one approach to allow us to characterize the expression of multiple genes is unsupervised methods for generating gene signatures by treatment group. Unsupervised methods are useful as they do not require any *a priori* information about the samples, nor do they focus on any subset of gene pathways or networks, allowing the user to generate new hypotheses more freely. Simple examples of these include gene ordering based on ranked-correlations or expression profiles based on clustering (van 't Veer et al. 2002; Chin et al. 2009). These can suggest genes and expression patterns that differentiate treatment groups, but may not provide a clear way to classify new samples or a quantification of specificity and sensitivity. Examples of machine learning and multivariate analysis approaches that are unbiased include support vector machines (Brown et al. 2000), neural networks (Khan et al. 2001), Baysian analysis (Chang et al. 2011), and random forests (Diaz-Uriarte and Alvarez de Andres 2006). Properly trained and tested, these approaches can classify gene expression profiles with great accuracy. However, extracting biological relevance can be daunting, particularly if they only provide sparse weightings across broad ranges of genes, as can often be found with support vector machines, or uninterpretable models, as can be found in neural networks. Even from significantly differentially expressed sets of genes obtained via Bayesian analysis and random forests, knowledge-driven analysis is

required to extract biological meaning. Searches on well-curated databases for gene product annotation such as the Gene Ontology, Molecular Signatures Database, and GeneSigDB can add organization by function (Subramanian et al. 2005; Chang and Nevins 2006; Culhane et al. 2010). Moreover, gene enrichment analysis for significantly enriched annotation terms can be performed with tools such as Gene Set Enrichment Analysis and GeneGO MetaCore tools (Subramanian et al. 2005; Reuters 2012).

Whether we consider differential expression across individual genes or gene sets, large numbers of hypotheses tests are commonly encountered in gene expression studies. This creates the problem of generating false discoveries, where false positives, apparently significant rejections of the null hypothesis, appear with greater frequency owing to the large number of tests. We can implement a number of methods to control and estimate the rate of false discoveries. Most methods used in gene expression analysis fall into methods that control the family-wise error rate (FWER) or the false discovery rate (FDR). FWER attempts to quantify and adjust for the rate of false discoveries among all tests of hypotheses, which is typically the most stringent approach for multiple testing correction. Examples of this include the Bonferroni correction and Hochberg method (Hochberg 1988; Bland and Altman 1995). Particularly in gene expression studies where effect sizes are small compared to sample numbers, FWER approaches can result in high false negative rates, effectively reducing exploratory capacity (Weller et al. 1998). FDR methods attempt to quantify and adjust for the rate of false discoveries among the significant genes or gene sets after correction. While being less stringent, effectively letting in more false

positives, we also limit the number of false negatives. This can be useful in experiments designed to be hypothesis generating, where we wish to maximize our window for discovery. Examples of this approach include the Benjamini-Hochberg method, beta-uniform mixture models, and Storey's method (Benjamini and Hochberg 1995; Allison et al. 2002; Storey 2002).

1.2 Ovarian cancer

Ovarian cancer is the eighth most common cancer and fifth most common cause of cancer deaths among women in the USA with an annual incidence rate of 12.2 per 100,000 and annual death rate of 8 per 100,000 in 2007 (Group 2012). Although the overall 5-year relative survival rate is 43.2%, mortality is high because 70% of ovarian cancers are diagnosed at advanced stage, with extensive metastasis within the peritoneal cavity, where the 5-year relative survival rate is 30% (Cho and Shih Ie 2009; Howlader et al. 2012). In the US in 2009, an estimated 1 in 72 women would develop ovarian cancer in their lifetime (Howlader et al. 2012). Globally, ovarian cancer is the sixth most common cancer in women, and more than 90% of primary malignant ovarian tumors are epithelial in origin (Sankaranarayanan and Ferlay 2006).

Unlike other solid tumors that go through multiple steps of extravasation before metastasizing through the blood circulatory system, ovarian cancer cells typically metastasize by direct contact with adjacent organs or by detaching from the primary tumor (Gupta and Massague 2006). Detached tumor cells can then travel in peritoneal fluids throughout the abdominal cavity. In this manner,

carcinoma can attach to reproductive organs, the omentum, or the sigmoid colon. Additionally, metastasized carcinoma can also be transported via the lymph node system (Eisenkop and Spirtos 2001).

The epithelial-mesenchymal transition (EMT) of ovarian surface epithelium (OSE) is thought to normally be involved in postovulatory repair, where the transition to a mesenchymal phenotype provides the motility and proliferation necessary for extracellular matrix remodeling (Salamanca et al. 2004). Early evidence of EMT's potential role in cancer was suggested in studies of kidney fibrosis in mouse models, where large numbers of fibroblast-specific protein-1 expressing fibroblasts arose via EMT in response to injury (Iwano et al. 2002). The presence of EMT in fibrosis was offered as an example of a mechanism present in both tumors and wound healing that could explain changes in cell phenotype. The transition is typical of cellular transformations crucial in embryogenesis, such as mesoderm formation, neural crest development, and secondary palate formation, as well as in organogenesis. EMT is also the first step in the epithelial-mesenchymal-epithelial transitions during ovarian carcinoma metastasis, beginning with the disruption of E-cadherin-mediated cell-cell interactions (Ahmed et al. 2007). This permits epithelial cells to detach from the basement membrane and loosens connections between carcinoma cells. Once detached these cells can now enter the peritoneal fluid, and be passively moved into the coelomic space. The cancer cells also acquire a mesenchymal phenotype becoming spindle-like, and more motile.

The reverse process, known as the mesenchymal-epithelial transition (MET) is involved in reverting the motile mesenchymal-like ovarian cancer cells created via

EMT to a more epithelial-like phenotype at the secondary tumor site. E-cadherin, known to induce the MET pathway, is expressed in both primary and metastatic ovarian carcinomas, but not normal ovarian surface epithelium (Veatch et al. 1994; Darai et al. 1997; Maines-Bandiera and Auersperg 1997; Davies et al. 1998). E-cadherin expression in human ovarian surface epithelium induces the localization of E-cadherin, catenins, and f-actin to the locations of cell-cell contact, gaining epithelial characteristics associated with MET (Auersperg et al. 1999). Consistent with this model, work in a human bladder cancer model has shown that MET contributes to the establishment of metastatic deposits, where targeted abrogation of fibroblast growth factor (FGF) pathways involved in MET both reverses MET and increases survival in TSU-Pr1 tumor cell line inoculated mice (Chaffer et al. 2005; Chaffer et al. 2006). MET occurs naturally during somitogenesis, kidney formation, and coelomic-cavity formation, and work done in these areas has identified important modulators likely to be involved in cancer metastasis (Saga and Takeda 2001; Vainio and Lin 2002). Given the plasticity of the native ovarian surface epithelium, MET is thought to be the molecular reversal of EMT (Wong and Leung 2007).

At the same time, our understanding about the mechanisms involved in EMT and MET is incomplete, particularly in its role in cancer progression. A major advance in understanding this dynamic was the identification of transcription factors capable of inducing EMT in cancer cells. Blanco et al (2002) noted the presence of Snail, a transcription factor involved in EMT in embryonic development, in human breast carcinomas, its expression inversely correlated with the grade of

tumor differentiation. High levels of expression of the transcription factor Twist was correlated with invasive breast lobular carcinoma, and further expression studies demonstrated Twist's ability to promote the loss of cell-cell adhesion, activated mesenchymal markers, and induce cell motility (Yang et al. 2004). E-cadherin is involved in signaling and capable of inducing MET in human ovarian surface epithelium (Auersperg 1999). Studies comparing primary ovarian carcinomas to metastases demonstrated lower Snail expression in metastases than in primary carcinomas, higher expression of TWIST1 and ZEB1 in metastases, and the regulation of Snail localization by Pak1, leading to E-cadherin re-expression in metastases (Elloul et al. 2010). EMT induced by TGF-β1 signaling through a Smads-dependent pathway in rat and human alveolar epithelial-like cells could be reversed, via the MAPK/ERK kinase pathway, by culturing with FGF-1 for 48 hours, suggesting that EMT and MET might arise from induction of separate pathways rather than reversing the induction of a single pathway (Ramos et al. 2010). These experiments outline the complex signaling involved in both EMT and MET coordinated by the actions of multiple transcription factors.

In 2005, Tarin suggested EMT did not actually occur in cancer metastasis, pointing out the most glaring of the gaps in the EMT model in cancer (Tarin et al. 2005). First, that stable epithelial mesenchymal transition had not been extensively documented or recognized by surgical pathologists when examining tumor samples. Moreover, that EMT had primarily been observed only in cell culture or engineered animal models, and that phenotypic descriptions used by researchers focused on molecular markers were not rigorous or based on changes in single molecular

markers. Finally, that markers described as being indicative of EMT were not specific for mesenchymal cells and were unreliable due to the genetic instability of tumors.

Supporters of the EMT model in cancer metastasis argued that EMT is not being used in the strict irreversible sense of transition between two differentiation states, but to describe the spectrum of phenotypic changes observed that inextricably link both molecular markers and biological process (Cardiff 2005; Yang and Weinberg 2008). A number of models to bridge this gap have been suggested, including incomplete EMT, epithelial-amoeboid transitions, and EMT-like states. EMT-like reflects a dedifferentiation rather than trans-differentiation process, where transformed epithelial cells may simply fail to differentiate normally, resulting in a state defined by cell cohesiveness, intermediate filament protein expression, and cell polarization (Klymkowsky and Savagner 2009). Incomplete EMT, on the other hand, suggests a signal cascade through a variety of mechanisms, ranging from TGF-B initiated cascades, to activation of downstream MAPK signaling, to activation of signaling by virally encoded oncogenes like v-Src and v-Ras that triggers some of the EMT properties without a complete transition of phenotypes (Christiansen and Rajasekaran 2006). Wolf et al (2003) suggest a third model of epithelial-amoeboid transition in which carcinoma cells gain mobility through protease-independent migration, adopting a spherical morphology without degradation of extracellular matrix barriers. As EMT continues to be unobserved in human tumor samples, while the molecular evidence for its role in cell lines and animals models grows, EMT's role in cancer pathogenesis remains unresolved.

Induction of this transition is of interest both for improving our understanding of this complex process as well as the potential to shift cancer cells into a less chemotherapeutically-resistant state (Thomson et al. 2005; Arumugam et al. 2009; Uramoto et al. 2010; Xie et al. 2012). microRNAs (miRNA) have been a potential transition inducer of interest owing to their regulatory impact on the transcription of multiple targets at once, and previous studies have established a role for miR-200 family microRNAs in the induction of MET in ovarian cancer cells in single time point gene expression experiments (Chen et al. 2011). We asked what the impact of a single point transfection of miR-429 from the miR-200 family miRNAs had on ovarian cancer cells and whether or not this effect was permanent, sampling across multiple time points at 0, 24, 48, and 144 hours after transfection. We used a control-adjusted time course analysis to show that by 24 and 48 hours, those cells exposed to miR-429 had gained morphologic and gene expression features consistent with a more epithelial state. And by 144 hours had returned to a more mesenchymal-like state in both morphology and expression, suggesting a rebound or plastic response to this miRNA.

1.3 Atherosclerosis

Atherosclerosis, the build up of fatty deposits, inflammation, proliferated cells, and scar tissue within the walls of arteries, is the leading cause of mortality and morbidity in the industrialized world. A chronic disease, its complications can lead to stenosis, stroke, and myocardial infarction, and is thought to be the underlying cause of most clinical cardiovascular events. In 2008, approximately one in every

six deaths in the United States was caused by coronary heart disease (CHD), and, in 2012, an estimated 1,200,000 Americans would experience myocardial infarctions (MI), in addition to 195,000 silent myocardial infarctions a year (Members et al. 2012). Strokes account for approximately 795,000 of cardiovascular disease incidents per year, and 1 in 18 deaths in the United States in 2008. Risk factors for atherosclerosis include high LDL cholesterol, low HDL cholesterol, high blood pressure, smoking, diabetes, obesity, age, family history, and insulin resistance (Anderson et al. 1991).

Atherosclerosis begins with a site of chronic inflammation in the arterial wall, initiated by endothelial dysfunction and structural changes followed by the accumulation of LDLs inside the vessel wall (Moore and Tabas 2011). The accumulation of oxidized lipids and lipoproteins drives the extravasation of immune cells attracted to adhesion molecules and chemokines expressed by the endothelial cells (Libby 2002). The continuing accumulation of lipids in these monocytes eventually leads to the formation of "fatty-streak" lesions, consisting of T cells and foam cells, which can appear as early as childhood. These plaques grow by accumulating lipid, and form a fibrous plaque through smooth muscle cell proliferation and collagen matrix growth. These plaques can then rupture, detaching to occlude elsewhere resulting in thromboembolism and strokes or cause a local thrombotic occlusion resulting in infarction. Even those plaques that are stable and do not rupture can cause stenosis and restrict blood flow to downstream tissue resulting in ischemia.

Coronary calcification (CAC) associated with atherosclerotic plaques has emerged as a high accuracy predictor for major adverse coronary heart disease events including myocardial infarction, angina, cardiac arrest and CHD death (Budoff et al. 2009b). Histological analysis and ultrasound studies have confirmed a direct relationship between plaque burden and coronary calcification (Baumgart et al. 1997; Mintz et al. 1997). The presence of calcification is now well established as a sign of atherosclerosis, and does not occur in the normal artery wall (Janowitz et al. 1991; Wexler et al. 1996). Absent or minimal calcification in asymptomatic individuals has been shown to be associated with a very low risk of adverse cardiovascular events when followed-up at a median of 4.1 years (Budoff et al. 2009a). Although previously believed to be the result of calcium precipitation or the degeneration of fibrous tissue, the mechanism of coronary calcification has been shown to be an active process similar to that of normal bone formation (Bostrom et al. 1993; Proudfoot et al. 1998).

Defined as the distance between the luminal-intimal interface and the media-adventitial interface of the common carotid artery, carotid intima-media thickness (CIMT) is visualized by B-mode vascular ultrasound (Pignoli et al. 1986). Increases in this distance are interpreted intimal thickenings from the early stages of atherosclerotic disease, particularly because carotid arteries have less muscular media than other arteries (Stary et al. 1992). Because intima-media thickness (IMT) can react dynamically to blood pressure and sheer stress, lower degrees of IMT can represent a mixture of response to these transient hemodynamics as well as atherosclerotic burden (Bots et al. 1997). It is now commonly accepted that

atherosclerosis is more likely at IMTs above 0.9 mm (Naghavi et al. 2006). Although total intima-media thickness can be correlated with future coronary heart disease risk, changes in CIMT have been found to be poorly predictive of changes in the potential for major adverse coronary events (Goldberger et al. 2010).

Firefighters, compared to other first responder personnel, have an elevated risk for major adverse coronary events that is thought to be linked to heat, dehydration, strong cardiovascular strain, smoke exposure, and shift work (Kales et al. 2003; Kales et al. 2007). Traditionally used coronary artery disease risk calculators like the ATP III version of the Framingham Risk Score (FRS) that are commonly used by clinicians may underestimate the risk of heart disease and atherosclerotic burden present in firefighters. By comparing FRS with CIMT and coronary artery calcification (CAC) in 159 male firefighters from Gwinnett County, Georgia, we determined that FRS misclassified a large number of individuals with clinically significant atherosclerosis. By using Receiver-Operator Characteristic curves to set new FRS thresholds, we were able to improve the sensitivity of the scoring method.

Percutaneous transluminal coronary angioplasty (PTCA) has revolutionized the treatment of coronary artery disease since its introduction in 1977 (Grüntzig et al. 1979). However, restenosis or the arterial healing response has proven to be problematic for PTCA due to negative remodeling, contraction formation and consequent late luminal loss in 30-60% of post-angioplasty patients (Fischman et al. 1994; Serruys et al. 1994). The use of bare metal stents (BMS) in PTCA has been effective in reducing restenosis by acting as a scaffold against elastic recoil and

negative remodeling (Sigwart et al. 1987; Fischman et al. 1994; Serruys et al. 1994). Referred to generally as percutaneous coronary intervention (PCI) the use of stents in PTCA has resulted in a significant reduction in many of the major adverse cardiac events associated with PTCA and is currently considered a standard procedure worldwide. However, the increased use of BMS in PTCA has resulted in the emergence of an unanticipated complication, *i.e.*, the occurrence of restenosis within the stent ("in-stent restenosis" or ISR) resulting in > 50% late lumen diameter loss in treated patients.

In an effort to reduce ISR, a new generation of drug-eluting stents (DES) has been designed to release anti-restenotic agents at the stent site. Built on top of stainless steel, cobalt, chrome, or platinum-chrome alloy stents these devices feature polymer coatings that deliver drug payloads in a controlled fashion and increasingly chosen for their biocompatibility to reduce inflammation and thrombocity (Cheol Whan et al. 2009; Kandzari et al. 2011). Drug eluting stents that have been released to market either carry paclitaxel or rapamycin-related compounds. At the present moment, the anti-restenotic drugs used in drug-eluting stents are sirolimus (Sirolimus Eluting Stents, SES), everolimus, and zotarolimus (Zotarolimus Eluting Stents, ZES). All three drugs have similar antimicrobial and immunosuppressive properties since they are derived from the same natural compound, rapamycin (Pendyala et al. 2008). Rapamycin acts by binding to the cytosolic receptor FKBP12, forming a complex that inhibits the activation of the mammalian target of rapamycin (mTOR) (Fischman et al. 1994). mTOR inhibition ultimately results in cell cycle arrest in the late G_1 phase, arresting smooth muscle

cell growth (Braun-Dullaeus et al. 1998; Marx and Marks 2001). Sirolimus is bound to the stent with a poly-ethylene-covinyl/poly-n-butyl methacrylate copolymer. ZES elute zotarolimus, a derivative of sirolimus that incorporates a phosphorylcholine coating that imparts high lipophilicity (Lewis and Stratford 2002). It has been suggested that ZES are better suited for stent based drug delivery since they have been shown to reduce endothelialisation and neointimal formation relative to SES (Burke et al. 2006). Although the impact of these stents has been characterized in longitudinal studies across multiple treatment centers, the broad transcriptomic impact of rapamycin-derived drug-eluting stents *in vivo* has not been studied (Cheol Whan et al. 2009; Park et al. 2010; Rasmussen et al. 2010; Kandzari et al. 2011). In order to better understand the molecular changes in coronary arteries at the site of stent implantation, we conducted a comparative microarray profiling study to examine differences in gene expression and pathway function in coronary arteries exposed to ZES, SES, and BMS in a porcine animal model. Through gene ontology analysis and comparison to prior work examining arterial response to BMS, we were able to characterize the progression of restenosis in arteries exposed to these two drug eluting stents and hypothesize that rapamycin-eluting stents were delaying, rather than permanently reducing, restenosis.

1.4 References

Ahmed N, Thompson EW, Quinn MA. 2007. Epithelial-mesenchymal interconversions in normal ovarian surface epithelium and ovarian carcinomas: an exception to the norm. *J Cell Physiol* **213**(3): 581-588.

Allison DB, Gadbury GL, Heo M, Fernendez JR, Lee C-K, Prolla TA, Weindruch R. 2002. A mixture model approach for the analysis of microarray gene expression data. *Computational Statistics & Data Analysis* **39**(1): 1-20.

Anderson KM, Wilson PW, Odell PM, Kannel WB. 1991. An updated coronary risk profile. A statement for health professionals. *Circulation* **83**(1): 356-362.

Arumugam T, Ramachandran V, Fournier KF, Wang H, Marquis L, Abbruzzese JL, Gallick GE, Logsdon CD, McConkey DJ, Choi W. 2009. Epithelial to mesenchymal transition contributes to drug resistance in pancreatic cancer. *Cancer Res* **69**(14): 5820-5828.

Auersperg N, Pan J, Grove BD, Peterson T, Fisher J, Maines-Bandiera S, Somasiri A, Roskelley CD. 1999. E-cadherin induces mesenchymal-to-epithelial transition in human ovarian surface epithelium. *Proceedings of the National Academy of Sciences* **96**(11): 6249-6254.

Baginsky S, Hennig L, Zimmermann P, Gruissem W. 2010. Gene Expression Analysis, Proteomics, and Network Discovery. *Plant Physiology* **152**(2): 402-410.

Baumgart D, Schmermund A, Goerge G, Haude M, Ge J, Adamzik M, Sehnert C, Altmaier K, Groenemeyer D, Seibel R et al. 1997. Comparison of electron beam computed tomography with intracoronary ultrasound and coronary angiography for detection of coronary atherosclerosis. *J Am Coll Cardiol* **30**(1): 57-64.

Benjamini Y, Hochberg Y. 1995. Controlling the false discovery rate: a practical and powerful approach to multiple testing. *Journal of the Royal Statistical Society Series B (Methodological)*: 289-300.

Blanco MJ, Moreno-Bueno G, Sarrio D, Locascio A, Cano A, Palacios J, Nieto MA. 2002. Correlation of Snail expression with histological grade and lymph node status in breast carcinomas. *Oncogene* **21**(20): 3241-3246.

Bland JM, Altman DG. 1995. Multiple significance tests: the Bonferroni method. *BMJ* **310**(6973): 170.

Bostrom K, Watson KE, Horn S, Wortham C, Herman IM, Demer LL. 1993. Bone morphogenetic protein expression in human atherosclerotic lesions. *J Clin Invest* **91**(4): 1800-1809.

Bots ML, Hofman A, Grobbee DE. 1997. Increased common carotid intima-media thickness. Adaptive response or a reflection of atherosclerosis? Findings from the Rotterdam Study. *Stroke* **28**(12): 2442-2447.

Braun-Dullaeus RC, Mann MJ, Dzau VJ. 1998. Cell Cycle Progression : New Therapeutic Target for Vascular Proliferative Disease. *Circulation* **98**(1): 82-89.

Brown MPS, Grundy WN, Lin D, Cristianini N, Sugnet CW, Furey TS, Ares M, Haussler D. 2000. Knowledge-based analysis of microarray gene expression data by using support vector machines. *Proceedings of the National Academy of Sciences* **97**(1): 262-267.

Budoff MJ, McClelland RL, Nasir K, Greenland P, Kronmal RA, Kondos GT, Shea S, Lima JA, Blumenthal RS. 2009a. Cardiovascular events with absent or minimal coronary calcification: the Multi-Ethnic Study of Atherosclerosis (MESA). *Am Heart J* **158**(4): 554-561.

Budoff MJ, Nasir K, McClelland RL, Detrano R, Wong N, Blumenthal RS, Kondos G, Kronmal RA. 2009b. Coronary calcium predicts events better with absolute calcium scores than age-sex-race/ethnicity percentiles: MESA (Multi-Ethnic Study of Atherosclerosis). *J Am Coll Cardiol* **53**(4): 345-352.

Burke SE, Kuntz RE, Schwartz LB. 2006. Zotarolimus (ABT-578) eluting stents. *Advanced Drug Delivery Reviews* **58**(3): 437-446.

Cardiff RD. 2005. Epithelial to Mesenchymal Transition Tumors: Fallacious or Snail's Pace? *Clin Cancer Res* **11**(24 Pt 1): 8534-8537.

Chaffer CL, Brennan JP, Slavin JL, Blick T, Thompson EW, Williams ED. 2006. Mesenchymal-to-epithelial transition facilitates bladder cancer metastasis: role of fibroblast growth factor receptor-2. *Cancer Res* **66**(23): 11271-11278.

Chaffer CL, Dopheide B, McCulloch DR, Lee AB, Moseley JM, Thompson EW, Williams ED. 2005. Upregulated MT1-MMP/TIMP-2 axis in the TSU-Pr1-B1/B2 model

of metastatic progression in transitional cell carcinoma of the bladder. *Clin Exp Metastasis* **22**(2): 115-125.

Chang J, Gatza M, Lucas J, Barry W, Vaughn P, Nevins J. 2011. SIGNATURE: A workbench for gene expression signature analysis. *BMC Bioinformatics* **12**(1): 443.

Chang JT, Nevins JR. 2006. GATHER: a systems approach to interpreting genomic signatures. *Bioinformatics* **22**(23): 2926-2933.

Chen J, Wang L, Matyunina LV, Hill CG, McDonald JF. 2011. Overexpression of miR-429 induces mesenchymal-to-epithelial transition (MET) in metastatic ovarian cancer cells. *Gynecologic Oncology* **121**(1): 200-205.

Cheol Whan L, Duk-Woo P, Seung-Hwan L, Young-Hak K, Myeong-Ki H, Jae-Joong K, Seong-Wook P, Sung-Cheol Y, In-Whan S, Jae-Hwan L et al. 2009. Comparison of the Efficacy and Safety of Zotarolimus-, Sirolimus-, and Paclitaxel-Eluting Stents in Patients With ST-Elevation Myocardial Infarction. *The American Journal of Cardiology* **104**(10): 1370-1376.

Chin MH, Mason MJ, Xie W, Volinia S, Singer M, Peterson C, Ambartsumyan G, Aimiuwu O, Richter L, Zhang J et al. 2009. Induced Pluripotent Stem Cells and Embryonic Stem Cells Are Distinguished by Gene Expression Signatures. *Cell Stem Cell* **5**(1): 111-123.

Cho KR, Shih Ie M. 2009. Ovarian cancer. *Annu Rev Pathol* **4**: 287-313.

Christiansen JJ, Rajasekaran AK. 2006. Reassessing epithelial to mesenchymal transition as a prerequisite for carcinoma invasion and metastasis. *Cancer Res* **66**(17): 8319-8326.

Culhane AC, Schwarzl T, Sultana R, Picard KC, Picard SC, Lu TH, Franklin KR, French SJ, Papenhausen G, Correll M et al. 2010. GeneSigDB, a curated database of gene expression signatures. *Nucleic Acids Research* **38**(suppl 1): D716-D725.

Dalma-Weiszhausz DD, Warrington J, Tanimoto EY, Miyada CG. 2006. The Affymetrix GeneChip Platform: An Overview. In *Methods in Enzymology*, Vol Volume 410 (ed. K Alan, O Brian), pp. 3-28. Academic Press.

Darai E, Scoazec JY, Walker-Combrouze F, Mlika-Cabanne N, Feldmann G, Madelenat P, Potet F. 1997. Expression of cadherins in benign, borderline, and malignant ovarian epithelial tumors: a clinicopathologic study of 60 cases. *Hum Pathol* **28**(8): 922-928.

Davies BR, Worsley SD, Ponder BA. 1998. Expression of E-cadherin, alpha-catenin and beta-catenin in normal ovarian surface epithelium and epithelial ovarian cancers. *Histopathology* **32**(1): 69-80.

Diaz-Uriarte R, Alvarez de Andres S. 2006. Gene selection and classification of microarray data using random forest. *BMC Bioinformatics* **7**(1): 3.

Eisenkop SM, Spirtos NM. 2001. The Clinical Significance of Occult Macroscopically Positive Retroperitoneal Nodes in Patients with Epithelial Ovarian Cancer. *Gynecologic Oncology* **82**(1): 143-149.

Elloul S, Vaksman O, Stavnes HT, Trope CG, Davidson B, Reich R. 2010. Mesenchymal-to-epithelial transition determinants as characteristics of ovarian carcinoma effusions. *Clin Exp Metastasis* **27**(3): 161-172.

Fischman DL, Leon MB, Baim DS, Schatz RA, Savage MP, Penn I, Detre K, Veltri L, Ricci D, Nobuyoshi M et al. 1994. A Randomized Comparison of Coronary-Stent Placement and Balloon Angioplasty in the Treatment of Coronary Artery Disease. *New England Journal of Medicine* **331**(8): 496-501.

Goldberger ZD, Valle JA, Dandekar VK, Chan PS, Ko DT, Nallamothu BK. 2010. Are changes in carotid intima-media thickness related to risk of nonfatal myocardial infarction? A critical review and meta-regression analysis. *American heart journal* **160**(4): 701-714.

Group USCSW. 2012. United States Cancer Statistics: 1999–2008 Incidence and Mortality Web-based Report. U.S. Department of Health and Human Services, Centers for Disease Control and Prevention and National Cancer Institute, Atlanta.

Grüntzig AR, Senning Å, Siegenthaler WE. 1979. Nonoperative Dilatation of Coronary-Artery Stenosis. *New England Journal of Medicine* **301**(2): 61-68.

Gupta GP, Massague J. 2006. Cancer Metastasis: Building a Framework. *Cell* **127**(4): 679-695.

Hochberg Y. 1988. A sharper Bonferroni procedure for multiple tests of significance. *Biometrika* **75**(4): 800-802.

Howlader N, Noone A, Krapcho M, Neyman N, Aminou R, Waldron W, Altekruse SF, Kosary CL, Ruhl J, Tatalovich Z et al. 2012. SEER Cancer Statistics Review, 1975-2009 (Vintage 2009 Populations). National Cancer Institute, Bethesda, MD.

Iwano M, Plieth D, Danoff TM, Xue C, Okada H, Neilson EG. 2002. Evidence that fibroblasts derive from epithelium during tissue fibrosis. *J Clin Invest* **110**(3): 341-350.

Janowitz WR, Agatston AS, Viamonte M, Jr. 1991. Comparison of serial quantitative evaluation of calcified coronary artery plaque by ultrafast computed tomography in persons with and without obstructive coronary artery disease. *Am J Cardiol* **68**(1): 1-6.

Kales SN, Soteriades ES, Christophi CA, Christiani DC. 2007. Emergency duties and deaths from heart disease among firefighters in the United States. *New England Journal of Medicine* **356**(12): 1207-1215.

Kales SN, Soteriades ES, Christoudias SG, Christiani DC. 2003. Firefighters and on-duty deaths from coronary heart disease: a case control study. *Environ Health* **2**(1): 14.

Kandzari DE, Mauri L, Popma JJ, Turco MA, Gurbel PA, Fitzgerald PJ, Leon MB. 2011. Late-Term Clinical Outcomes With Zotarolimus- and Sirolimus-Eluting Stents: 5-Year Follow-Up of the ENDEAVOR III (A Randomized Controlled Trial of the Medtronic Endeavor Drug [ABT-578] Eluting Coronary Stent System Versus the Cypher Sirolimus-Eluting Coronary Stent System in De Novo Native Coronary Artery Lesions). *J Am Coll Cardiol Intv* **4**(5): 543-550.

Kerr MK, Martin M, Churchill GA. 2000. Analysis of variance for gene expression microarray data. *J Comput Biol* **7**(6): 819-837.

Khan J, Wei JS, Ringner M, Saal LH, Ladanyi M, Westermann F, Berthold F, Schwab M, Antonescu CR, Peterson C et al. 2001. Classification and diagnostic prediction of cancers using gene expression profiling and artificial neural networks. *Nat Med* **7**(6): 673-679.

Klymkowsky MW, Savagner P. 2009. Epithelial-mesenchymal transition: a cancer researcher's conceptual friend and foe. *Am J Pathol* **174**(5): 1588-1593.

Lewis AL, Stratford PW. 2002. Phosphorylcholine-Coated Stents. *Journal of Long-Term Effects of Medical Implants* **12**(4): 20.

Libby P. 2002. Inflammation in atherosclerosis. *Nature* **420**(6917): 868-874.

Lockhart DJ, Dong H, Byrne MC, Follettie MT, Gallo MV, Chee MS, Mittmann M, Wang C, Kobayashi M, Horton H et al. 1996. Expression monitoring by hybridization to high-density oligonucleotide arrays. *Nat Biotechnol* **14**(13): 1675-1680.

Maines-Bandiera SL, Auersperg N. 1997. Increased E-cadherin expression in ovarian surface epithelium: an early step in metaplasia and dysplasia? *Int J Gynecol Pathol* **16**(3): 250-255.

Marx SO, Marks AR. 2001. Bench to Bedside: The Development of Rapamycin and Its Application to Stent Restenosis. *Circulation* **104**(8): 852-855.

Members WG, Roger VrL, Go AS, Lloyd-Jones DM, Benjamin EJ, Berry JD, Borden WB, Bravata DM, Dai S, Ford ES et al. 2012. Heart Disease and Stroke Statistics,Äî2012 Update. *Circulation* **125**(1): e2-e220.

Mintz GS, Pichard AD, Popma JJ, Kent KM, Satler LF, Bucher TA, Leon MB. 1997. Determinants and correlates of target lesion calcium in coronary artery disease: a clinical, angiographic and intravascular ultrasound study. *J Am Coll Cardiol* **29**(2): 268-274.

Moore KJ, Tabas I. 2011. Macrophages in the Pathogenesis of Atherosclerosis. *Cell* **145**(3): 341-355.

Naghavi M, Falk E, Hecht HS, Jamieson MJ, Kaul S, Berman D, Fayad Z, Budoff MJ, Rumberger J, Naqvi TZ et al. 2006. From Vulnerable Plaque to Vulnerable Patient,ÄîPart III: Executive Summary of the Screening for Heart Attack

Prevention and Education (SHAPE) Task Force Report. *The American Journal of Cardiology* **98**(2, Supplement 1): 2-15.

Park D-W, Kim Y-H, Yun S-C, Kang S-J, Lee S-W, Lee C-W, Park S-W, Seong I-W, Lee J-H, Tahk S-J et al. 2010. Comparison of Zotarolimus-Eluting Stents With Sirolimus- and Paclitaxel-Eluting Stents for Coronary Revascularization: The ZEST (Comparison of the Efficacy and Safety of Zotarolimus-Eluting Stent with Sirolimus-Eluting and PacliTaxel-Eluting Stent for Coronary Lesions) Randomized Trial. *Journal of the American College of Cardiology* **56**(15): 1187-1195.

Pendyala L, Jabara R, Shinke T, Chronos N, Robinson K, Li J, Hou D. 2008. Drug-Eluting Stents: Present and Future. *Cardiovascular & Hematological Agents in Medicinal Chemistry* **6**: 105-115.

Pignoli P, Tremoli E, Poli A, Oreste P, Paoletti R. 1986. Intimal plus medial thickness of the arterial wall: a direct measurement with ultrasound imaging. *Circulation* **74**(6): 1399-1406.

Proudfoot D, Skepper JN, Shanahan CM, Weissberg PL. 1998. Calcification of human vascular cells in vitro is correlated with high levels of matrix Gla protein and low levels of osteopontin expression. *Arterioscler Thromb Vasc Biol* **18**(3): 379-388.

Ramos C, Becerril C, Montano M, Garcia-De-Alba C, Ramirez R, Checa M, Pardo A, Selman Ms. 2010. FGF-1 reverts epithelial-mesenchymal transition induced by TGF-B1 through MAPK/ERK kinase pathway. *American Journal of Physiology - Lung Cellular and Molecular Physiology* **299**(2): L222-L231.

Rasmussen K, Maeng M, Kaltoft A, Thayssen P, Kelbæk H, Tilsted HH, Abildgaard U, Christiansen EH, Engstrøm T, Krusell LR et al. 2010. Efficacy and safety of zotarolimus-eluting and sirolimus-eluting coronary stents in routine clinical care (SORT OUT III): a randomised controlled superiority trial. *The Lancet* **375**(9720): 1090-1099.

Reuters T. 2012. Metacore. New York, NY.

Saga Y, Takeda H. 2001. The making of the somite: molecular events in vertebrate segmentation. *Nat Rev Genet* **2**(11): 835-845.

Salamanca CM, Maines-Bandiera SL, Leung PCK, Hu Y-L, Auersperg N. 2004. Effects of Epidermal Growth Factor/Hydrocortisone on the Growth and Differentiation of Human Ovarian Surface Epithelium. *Journal of the Society for Gynecologic Investigation* **11**(4): 241-251.

Sankaranarayanan R, Ferlay J. 2006. Worldwide burden of gynaecological cancer: the size of the problem. *Best Pract Res Clin Obstet Gynaecol* **20**(2): 207-225.

Serruys PW, de Jaegere P, Kiemeneij F, Macaya C, Rutsch W, Heyndrickx G, Emanuelsson H, Marco J, Legrand V, Materne P et al. 1994. A Comparison of Balloon-Expandable-Stent Implantation with Balloon Angioplasty in Patients with Coronary Artery Disease. *New England Journal of Medicine* **331**(8): 489-495.

Sigwart U, Puel J, Mirkovitch V, Joffre F, Kappenberger L. 1987. Intravascular Stents to Prevent Occlusion and Re-Stenosis after Transluminal Angioplasty. *New England Journal of Medicine* **316**(12): 701-706.

Smyth GJ. 2004. Linear Models and Empirical Bayes Methods for Accessing Differential Expression in Microarray Expreiment. *Stat Appl Genet Mol Biol*.

Stary HC, Blankenhorn DH, Chandler AB, Glagov S, Insull W, Jr., Richardson M, Rosenfeld ME, Schaffer SA, Schwartz CJ, Wagner WD et al. 1992. A definition of the intima of human arteries and of its atherosclerosis-prone regions. A report from the Committee on Vascular Lesions of the Council on Arteriosclerosis, American Heart Association. *Circulation* **85**(1): 391-405.

Storey JD. 2002. A direct approach to false discovery rates. *Journal of the Royal Statistical Society: Series B (Statistical Methodology)* **64**(3): 479-498.

Subramanian A, Tamayo P, Mootha VK, Mukherjee S, Ebert BL, Gillette MA, Paulovich A, Pomeroy SL, Golub TR, Lander ES et al. 2005. Gene set enrichment analysis: A knowledge-based approach for interpreting genome-wide expression profiles. *Proceedings of the National Academy of Sciences of the United States of America* **102**(43): 15545-15550.

Tarin D, Thompson EW, Newgreen DF. 2005. The fallacy of epithelial mesenchymal transition in neoplasia. *Cancer Res* **65**(14): 5996-6000; discussion 6000-5991.

Thomson S, Buck E, Petti F, Griffin G, Brown E, Ramnarine N, Iwata KK, Gibson N, Haley JD. 2005. Epithelial to mesenchymal transition is a determinant of sensitivity of non-small-cell lung carcinoma cell lines and xenografts to epidermal growth factor receptor inhibition. *Cancer Res* **65**(20): 9455-9462.

Tusher VG, Tibshirani R, Chu G. 2001. Significance analysis of microarrays applied to the ionizing radiation response. *Proc Natl Acad Sci U S A* **98**(9): 5116-5121.

Uramoto H, Iwata T, Onitsuka T, Shimokawa H, Hanagiri T, Oyama T. 2010. Epithelial-mesenchymal transition in EGFR-TKI acquired resistant lung adenocarcinoma. *Anticancer Res* **30**(7): 2513-2517.

Vainio S, Lin Y. 2002. Coordinating early kidney development: lessons from gene targeting. *Nat Rev Genet* **3**(7): 533-543.

van 't Veer LJ, Dai H, van de Vijver MJ, He YD, Hart AAM, Mao M, Peterse HL, van der Kooy K, Marton MJ, Witteveen AT et al. 2002. Gene expression profiling predicts clinical outcome of breast cancer. *Nature* **415**(6871): 530-536.

Veatch AL, Carson LF, Ramakrishnan S. 1994. Differential expression of the cell-cell adhesion molecule E-cadherin in ascites and solid human ovarian tumor cells. *International Journal of Cancer* **58**(3): 393-399.

Weller JI, Song JZ, Heyen DW, Lewin HA, Ron M. 1998. A New Approach to the Problem of Multiple Comparisons in the Genetic Dissection of Complex Traits. *Genetics* **150**(4): 1699-1706.

Wexler L, Brundage B, Crouse J, Detrano R, Fuster V, Maddahi J, Rumberger J, Stanford W, White R, Taubert K et al. 1996. Coronary Artery Calcification: Pathophysiology, Epidemiology, Imaging Methods, and Clinical Implications. *Circulation* **94**(5): 1175-1192.

Wolf K, Mazo I, Leung H, Engelke K, von Andrian UH, Deryugina EI, Strongin AY, Brocker EB, Friedl P. 2003. Compensation mechanism in tumor cell migration: mesenchymal-amoeboid transition after blocking of pericellular proteolysis. *J Cell Biol* **160**(2): 267-277.

Wong AS, Leung PC. 2007. Role of endocrine and growth factors on the ovarian surface epithelium. *J Obstet Gynaecol Res* **33**(1): 3-16.

Xie M, Zhang L, He CS, Xu F, Liu JL, Hu ZH, Zhao LP, Tian Y. 2012. Activation of Notch-1 enhances epithelial-mesenchymal transition in gefitinib-acquired resistant lung cancer cells. *J Cell Biochem* **113**(5): 1501-1513.

Yang J, Mani SA, Donaher JL, Ramaswamy S, Itzykson RA, Come C, Savagner P, Gitelman I, Richardson A, Weinberg RA. 2004. Twist, a Master Regulator of Morphogenesis, Plays an Essential Role in Tumor Metastasis. *Cell* **117**(7): 927-939.

Yang J, Weinberg RA. 2008. Epithelial-mesenchymal transition: at the crossroads of development and tumor metastasis. *Dev Cell* **14**(6): 818-829.

Zhang S, Cao J. 2009. A close examination of double filtering with fold change and t test in microarray analysis. *BMC Bioinformatics* **10**(1): 402.

CHAPTER 2

IMPROVING FRAMINGHAM RISK SCORE ESTIMATION OF CORONARY CALCIFICATION AND CAROTID INTIMA-MEDIAL THICKNESS IN FIREFIGHTERS

2.1 Introduction

Cardiovascular disease (CVD) is the largest cause (45%) of on-duty firefighter fatalities, accounting for a larger fraction of deaths than by burns, asphyxiation, or other injuries (TriData Corporation 2002; Fahy 2005). Most of these CVD fatalities were caused by coronary heart disease (CHD), of which 32% occurred during fire suppression and 31% occurred during alarm response or return (Kales et al. 2007). In other public service sectors such as police work and emergency medical services, on-duty CHD deaths only account for 22% and 11% of deaths, respectively (Kales et al. 2003; Fahy 2005). In addition to the standard risk factors for CHD, firefighters are also subject to less common cardiovascular stressors such as shift work, smoke exposure, acute and irregular cardiovascular strain, heat, dehydration, and excess physical workload (Soteriades et al. 2011). The impact of CHD on firefighting readiness and emergency resources can be appreciated when we add the estimated 17 non-fatal, line-of-duty CHD events that also occur for each CHD death (Karter and

Molis 2006). Monitoring and management of firefighter cardiac health is important for both individual health and public safety.

A number of mathematical functions using traditional risk factors as variables have been written to predict coronary heart disease risk (Beswick and Brindle 2006). From both a personal health and public policy point of view, we are interested in the degree to which such functions correspond and predict coronary heart disease risk in firefighters. One of the most commonly used risk scoring methods is based on the data from the Framingham Heart Study cohort, based on an original cohort of 5,209 adults from Framingham, Massachusetts as well as their children, spouses, and grandchildren, known as the Framingham Risk Score (FRS) (Anderson et al. 1991a; Anderson et al. 1991b; Wilson et al. 1998). The updated FRS, endorsed by the National Cholesterol Education Program Adult Treatment Panel III and used by clinicians, takes into account age, total cholesterol, smoking status, high density lipoprotein fraction, and systolic blood pressure to estimate 10 year "hard" CHD (myocardial infarction or coronary heart disease death) risk (National Cholesterol Education Program Expert Panel 2002). Some of the limitations of the FRS include its emphasis on older patients, an influence from its original cohort make-up; its homogeneous white middle-class demography; and 10-year risk quantification that fails to account for lifetime risk, particularly in younger patients (Akosah et al. 2003; Hemann et al. 2007). Younger individuals (men <55 and women <65 years of age) with low- or medium-risk FRS scores, but early onset CHD are often misclassified as not meeting the criteria for pharmacotherapy (Akosah et al. 2003).

As a result, there is an interest in non-invasive diagnostic tools that can improve risk assessment using well-quantified measures of CHD. Coronary artery calcification (CAC) is a marker of atherosclerosis that can be quantified using electron beam computed tomography and multi-detector computed tomography, and may help to assess the extent of subclinical atherosclerosis (Greenland et al. 2007). Tissue and ultrasound studies have confirmed a direct relationship between atherosclerotic plaque burden and the quantity of CAC (Baumgart et al. 1997; Mintz et al. 1997). Also in prospective studies where follow-up was performed, the amount of CAC has been shown in a number of studies to predict cardiac events in asymptomatic individuals 3-5 years later (Wayhs et al. 2002; Raggi et al. 2003; Shaw et al. 2003). Carotid intima-media thickness (CIMT), measured by B-mode ultrasound, has also been used as an assessment for the presence of coronary atherosclerosis and an independent predictor of future cardiovascular events (Naghavi et al. 2006). Again in prospective studies asymptomatic individuals with abnormal CIMT were shown to have increased risk of myocardial infarctions and stroke 4 to 7 years later, with a direct correspondence between degree of thickness and risk of coronary event (Chambless et al. 1997; Hodis et al. 1998; O'Leary et al. 1999b).

In our study, we were interested in assessing the utility of the Framingham Risk Score in evaluating the atherosclerotic risk in asymptomatic firefighters. To this end we determined FRS for 159 male firefighters from Gwinnett County, Georgia, and compared their risk categorization against their known atherosclerotic burden as determined by CIMT and CAC. While the 20% FRS threshold,

corresponding to medium risk, had a high specificity for both CAC and CIMT, it also had a low sensitivity (17% and 40%, respectively), indicating that a large percentage of individuals with clinically significant atherosclerosis are being misclassified. By adjusting the FRS threshold downward, we were able to raise the sensitivity greatly with only a modest loss of specificity. We also proposed the use of a smoking adjustment as a proxy for firefighter exposure to combustion products.

2.2 Methods

The Firefighter Heart Disease Prevention (FHDP) study was designed as a cross-sectional investigation of subclinical atherosclerosis as defined by noninvasive imaging, and multiple phenotypes and genotypes previously established to be associated with increased cardiovascular risk. Following recruitment and informed consent, firefighters completed a series of questionnaires that address standard demographic, nutrition, exercise, lifestyle, and family history variables. Standard physiologic measurements were obtained including, resting 12-lead electrocardiogram (ECG), blood pressure, ankle-brachial index (ABI), height/weight, and waist-to-hip measurements.

One hundred and fifty-nine active duty firefighters older than 40 years were recruited from the Gwinnett County Fire Department that serves a population of approximately 800,000 individuals. The study was approved by the Institutional Review Boards of Saint Joseph's Hospital and Georgia Institute of Technology.

2.2.1 Blood pressure measurement

Following five minutes of rest in the sitting position, blood pressure was determined in the right arm following American Heart Association criteria (Pickering et al. 2005). Three measurements were made one minute apart. Heart rate and blood pressure were obtained prior to blood draw.

2.2.2 Coronary artery calcium scoring

Calcium scoring computed tomographic images were performed on a 64-slice multi-detector computed-tomography scanner (MDCT) (Somatom Sensation 64, Siemens, Forchhcim, Germany). The scan parameters were tube voltage 110 kY, tube current 250 mAs effective, collimation 64 x 0.6 mm, and rotation time 330 ms. Image acquisition was triggered to 60% to 80% timing interval after the Q, R, and S wave (QRS) complex during diastole throughout a breath hold by the patient (Taylor et al. 2004). A standard calcium-scoring kernel (B35f) was used for reconstruction of the MDCT-data. An experienced reader scored the images. Images were retrospectively reconstructed with a slice thickness of 3.0 mm and scoring of the common carotid, carotid bulb, and internal carotid artery vessels was performed. The total number of calcified lesions in the coronary anatomy was documented and the total Agatston score was calculated for all calcified lesions. Percentile rank score was based on the age and sex of the patient as described previously (Agatston et al. 1990).

2.2.3 Carotid Arterial Wall Imaging

Carotid intima media thickness measurements were performed on an ultrasound machine equipped with software that has been demonstrated to accurately measure

carotid plaque thickness (Toshiba Xario Ultrasound, Tokyo, Japan) (O'Leary et al. 1999a; Tanaka et al. 2001). The machine was equipped with a high resolution 7.5 MHz linear array transducer. Scanning was performed of the common carotid, carotid bulb, and internal carotid arteries. Five measurements of the carotid-intimal medial thickness were recorded of each vessel utilizing a method for the determination of the intimal-medial thickness that has been previously described (Pignoli et al. 1986). The measurements in each vessel were performed as follows: two within the common carotid artery, two within the internal carotid artery, and one within the carotid bulb. One measurement in each common and internal carotid artery was recorded within the relatively straight portion of each vessel at the area of greatest intimal-medial thickness. One measurement within each common and internal carotid artery was recorded at 1-cm interval from the carotid bulb. All recordings were performed in the far wall of the vessel using the same depth for each measurement.

2.2.4 Laboratory Tests

Blood samples were obtained following a 16-hour fast. Plasma was prepared from blood within 30 minutes and blood and plasma were all kept at 4°C. Plasma lipid and lipoprotein cholesterol concentrations were determined by the methods of the Lipid Research Clinics (Office USGP 1982). Triglyceride, total cholesterol, and lipoprotein cholesterol values were measured by enzymatic procedures. High-density lipoprotein (HDL) cholesterol was determined by the dextran sulfate-magnesium precipitation procedure (Thompson and Roy 1981). Low-density

lipoprotein cholesterol was calculated from the following equation: Low density lipoprotein (LDL) cholesterol = total cholesterol - [HDL cholesterol + (triglycerides/5)] (Wagner et al. 2000).

2.2.5 Coronary calcium and carotid intima-media thickness thresholds

Based on prior studies, the American College of Cardiology Foundation (ACCF) has classified patients without detectable coronary calcification (CAC score = 0) as low risk, having a very low rate of CHD death or MI three to five years later (Greenland et al. 2007). Those patients with any measurable calcium were determined to have a relative risk ratio of 4.3 (95% confidence interval = 3.5 to 5.2) compared to the zero calcium patient group, from the ACCF meta-analysis. The Screening for Heart Attack Prevention and Education Task Force classifies individuals with CIMT greater than or equal to 1 mm as high risk and having a positive result for subclinical atherosclerosis (Naghavi et al. 2006). We follow these conclusions when classifying risks based on calcium scores and carotid intima media thickness.

2.2.6 Framingham Risk Score standards

The Third Report of the National Cholesterol Education Program Expert Panel on Detection, Evaluation, and Treatment of High Blood Cholesterol in Adults (National Cholesterol Education Program Expert Panel 2002) recommends the use of the Framingham Risk scoring to assess 10 year risk for coronary heart disease in individuals who otherwise do not have coronary artery disease (CHD) or other clinical atherosclerotic diseases. Age, total cholesterol, HDL cholesterol, systolic

blood pressure, treatment for hypertension, and cigarette smoking are included in the Framingham calculation of 10-year risk. The primary endpoint in the 10-year risk assessment is myocardial infarction or coronary heart disease death. Although the Framingham risk assessment also has been used to estimate total CHD at the rate of about two-thirds to three-fourths of hard CHD, ATP III does not recommend this use. The risk probabilities are divided into three categories. Low risk is described as less than 10% risk by Framingham scoring (FRS). Medium risk is 10 to 20%, while high risk (CHD risk equivalent) is greater than 20% by FRS.

2.3 Results

2.3.1 Baseline characteristics

Our study sample consisted of 159 male firefighters (mean age 46.5 years) (Table 2.1) not on any medications and without known coronary artery disease (CAD). Each participant underwent clinical and serological risk factor screening, MDCT, and CIMT. One of our primary interests is how well coronary artery calcium scoring (CAC) by MDCT and carotid-intimal media thickness by ultrasound imaging aligns with traditional CAD risk factors. We asked if average risk factor values were significantly different between groups as defined by well-accepted thresholds for CAC and CIMT determined by Student's t-test. When comparing individuals with no detectable coronary calcification (CAC=0) with individuals with measurable calcification (CAC >0), there were significant differences in ages, diastolic blood pressure, and systolic blood pressure (p-value = 0.0028 0.0084, 0.0045, respectively) (Table 2.2). Total cholesterol, high-density lipoprotein, and low-

Table 2.1. *Characteristics (means) of the sampled firefighter population (n=159)*

Age (years)	46.55	± 5.08
Systolic blood pressure (mm Hg)	124.13	± 11.1
Diastolic blood pressure (mm Hg)	78.18	± 8
Total cholesterol (mg/dL)	203.68	± 34.82
HDL cholesterol (mg/dL)	48.38	± 13.78
LDL cholesterol (mg/dL)	134.27	± 31.79
Framingham Risk Score (10 yr):		
Low		128
Med		22
High		9

Table 2.2. *Comparison of common characteristics between firefighters at different risk levels as determined by CAC*

	CAC		
	Positive (CAC>0)	Negative (CAC = 0)	T-test p-value
N	37	122	
Age (yrs)	48.7 +/- 5.6	45.9 +/- 4.7	**0.0027**
Diastolic BP avg (mm Hg)	81.2 +/- 8.9	77.27 +/- 7.5	**0.0084**
Systolic BP avg (mm Hg)	128.6 +/- 13.6	122/7 +/- 9.9	**0.0045**
Total cholesterol (mg/dL)	209.4 +/- 40.7	201.9 +/- 32.9	0.2545
High-density lipoprotein cholesterol (mg/dL)	49.8 +/- 16.8	47.9 +/- 12.8	0.4836
Low-density lipoprotein cholesterol (mg/dL)	139.9 +/- 39.0	132.6 +/- 29.2	0.2211

Table 2.3. *Comparison of common characteristics between firefighters at different risk levels as determined by CIMT*

	CIMT		
	Positive	Negative	T-test
	(CIMT >0.9mm)	(CIMT < 0.9 mm)	p-Value
N	15	144	
Age (yrs)	53.21 +/- 5.59	45.91 +/- 4.58	**1.013E-07**
Diastolic BP avg (mm Hg)	82.71 +/- 8.21	77.74 +/- 7.9	**0.0267**
Systolic BP avg (mm Hg)	133.47 +/- 14.36	123.22 +/- 10.40	**0.00087**
Total cholesterol (mg/dL)	213.57 +/- 31.15	202.73 +/- 35.22	0.2688
High-density lipoprotein cholesterol (mg/dL)	46.78 +/- 12.82	48.53 +/- 13.95	0.6521
Low-density lipoprotein cholesterol (mg/dL)	148 +/- 32.14	132.95 +/- 31.55	0.0908

density lipoproteins levels did not differ significantly between these two groups. The same pattern was also true when comparing individuals with carotid intima-media thicknesses (CIMT) greater than 0.9 mm and those whose CIMTs were less than 0.9 mm, where there were significant differences in ages, diastolic blood pressure, and systolic blood pressure (p-value = $1x10^{-7}$, 0.026, 0.00087, respectively) (Table 2.3). In order to set a new FRS threshold and then test its utility, we randomly split our 159-person population into a training group of 106 individuals and a testing group of 53 individuals that will be used for threshold validation. Given our sample size larger than 100, a 1/3rds to 2/3rds split has been previously determined to retain both high classification and testing accuracy in high dimensional data sets (Dobbin and Simon 2011).

2.3.2 Standard FRS thresholds fail to recognize existing atherosclerosis

To first analyze the utility of the Framingham Risk Score we asked if its risk categories were well correlated with our measures of actual atherosclerotic burden using CAC and CIMT. For the training group, we calculated Framingham Risk Scores (FRS), using their risk factor and medical history data. We then split these scores by Framingham risk categories: high (> 20% risk of a major adverse coronary event within 10 years), medium (10-20% risk), and low (<10% risk). Out of 106 individuals, 85 have FRS below 10%, 17 have FRS between 10% and 20%, and 4 have FRS above 20%. Out of the 85 with FRS below 10%, 16 were positive for coronary calcification and two were positive by CIMT (as well as CAC) (Figures 2.1 and 2.2). Out of the 17 with FRS between 10 and 20%, three were positive for

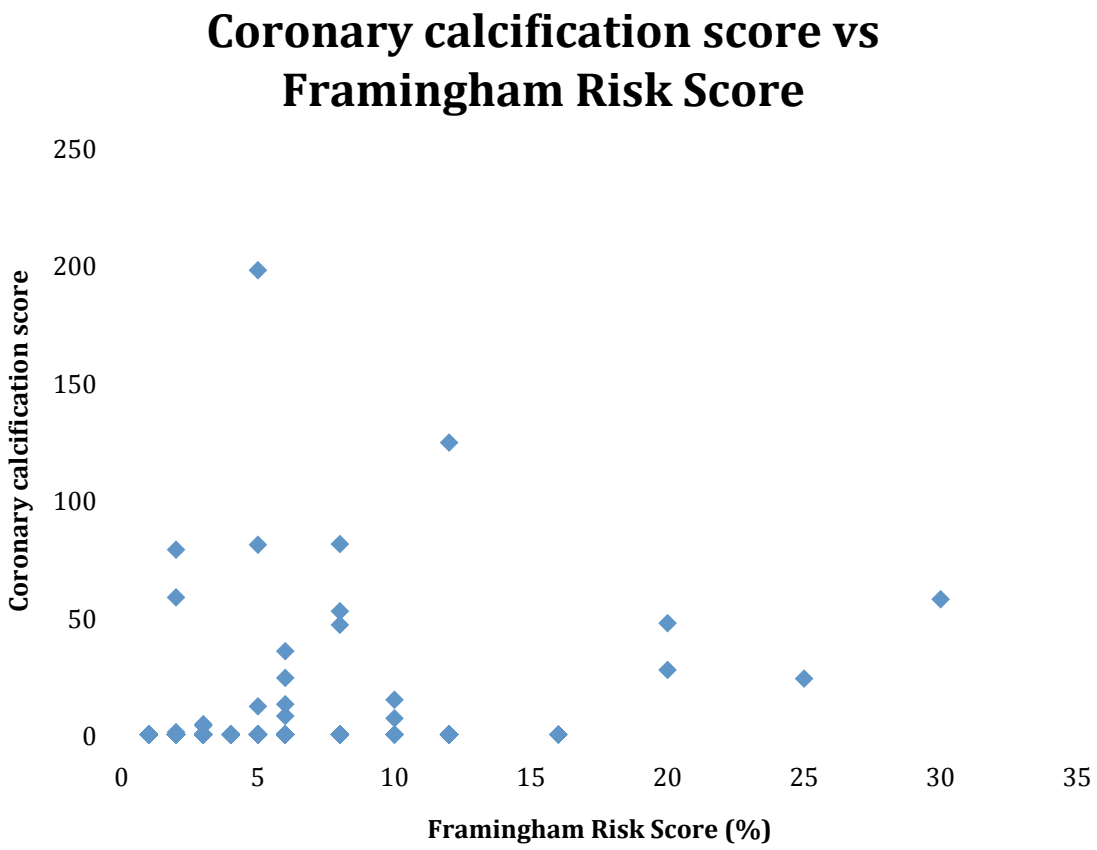

Figure 2.1. *Coronary artery calcification vs Framingham Risk Score*
Coronary artery calcification scores (CAC) above zero are classified as clinically significant for atherosclerosis. The majority of atherosclerosis positive individuals as determined by CAC, particularly those with high scores, are also classified as having low or moderate risk by Framingham Risk Score. The Pearson correlation between the two measures is relatively weak (r=0.3184629, p-value=0.000878).

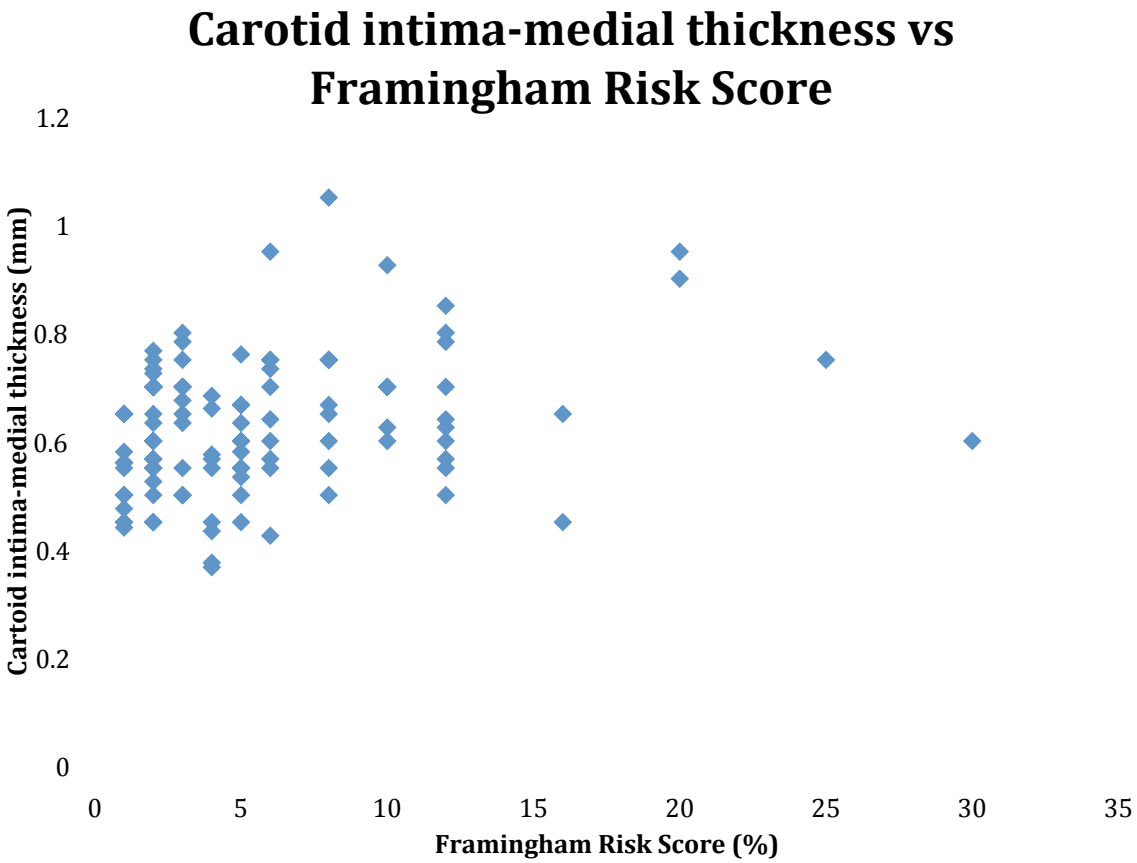

Figure 2.2. *Carotid intima-media thickness vs Framingham Risk Score*
Carotid intima-media thicknesses (CIMT) above 0.9 mm are classified as clinically significant for atherosclerosis. Again, the majority of atherosclerosis positive individuals as determined by CIMT are also classified as having low or moderate risk by Framingham Risk Score. The Pearson correlation between the two measures is relatively weak (r=0.3395805, p-value = 0.0003692).

coronary calcification and one was positive by CIMT (but not by CAC). Of the four individuals in the high risk FRS group, all were positive for coronary calcification and two were positive by CIMT.

Nineteen out of 23 of the sampled individuals with clinically significant coronary calcification that indicates the presence of atherosclerosis are classified as low or medium risk by FRS. At the 20% FRS threshold, FRS has 100% specificity for significant coronary calcium, but only 17% sensitivity (Table 2.4). Likewise for significant carotid intima-media thickness at the 20% FRS threshold, FRS has 98% specificity, and only 40% sensitivity (Table 2.5). Even at a more conservative 10% FRS threshold, FRS has 83% specificity for significant coronary calcium, and 30% sensitivity. And a 10% FRS threshold has 82% specificity for significant carotid intima-media thickness, and 60% sensitivity. This low sensitivity represents a large number of affected individuals who would appear as low risk by Framingham Risk Score.

2.3.3 Optimizing FRS thresholds for specificity and sensitivity

Because of the high cost of misclassifying affected individuals as low risk, we sought to find a new optimal FRS threshold that provided a better balance between specificity and sensitivity. Using a receiver-operator characteristic (ROC) curve, we determined new FRS thresholds for capturing significant coronary calcification (Figure 2.3) or carotid intima-media thickness (Figure 2.4). The ROC curve provides an intuitive path for optimizing specificity and sensitivity. For coronary calcification, this optimized FRS threshold is 6% risk, while for CIMT the optimized

Table 2.4. *Low sensitivity for CAC at traditional FRS thresholds*

	FRS	
CAC	Positive (high)	Negative (low-med)
Positive (>0)	4	19
Negative (=0)	0	83
	Specificity	1.00
	Sensitivity	0.17

Table 2.5. *Low sensitivity for CIMT at traditional FRS thresholds*

	FRS	
CIMT	Positive (high)	Negative (low-med)
Positive (>0.9mm)	2	3
Negative (<0.9mm)	2	99
	Specificity	0.98
	Sensitivity	0.40

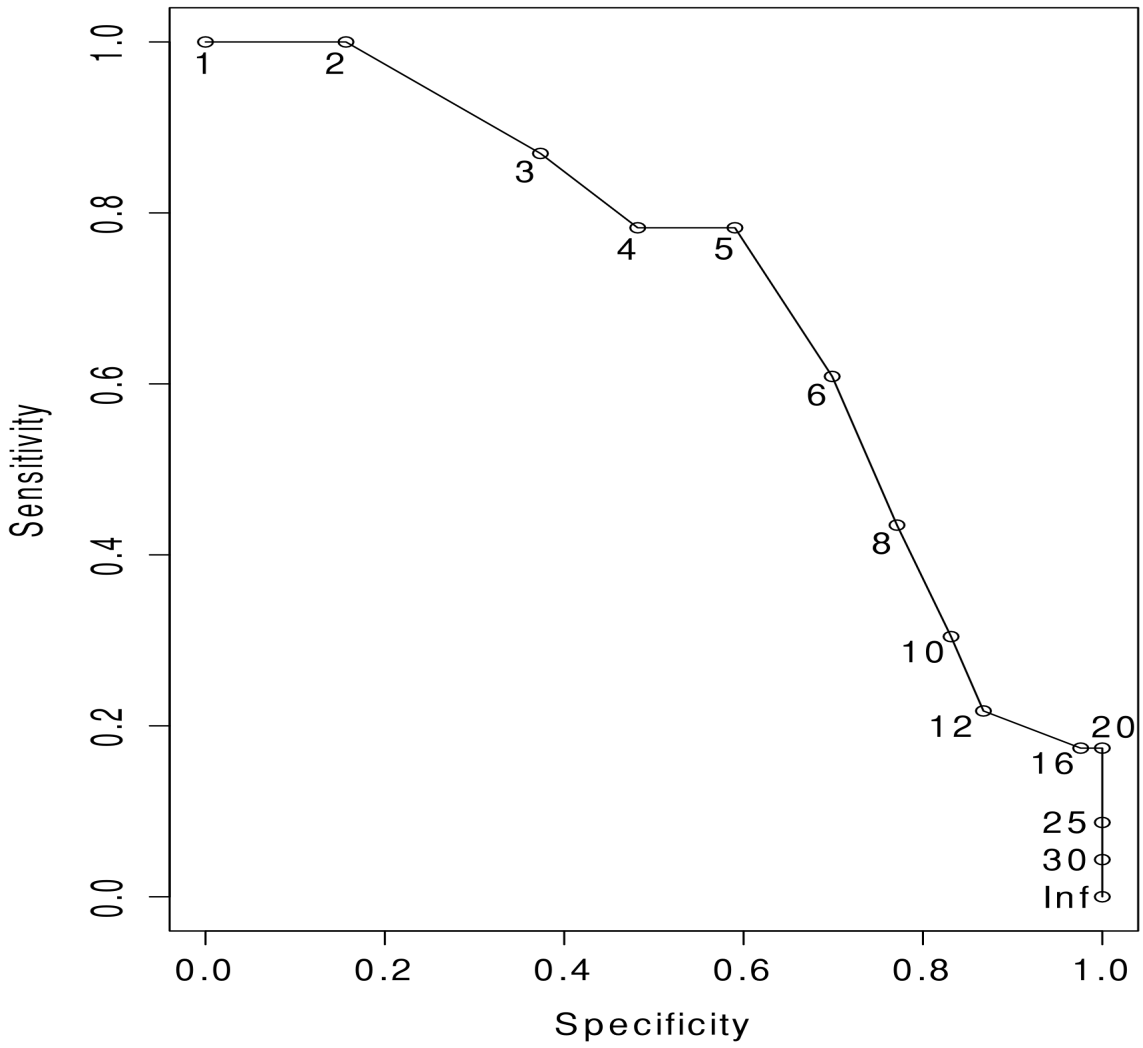

Figure 2.3. *Receiver-operator characteristic curve for Framingham Risk Score in predicting coronary artery calcification status*
The receiver-operator characteristic curve (ROC) plots specificities and sensitivities of all possible threshold percentage values of the Framingham Risk Scores (FRS) when calling coronary calcification status. Here positive calcification status is defined as any score above zero. The numbered points represent FRS thresholds above which significant risk of major adverse coronary events would be predicted.

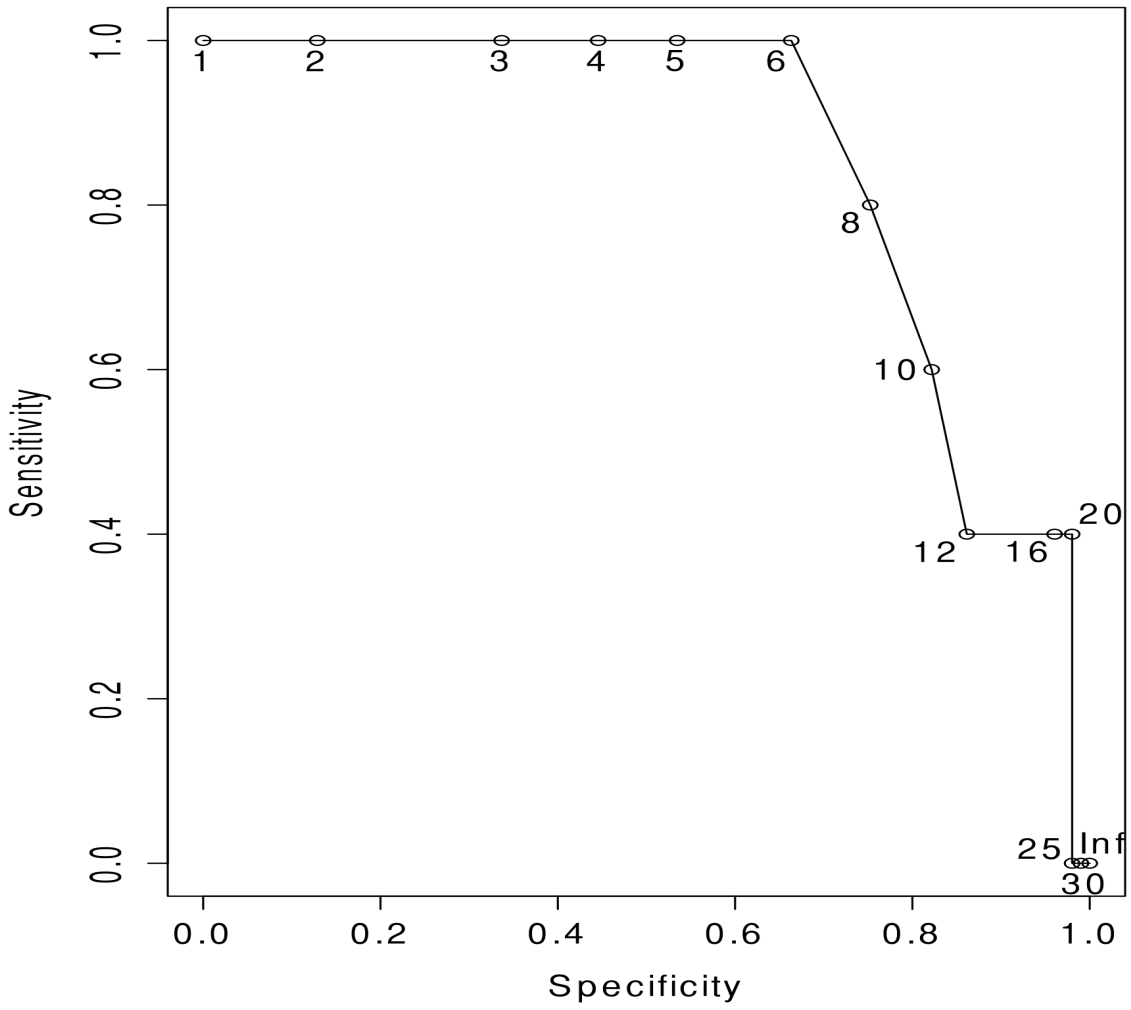

Figure 2.4. *Receiver-operator characteristic curve for Framingham Risk Score in predicting carotid intima-media thickness status*
The receiver-operator characteristic curve (ROC) plots specificities and sensitivities of all possible threshold values of the Framingham Risk Scores (FRS) when calling carotid intima-medial thickness status. Here a CIMT status associated with clinically significant atheroslerosis is defined as any score above 0.9 mm. The numbered points represent FRS thresholds above which significant risk of major adverse coronary events would be predicted.

threshold is 8% risk. Both are lower than the current ATP III 10% threshold for designating low risk.

2.3.4 Testing optimized FRS thresholds reveals improved sensitivity

To test the performance of these new thresholds, we applied them to a test population of 53 firefighters with similar characteristics and known CAC and CIMT status and calculate specificity and sensitivity measures for each. At the 6% FRS threshold for coronary calcium, specificity decreases to 74%, while sensitivity increases to 50% (Table 2.6). Using the 8% FRS threshold for CIMT, specificity decreases to 91%, while sensitivity increases to 67% (Table 2.7). These new lowered thresholds improve the sensitivity of the FRS calculation at a modest cost to specificity.

2.3.5 Treating firefighters as smokers

The ATP III guidelines recently quantified additional CHD risk from smoking as a sliding scale by subject age (Table 2.8), where points are added based on the subject's age group. Fewer points are added at increased ages to account for exposure over time. To account for chronic firefighter exposure to toxins and particles generated by ignition at firefighting incidents, we examined the effects of treating all firefighters as smokers for the purposes of the FRS calculation, regardless of their actual smoking status. Following this recalculation, we determined the specificity and sensitivity of the traditional 20% FRS thresholds for CAC and CIMT using our training group. For CAC, the FRS threshold had a specificity

Table 2.6. *Improved FRS correspondence to CAC at 6% risk threshold*

	FRS	
CAC	Positive (>6%)	Negative (<=6%)
Positive (>0)	7	7
Negative (=0)	10	29
	Specificity	0.74
	Sensitivity	0.50

Table 2.7. *Improved FRS correspondence to CIMT at 8% risk threshold*

	FRS	
CIMT	Positive (>8%)	Negative (<=8%)
Positive (>0.9mm)	6	3
Negative (<0.9mm)	4	40
	Specificity	0.91
	Sensitivity	0.67

Table 2.8. *FRS smoking adjustment*

	Points				
	Age 20-39	Age 40-49	Age 50-59	Age 60-69	Age 70-79
Nonsmoker	0	0	0	0	0
Smoker	8	5	3	1	1

Table 2.9. *Changes in traditional FRS threshold correspondence with CAC with smoking adjustment*

	FRS with smoking adjustment	
CAC	Positive (high)	Negative (low-med)
Positive (>0)	6	17
Negative (=0)	6	77
	Specificity	0.93
	Sensitivity	0.26

Table 2.10. *Changes in traditional FRS threshold correspondence with CIMT with smoking adjustment*

	FRS with smoking adjustment	
CIMT	Positive (high)	Negative (low-med)
Positive (>0.9mm)	5	0
Negative (<0.9mm)	7	94
	Specificity	0.93
	Sensitivity	1.00

of 93%, and a sensitivity of 26% (Table 2.9). While for CIMT, the FRS threshold had a specificity of 93% and a sensitivity of 100% (Table 2.10).

We also generated ROC curves for FRS thresholds for coronary calcification and CIMT including this smoking adjustment (Figures 2.5 and 2.6). These ROC curves yielded an optimized FRS threshold for significant coronary calcium of 12% and an optimized FRS threshold of 20% for CIMT. We again tested the performance of these new thresholds by applying them to our test population of 53 firefighters. The new FRS threshold for significant coronary calcium of 12% yielded a specificity of 51% and sensitivity of 43% (Table 2.11). For CIMT, the FRS threshold of 20% yielded a specificity of 88% and sensitivity of 75% (Table 2.12).

2.4 Discussion

The standard threshold (positive FRS > 20%) assigns a large proportion of firefighters with existing atherosclerosis into low and medium risk categories (Table 2.1 – 2.3). Although the Framingham Risk assessment was designed to measure the probability of future myocardial infarction and death from coronary artery disease, the presence of current significant coronary calcification or carotid intima-media thickening would suggest that these individuals are in fact already at high risk for coronary artery disease. Indeed, coronary calcification is an indicator of subclinical atherosclerosis and when combined with risk factors can be considered a CHD risk equivalent (National Cholesterol Education Program Expert Panel 2002). CIMT also is a predictor of future cardiovascular events and has been used in many

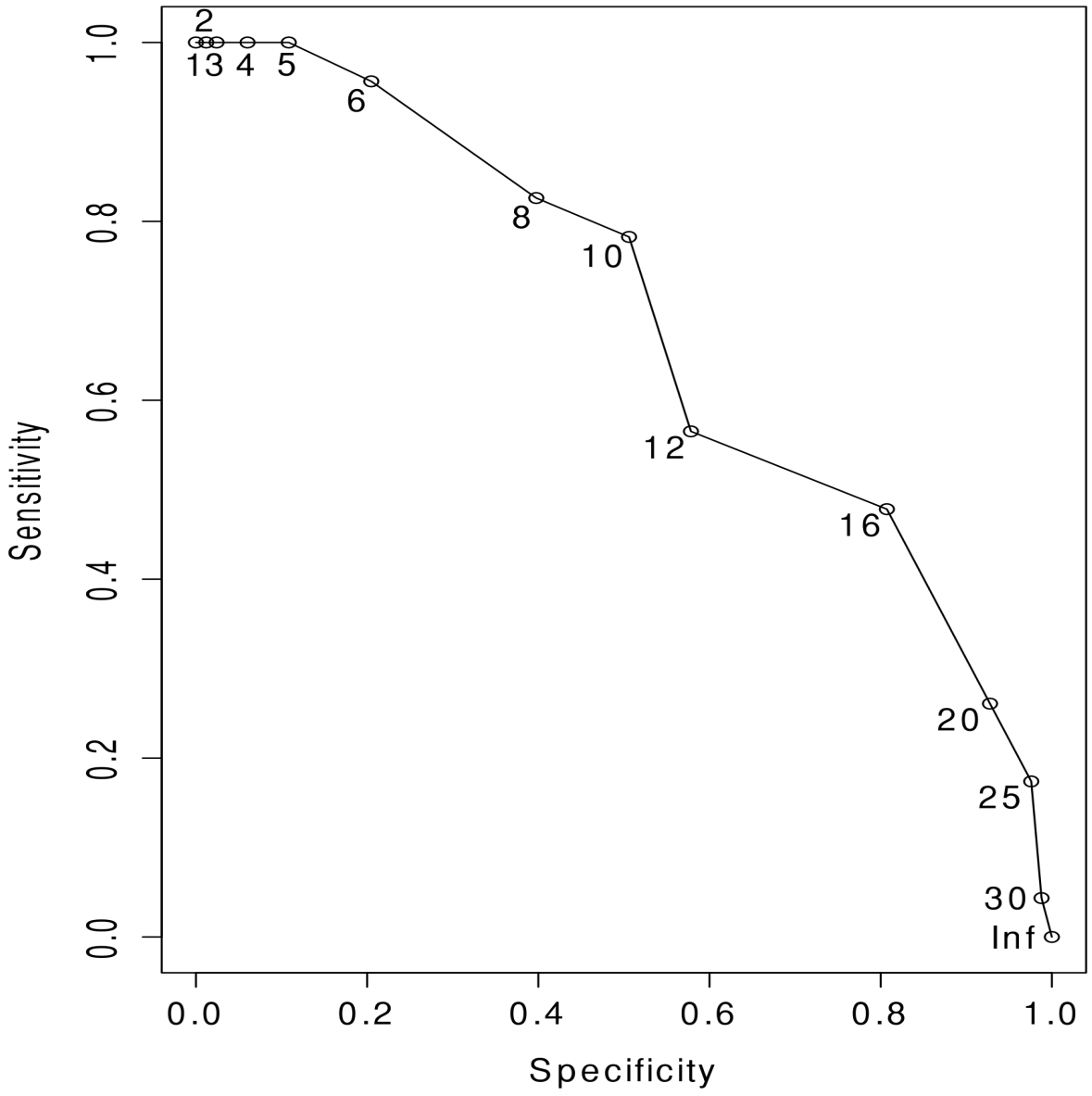

Figure 2.5. *Receiver-operator characteristic curve for Framingham Risk Score prediction of coronary calcification with smoking adjustment.*
The receiver-operator characteristic curve (ROC) plots specificities and sensitivities of all possible threshold values of the Framingham Risk Scores (FRS) when calling coronary calcification status. Here positive calcification status is defined as any score above zero. The numbered points represent FRS thresholds above which significant risk of major adverse coronary events would be predicted when the smoking adjustment is applied to this score regardless of the individual firefighter's actual smoking status.

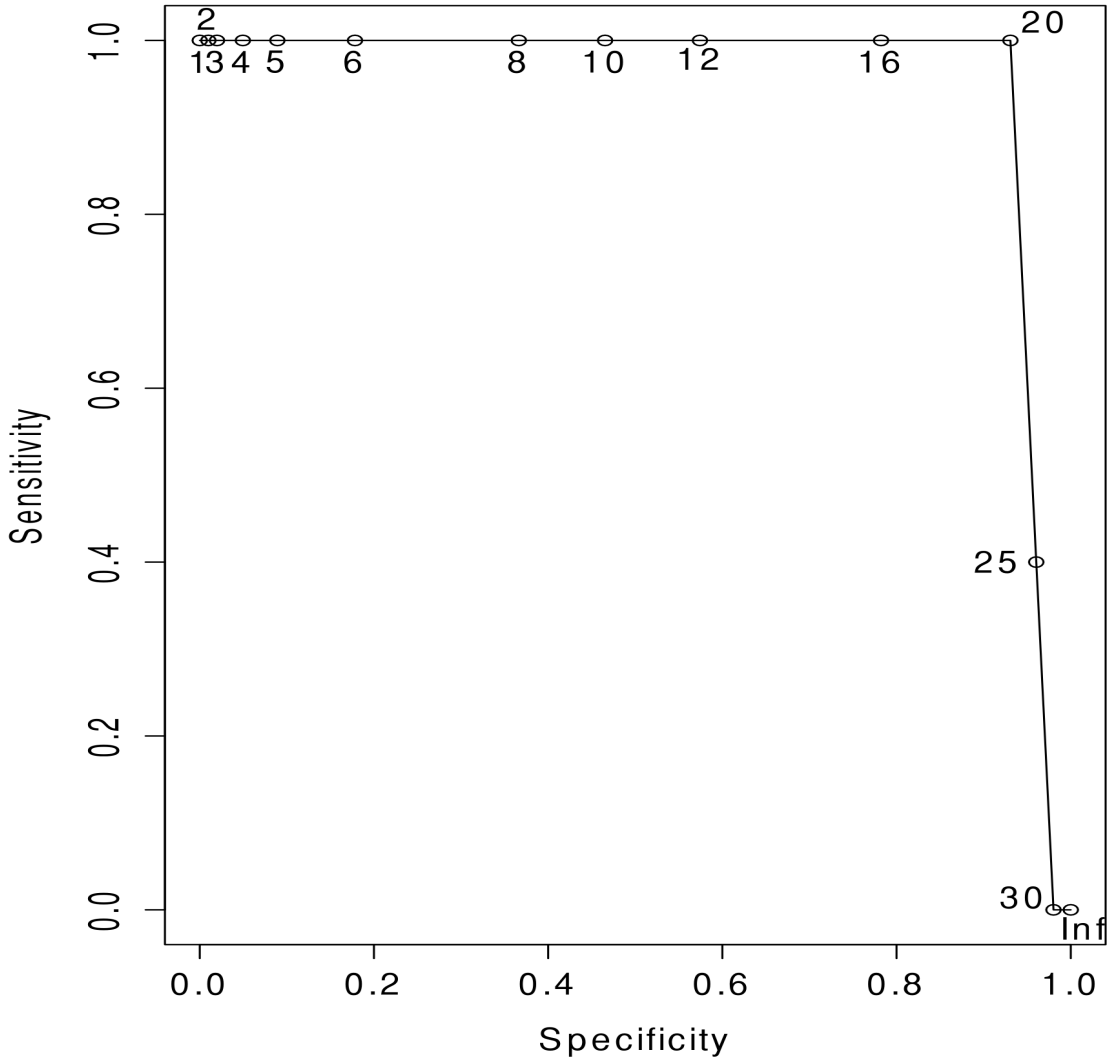

Figure 2.6. *Receiver-operator characteristic curve for Framingham Risk Score prediction of carotid intima-medial thickness with smoking adjustment*
The receiver-operator characteristic curve (ROC) plots specificities and sensitivities of all possible threshold values of the Framingham Risk Scores (FRS) when calling carotid intima-medial thickness status. Here a CIMT status associated with clinically significant atheroslerosis is defined as any score above 0.9 mm. The numbered points represent FRS thresholds above which significant risk of major adverse coronary events would be predicted. when the smoking adjustment is applied to this score regardless of the individual firefighter's actual smoking status.

Table 2.11. *Changes in FRS correspondence with CAC with smoking adjustment at 12% threshold*

	FRS with smoking adjustment	
CAC	Positive (>12%)	Negative (<=12%)
Positive (>0)	6	8
Negative (=0)	19	20
	Specificity	0.51
	Sensitivity	0.43

Table 2.12. *Changes in FRS correspondence with CIMT with smoking adjustment at 20% threshold*

	FRS with smoking adjustment	
CIMT	Positive (>20%)	Negative (<=20%)
Positive (>0.9mm)	3	1
Negative (<0.9mm)	6	43
	Specificity	0.88
	Sensitivity	0.75

other studies as a surrogate end point (Salonen and Salonen 1993; Belcaro et al. 1996; Bots et al. 1997; Chambless et al. 1997; O'Leary et al. 1999a).

In order to correct the shortcomings of applying the standard FRS thresholds to firefighters, we used receiver-operator characteristic curves to determine new thresholds that would improve the sensitivity while maintaining the high degree of specificity held by the existing threshold. This resulted in lower thresholds, 6% for CAC and 8% for CIMT, for predicting CAD. We were able to generate substantial gains in sensitivity (17% improved to 50% for CAC, and 40% improved to 67% for CIMT) with a modest loss of specificity (100% to 74% for CAC, and 98% to 91% for CIMT). We argue that misdiagnosing affected individuals as healthy is far costlier than misdiagnosing healthy individuals as affected. The Multi-Ethnic Study of Atherosclerosis and the Prospective Army Coronary Calcium Project also found that individuals with low FRS (5.1-20%) also had clinically significant atherosclerosis as determined by CAC, indicating that this pattern is not exclusive to firefighters (Taylor et al. 2010; Okwuosa et al. 2011).

Despite the widespread use of self-contained breathing apparatuses by firefighters during fire suppression activities, this respiratory protection is often removed during the salvage and overhaul duties immediately following (Rosenstock and Olsen 2007). Significant exposure to the products of combustion, including toxic chemicals, such as carbon monoxide, benzene, sulphur dioxide, hydrogen cyanide, acrolein, and fine particulate matter occurs during the overhaul process (Gold et al. 1978; Burgess et al. 2001). Exposure to both toxic chemicals and fine particulate matter has been implicated in the progression of coronary heart disease (Brandt-

Rauf et al. 1988; Baxter et al. 2010). Specifically, long-term exposure to particulate matter may increase the risk of subclinical atherosclerosis through an oxidative stress mechanism due to the high content of redox-cycling chemicals in ultrafine particles (<0.18 μm in diameter) found abundantly in post-suppression air (Araujo and Nel 2009). To account for this exposure over time, we altered the Framingham Risk Score calculation to include all firefighters as smokers. Following the application of ROC curves, we set new thresholds of 12% FRS for CAC and 20% FRS for CIMT. Application of these thresholds to our test group revealed gains in sensitivity for the predictive power of smoking-adjusted FRS for clinically significant CIMT, but a loss in both specificity and sensitivity when it came to CAC.

Our attempts to adjust the thresholds by ROC and smoking correction demonstrate that substantial changes can be made in the sensitivity of traditional testing, though our smoking adjustment improved the correspondence of FRS to CIMT and not CAC. The presence of clinically significant CAC and CIMT at low FRS combined with increased risk of CAD in firefighters even when compared to other first responders suggests that all firefighters should be screened for CAD regardless of their classification by traditional means such as FRS. In this setting, non-invasive tests like CAC and CIMT could compliment FRS in determining the aggressiveness of treatment.

Given our experimental design, it is difficult to accurately contrast coronary health markers in firefighters against those observed in the general population, though it appears that other large scale studies have found clinically significant CAC and CIMT in low-risk FRS categorized individuals as well (Folsom et al. 2008; Lester

et al. 2009; Khalil et al. 2010; Polak et al. 2011). We suggest follow-up studies that examine firefighter and non-firefighter populations in parallel. Moreover, long-term studies that encompass 5 and 10 year follow on surveying for major adverse coronary events would help to affirm our predictions of early signs of risk. Finally long-term studies of toxin and particulate exposure impact on firefighter coronary health are also warranted.

2.5 References

Agatston AS, Janowitz WR, Hildner FJ, Zusmer NR, Viamonte M, Jr., Detrano R. 1990. Quantification of coronary artery calcium using ultrafast computed tomography. *J Am Coll Cardiol* **15**(4): 827-832.

Akosah KO, Schaper A, Cogbill C, Schoenfeld P. 2003. Preventing myocardial infarction in the young adult in the first place: how do the national cholesterol education panel iii guidelines perform? *J Am Coll Cardiol* **41**(9): 1475-1479.

Anderson KM, Odell PM, Wilson PW, Kannel WB. 1991a. Cardiovascular disease risk profiles. *Am Heart J* **121**(1 Pt 2): 293-298.

Anderson KM, Wilson PW, Odell PM, Kannel WB. 1991b. An updated coronary risk profile. A statement for health professionals. *Circulation* **83**(1): 356-362.

Araujo JA, Nel AE. 2009. Particulate matter and atherosclerosis: role of particle size, composition and oxidative stress. *Part Fibre Toxicol* **6**: 24.

Baumgart D, Schmermund A, Goerge G, Haude M, Ge J, Adamzik M, Sehnert C, Altmaier K, Groenemeyer D, Seibel R et al. 1997. Comparison of electron beam computed tomography with intracoronary ultrasound and coronary angiography for detection of coronary atherosclerosis. *J Am Coll Cardiol* **30**(1): 57-64.

Baxter CS, Ross CS, Fabian T, Borgerson JL, Shawon J, Gandhi PD, Dalton JM, Lockey JE. 2010. Ultrafine Particle Exposure During Fire Suppression-Is It an

Important Contributory Factor for Coronary Heart Disease in Firefighters? *Journal of Occupational and Environmental Medicine* **52**(8): 791-796 710.1097/JOM.1090b1013e3181ed1092c1096e.

Belcaro G, Nicolaides AN, Laurora G, Cesarone MR, De Sanctis M, Incandela L, Barsotti A. 1996. Ultrasound Morphology Classification of the Arterial Wall and Cardiovascular Events in a 6-Year Follow-up Study. *Arteriosclerosis, Thrombosis, and Vascular Biology* **16**(7): 851-856.

Beswick A, Brindle P. 2006. Risk scoring in the assessment of cardiovascular risk. *Curr Opin Lipidol* **17**(4): 375-386.

Bots ML, Hoes AW, Koudstaal PJ, Hofman A, Grobbee DE. 1997. Common Carotid Intima-Media Thickness and Risk of Stroke and Myocardial Infarction : The Rotterdam Study. *Circulation* **96**(5): 1432-1437.

Brandt-Rauf PW, Fallon LF, Jr., Tarantini T, Idema C, Andrews L. 1988. Health hazards of fire fighters: exposure assessment. *Br J Ind Med* **45**(9): 606-612.

Burgess JL, Nanson CJ, Bolstad-Johnson DM, Gerkin R, Hysong TA, Lantz RC, Sherrill DL, Crutchfield CD, Quan SF, Bernard AM et al. 2001. Adverse respiratory effects following overhaul in firefighters. *Journal of Occupational and Environmental Medicine* **43**(5): 467-473.

Chambless LE, Heiss G, Folsom AR, Rosamond W, Szklo M, Sharrett AR, Clegg LX. 1997. Association of coronary heart disease incidence with carotid arterial wall thickness and major risk factors: the Atherosclerosis Risk in Communities (ARIC) Study, 1987-1993. *Am J Epidemiol* **146**(6): 483-494.

Dobbin KK, Simon RM. 2011. Optimally splitting cases for training and testing high dimensional classifiers. *BMC medical genomics* **4**: 31.

Fahy RF. 2005. U.S. firefighter fatalities due to sudden cardiac death, 1995–2004., Vol 2012. National Fire Protection Association, Quincy, MA.

Folsom AR, Kronmal RA, Detrano RC, O'Leary DH, Bild DE, Bluemke DA, Budoff MJ, Liu K, Shea S, Szklo M et al. 2008. Coronary artery calcification compared with carotid intima-media thickness in the prediction of cardiovascular

disease incidence: the Multi-Ethnic Study of Atherosclerosis (MESA). *Archives of internal medicine* **168**(12): 1333-1339.

Gold A, Burgess WA, Clougherty EV. 1978. Exposure of firefighters to toxic air contaminants. *Am Ind Hyg Assoc J* **39**(7): 534-539.

Greenland P, Bonow RO, Brundage BH, Budoff MJ, Eisenberg MJ, Grundy SM, Lauer MS, Post WS, Raggi P, Redberg RF et al. 2007. ACCF/AHA 2007 Clinical Expert Consensus Document on Coronary Artery Calcium Scoring By Computed Tomography in Global Cardiovascular Risk Assessment and in Evaluation of Patients With Chest Pain: A Report of the American College of Cardiology Foundation Clinical Expert Consensus Task Force (ACCF/AHA Writing Committee to Update the 2000 Expert Consensus Document on Electron Beam Computed Tomography) Developed in Collaboration With the Society of Atherosclerosis Imaging and Prevention and the Society of Cardiovascular Computed Tomography. *J Am Coll Cardiol* **49**(3): 378-402.

Hemann BA, Bimson WF, Taylor AJ. 2007. The Framingham Risk Score: an appraisal of its benefits and limitations. *The American Heart Hospital Journal* **5**(2): 91-96.

Hodis HN, Mack WJ, LaBree L, Selzer RH, Liu CR, Liu CH, Azen SP. 1998. The role of carotid arterial intima-media thickness in predicting clinical coronary events. *Ann Intern Med* **128**(4): 262-269.

Kales SN, Soteriades ES, Christophi CA, Christiani DC. 2007. Emergency duties and deaths from heart disease among firefighters in the United States. *New England Journal of Medicine* **356**(12): 1207-1215.

Kales SN, Soteriades ES, Christoudias SG, Christiani DC. 2003. Firefighters and on-duty deaths from coronary heart disease: a case control study. *Environ Health* **2**(1): 14.

Karter MJ, Molis JL. 2006. Firefighter Injuries in the United States. National Fire Protection Association, Quincy, MA.

Khalil Y, Mukete B, Durkin MJ, Coccia J, Matsumura ME. 2010. A comparison of assessment of coronary calcium vs carotid intima media thickness for determination of vascular age and adjustment of the Framingham Risk Score. *Prev Cardiol* **13**(3): 117-121.

Lester SJ, Eleid MF, Khandheria BK, Hurst RT. 2009. Carotid intima-media thickness and coronary artery calcium score as indications of subclinical atherosclerosis. *Mayo Clinic proceedings* **84**(3): 229-233.

Mintz GS, Pichard AD, Popma JJ, Kent KM, Satler LF, Bucher TA, Leon MB. 1997. Determinants and correlates of target lesion calcium in coronary artery disease: a clinical, angiographic and intravascular ultrasound study. *J Am Coll Cardiol* **29**(2): 268-274.

Naghavi M, Falk E, Hecht HS, Jamieson MJ, Kaul S, Berman D, Fayad Z, Budoff MJ, Rumberger J, Naqvi TZ et al. 2006. From Vulnerable Plaque to Vulnerable Patient,ÄîPart III: Executive Summary of the Screening for Heart Attack Prevention and Education (SHAPE) Task Force Report. *The American Journal of Cardiology* **98**(2, Supplement 1): 2-15.

National Cholesterol Education Program Expert Panel. 2002. Third Report of the National Cholesterol Education Program (NCEP) Expert Panel on Detection, Evaluation, and Treatment of High Blood Cholesterol in Adults (Adult Treatment Panel III) Final Report. In *Circulation*, Vol 106, p. 3143.

O'Leary DH, Polak JF, Kronmal RA, Manolio TA, Burke GL, Wolfson SK. 1999a. Carotid-Artery Intima and Media Thickness as a Risk Factor for Myocardial Infarction and Stroke in Older Adults. *New England Journal of Medicine* **340**(1): 14-22.

O'Leary DH, Polak JF, Kronmal RA, Manolio TA, Burke GL, Wolfson SK, Jr. 1999b. Carotid-artery intima and media thickness as a risk factor for myocardial infarction and stroke in older adults. Cardiovascular Health Study Collaborative Research Group. *N Engl J Med* **340**(1): 14-22.

Office USGP. 1982. Lipid Research Manual of Laboratory Operations: Lipid and Lipoprotein Analysis. Vol 1, Washington DC.

Okwuosa TM, Greenland P, Ning H, Liu K, Bild DE, Burke GL, Eng J, Lloyd-Jones DM. 2011. Distribution of coronary artery calcium scores by Framingham 10-year risk strata in the MESA (Multi-Ethnic Study of Atherosclerosis) potential implications for coronary risk assessment. *J Am Coll Cardiol* **57**(18): 1838-1845.

Pickering TG, Hall JE, Appel LJ, Falkner BE, Graves J, Hill MN, Jones DW, Kurtz T, Sheps SG, Roccella EJ. 2005. Recommendations for Blood Pressure Measurement in Humans and Experimental Animals. *Hypertension* **45**(1): 142-161.

Pignoli P, Tremoli E, Poli A, Oreste P, Paoletti R. 1986. Intimal plus medial thickness of the arterial wall: a direct measurement with ultrasound imaging. *Circulation* **74**(6): 1399-1406.

Polak JF, Pencina MJ, Pencina KM, O'Donnell CJ, Wolf PA, D'Agostino RB, Sr. 2011. Carotid-wall intima-media thickness and cardiovascular events. *N Engl J Med* **365**(3): 213-221.

Raggi P, Cooil B, Shaw LJ, Aboulhson J, Takasu J, Budoff M, Callister TQ. 2003. Progression of coronary calcium on serial electron beam tomographic scanning is greater in patients with future myocardial infarction. *Am J Cardiol* **92**(7): 827-829.

Rosenstock L, Olsen J. 2007. Firefighting and death from cardiovascular causes. *New England Journal of Medicine* **356**(12): 1261-1263.

Salonen JT, Salonen R. 1993. Ultrasound B-mode imaging in observational studies of atherosclerotic progression. *Circulation* **87**(3 Suppl): II56-65.

Shaw LJ, Raggi P, Schisterman E, Berman DS, Callister TQ. 2003. Prognostic value of cardiac risk factors and coronary artery calcium screening for all-cause mortality. *Radiology* **228**(3): 826-833.

Soteriades ES, Smith DL, Tsismenakis AJ, Baur DM, Kales SN. 2011. Cardiovascular disease in US firefighters: a systematic review. *Cardiol Rev* **19**(4): 202-215.

Tanaka H, Dinenno FA, Monahan KD, DeSouza CA, Seals DR. 2001. Carotid Artery Wall Hypertrophy With Age Is Related to Local Systolic Blood Pressure in Healthy Men. *Arteriosclerosis, Thrombosis, and Vascular Biology* **21**(1): 82-87.

Taylor AJ, Bindeman J, Bhattarai S, Feuerstein IM, O'Malley PG. 2004. Subclinical calcified atherosclerosis in men and its association with a family history of premature coronary heart disease in first- and second-degree relatives. *Prev Cardiol* **7**(4): 163-167.

Taylor AJ, Fiorilli PN, Wu H, Bauer K, Bindeman J, Byrd C, Feuerstein IM, O'Malley PG. 2010. Relation between the Framingham Risk Score, coronary calcium, and incident coronary heart disease among low-risk men. *Am J Cardiol* **106**(1): 47-50.

Thompson GM, Roy AV. 1981. The dextran sulfate--MgSO4 precipitation as a method for quantitation of high-density lipoprotein cholesterol. *Am J Clin Pathol* **75**(2): 267-270.

TriData Corporation. 2002. Firefighter Fatality Retrospective Study. Vol 2012. Federal Emergency Management Agency United States Fire Administration National Fire Data Center, Arlington, VA.

Wagner AM, Sanchez-Quesada JL, Perez A, Rigla M, Cortes M, Blanco-Vaca F, Ordonez-Llanos J. 2000. Inaccuracy of calculated LDL-cholesterol in type 2 diabetes: consequences for patient risk classification and therapeutic decisions. *Clin Chem* **46**(11): 1830-1832.

Wayhs R, Zelinger A, Raggi P. 2002. High coronary artery calcium scores pose an extremely elevated risk for hard events. *J Am Coll Cardiol* **39**(2): 225-230.

Wilson PW, D'Agostino RB, Levy D, Belanger AM, Silbershatz H, Kannel WB. 1998. Prediction of coronary heart disease using risk factor categories. *Circulation* **97**(18): 1837-1847.

CHAPTER 3

INFLAMMATION AND EXTRACELULAR MATRIX GENES DIFFERENTIALLY EXPRESSED IN CORONARY ARTERIES FOLLOWING ZOTAROLIMUS- AND SIROLIMUS-ELUTING STENT IMPLANTATION

3.1. INTRODUCTION

Percutaneous transluminal coronary angioplasty (PTCA) has revolutionized the treatment of coronary artery disease since its introduction in 1977 (Grüntzig et al. 1979). However, restenosis or the arterial healing response has proven to be problematic for PTCA due to negative remodeling, contraction formation and consequent late luminal loss in 30-60% of post-angioplasty patients (Fischman et al. 1994; Serruys et al. 1994). The use of bare metal stents (BMS) in PTCA has been effective in reducing restenosis by acting as a scaffold against elastic recoil and negative remodeling (Sigwart et al. 1987; Fischman et al. 1994; Serruys et al. 1994). Referred to generally as percutaneous coronary intervention (PCI) the use of stents in PTCA has resulted in a significant reduction in many of the major adverse cardiac events associated with PTCA and is currently considered a standard procedure worldwide. However, the increased use of BMS in PTCA has resulted in the emergence of an unanticipated complication, *i.e.*, the occurrence of restenosis within

the stent ("in-stent restenosis" or ISR) resulting in > 50% late lumen diameter loss in treated patients.

In an effort to reduce ISR, a new generation of drug-eluting stents (DES) has been designed to release anti-restenotic agents at the stent site. The two most common anti-restenotic drugs used in drug-eluting stents, are sirolimus (Sirolimus Eluting Stents, SES) and zotarolimus (Zotarolimus Eluting Stents, ZES). Both drugs have similar antimicrobial and immunosuppressive properties since they are derived from the same natural compound, rapamycin (Pendyala et al. 2008). Rapamycin acts by binding to the cytosolic receptor FKBP12, forming a complex that inhibits the activation of the mammalian target of rapamycin (mTOR) (Fischman et al. 1994). mTOR inhibition ultimately results in cell cycle arrest in the late G_1 phase, arresting smooth muscle cell growth (Braun-Dullaeus et al. 1998; Marx and Marks 2001). Sirolimus is bound to the stent with a poly-ethylene-covinyl/poly-n-butyl methacrylate copolymer. ZES elute zotarolimus, a derivative of sirolimus that incorporates a phosphorylcholine coating that imparts high lipophilicity (Lewis and Stratford 2002). It has been suggested that ZES are better suited for stent based drug delivery since they have been shown to reduce endothelialisation and neointimal formation relative to SES (Burke et al. 2006).

Despite the apparent design advantage of ZES, recent clinical studies show that both short-term (1 month) and long term (1 year) use of ZES results in an elevated rate of ISR, stent thrombosis, lesion revascularization, and vessel revascularization relative to SES (Cheol Whan et al. 2009; Rasmussen et al. 2010). While these and other

comparative studies have revealed significant differences between BMS, SES and ZES at both the clinical and histological levels, the molecular basis of these differences remains poorly understood.

In an effort to better understand the molecular basis of the variable response of coronary arteries to the different classes of stents, we conducted a comparative microarray profiling study to examine differences in gene expression and pathway function in coronary arteries exposed to ZES, SES, and BMS in a porcine animal model.

3.2. MATERIAL AND METHODS

3.2.1 Stent characteristics

SES (Cypher®, 13 mm in length, Johnson & Johnson, Bridgewater, New Jersey) contain sirolimus combined with non-erodable polymers (polyethylene-co-vinyl acetate [PEVA] and poly-n-butyl methacrylate [PBMA]). The thickness of the coating is about 12.6-μm. The dose of the drug on the SES surface is 10 μg/mm of stent length. Both SES and bare metal stents (BMS, 12 mm in length, Driver®, Medtronic Cardiovascular, Minneapolis, MN) were purchased as commercially available products. ZES (Endeavor®, 12 mm in length, Medtronic Cardiovascular) were provided by Medtronic formulated with zotarolimus, a chemical analogue of sirolimus, and were coated with phosphorylcholine (PC). The dose of the drug on the ZES surface is 10 μg/mm of stent length with a coating thickness of 4.8-μm. ZES has a relatively rapid drug elution profile as 90% of the drug is released during the

first 10-14 days as compared with the SES, in which 80% elution occurs over 30 days. All of the devices were FDA approved and currently in clinical use.

3.2.2 Animals and experimental protocol

Animal handling and care followed the recommendations of the National Institutes of Health (NIH) guide for The Care and Use of Laboratory Animals, and were consistent with guidelines of the American Heart Association (AHA). All protocols were approved by the Saint Joseph's Translational Research Institute Animal Care and Use Committee in accordance with the Association for Assessment and Accreditation of Laboratory Animal Care guidelines. Juvenile Yorkshire farm animals (n = 6), females or castrated males, approximately 40-50 kg and 4-5 months of age were enrolled into three different randomized groups: 1) BMS (n = 2); 2) SES (n = 2); and 3) ZES (n = 2). Two coronary arteries in each animal were implanted with two overlapping stents, for a total of four stents of the same type in each animal.

All animals received a combination of 81 mg aspirin and 75 mg clopidogrel by mouth daily for 3 days prior to stent implantation. The drug regimen was continued until termination of the experiment. For stent implantation, the animals were sedated by intramuscular injection of ketamine 20 mg/kg, xylazine 2 mg/kg, and atropine 0.05 mg/kg. After intubation, general anesthesia was induced and maintained with isofluorane (2.5%). Cardiac cycle and blood pressure were continuously monitored.

Cardiac catheterization was performed with full heparinization (200 units/kg), and the stents were implanted using quantitative coronary angiography (QCA) guidance to obtain a stent-to-arterial diameter ratio (S/A ratio) = 1.1:1 with an overlapping segment of one-third to one-half of single stent length. Activated clotting time (ACT) measurements were performed approximately every 30 min, and additional heparin was administered when ACT was below 5 min.

At one month, baseline angiography was performed by a single angiographer using consistent contrast injection volumes.

3.2.3 RNA extraction and microarray

After 28 days, tissue samples were collected from the stented segment of both arteries from each animal (Table 3.1). Tissue was manually dissected from each stent and 10-20 mg was ground with a Polytron homogenizer (Kinematica AG, Lucerne, Switzerland) in RNeasy lysis buffer (Qiagen Inc., Valencia, California). RNA was isolated according to the manufacturer's instructions. Quantity and quality of RNA was determined with a NanoDrop spectrophotometer (Thermo Scientific Inc., Wilmington, Delaware) and BioAnalyser total RNA PicoChip assay (Agilent Technologies Inc., Santa Clara, California). 50 ng of the total RNA was converted into cDNA and amplified with the Applause 3'-Amp System (NuGEN Technologies Inc., San Carlos, California). 3 μg of amplified cDNA was fragmented and labeled with Encore™ Biotin Module (NuGEN Technologies Inc.). The resulting cDNA was hybridized to the GeneChip Porcine Genome array (Affymetrix Inc., Santa Clara,

Table 3.1. *Analyzed stents and their implant positions.* We generated 12 individual gene expression profiles (Affymetrix Porcine Genome Array) from artery samples taken from two SES implanted animals, two ZES implanted animals, and two BMS implanted animals. Two coronary arteries in each animal were implanted with two overlapping stents, for a total of four stents of the same type in each animal. For each artery the tissues surrounding overlapping stents were processed together, generating two gene expression profiles per animal, one for each artery. Stents, animals, and stented coronary arteries are listed here.

Stent	Animal #	Artery
Bare metal	4746	Right coronary Left anterior descending
	4747	Right coronary Left anterior descending
Sirolimus eluting	4745	Left circumflex Right coronary
	4750	Right coronary Left anterior descending
Zotarolimus eluting	4757	Right coronary Left anterior descending
	4751	Right coronary Left anterior descending

California) for 16 hours at 45˚C. The arrays then were washed, stained and scanned according to the Affymetrix Technical Manual.

3.2.4 Microarray data analysis

Affymetrix .CEL files were processed using the Affymetrix Expression Console (EC) Software Version 5.0. Files were processed using the default MAS5 3' expression workflow. All reported microarray data are described in accordance with MIAME guidelines and deposited in the National Center for Biotechnology Information's Gene Expression Omnibus database with the accession numbers GSM712656, GSM712657, GSM712658, GSM712659, GSM712660, GSM712661, GSM712662, GSM712663, GSM712664, GSM712665, GSM712666, and GSM712667. Probe sets that were called absent by default MAS5 criteria in all 24 samples were removed before further processing. Probe set results were further evaluated using Spotfire DecisionSite software. Using a beta-uniform model to control the false discovery rate to less than 0.25 for our pooled pair-wise stent comparisons, we determined a new multiple testing-adjusted p-value threshold of 0.016 (Coombes 2010). Probes were considered differentially expressed if they had a fold change value of ≥ 2 or <= -2 and a p-value < .016 (Student's t-test).

3.3. RESULTS

Relative to BMS-exposed arteries, 955 and 508 genes were differentially expressed in SES-exposed and ZES-exposed arteries, respectively (Table 3.2). More genes were down regulated than up regulated in both of the drug-eluting stent- exposed samples relative to the BMS-exposed samples. For the SES-exposed samples 470

Table 3.2. *Significantly differentially expressed genes.* Numerous and characteristic genes distinguish expression patterns in arterial tissue exposed to sirolimus-eluting compared to bare metal (SES-BMS), zotarolimus-eluting compared to bare metal (ZES-BMS), and zotarolimus-eluting compared to sirolimus-eluting stents (ZES-SES). This table lists those genes with fold change greater than two between groups and t-test p-value < 0.05 for significant differences in average expression levels between groups. Displayed are those genes with the 10 largest fold changes up or down for each comparison.

Gene Title	Gene Symbol	Fold change	t-test p-value
SES-BMS comparison			
arginase liver	ARG1	118.37	0.00274
interleukin 1 beta	IL1B	71.60	0.00910
similar to dual specificity phosphatase 5	LOC100157144	39.48	0.00053
nucleoside phosphorylase	NP	38.77	0.00258
interleukin 8	IL8	35.00	0.02333
muscle specific intermediate filament desmin	LOC396725	-28.56	0.02247
similar to potassium channel subfamily K member 10	LOC100155276	-19.34	0.00720
vitronectin	VTN	-19.03	0.00712
similar to Interferon induced protein with tetratricopeptide repeats 2	LOC100155467	-18.72	0.01335
Aquaporin 8	LOC100127152	-18.51	0.00486
ZES-BMS comparison			
arginase liver	ARG1	64.17	0.00570
amelogenin	AMELX	41.98	0.00223
Serum amyloid A2	LOC733603	22.69	0.01469
Similar to orphan G-protein coupled receptor bRGR1	LOC100153615	20.87	0.04727
similar to Carbonic anhydrase 2	LOC100154873	19.76	0.00293
casein kappa	CSN3	-30.04	0.00187
Neurotrophin 3	NTF3	-22.71	0.00224
transforming growth factor beta 2	TGFB2	-20.77	0.03254
sialoadhesin	SIGLEC-1	-20.43	0.00316
similar to uncharacterized protein C22orf13	LOC100154708	-20.09	0.00035

Table 3.2 (continued)

ZES-SES comparison			
Aquaporin 8	LOC100127152	16.89	0.00230
anti Mullerian hormone	AMH	15.52	0.00014
Ras homolog gene family member F	RHOF	14.57	0.00075
transcription factor AP 2 gamma	CH242-255C19.1	12.39	0.00059
similar to Polymerase (RNA) I polypeptide D	LOC100152160	11.63	0.02974
stefin A8	LOC396867	-30.30	0.01232
Similar to coagulation factor XIII A1 subunit	LOC100153504	-19.08	0.00279
metallothionein	MT1A	-17.16	0.01625
haptocorrin	LOC396873	-14.58	0.03641
similar to Apolipoprotein B mRNA editing enzyme catalytic polypeptide like 2	LOC100156477	-13.90	0.00256

were up regulated and 485 down regulated while for the ZES-exposed samples, 188 were up regulated and 320 down regulated relative to the BMS-exposed samples. Comparing ZES-exposed samples with SES-exposed samples, 206 genes are up regulated in ZES compared to SES and 208 genes are down regulated.

Some of the differentially expressed genes observed in the SES-BMS comparison and differentially expressed genes observed in the ZES-BMS comparison overlap. This overlap consists of 158 genes identified as being significantly differentially expressed in the SES-exposed and ZES-exposed arteries. All of these overlapping genes were differentially expressed co-directionally. That is, 93 of the 158 genes were up regulated in both the SES-BMS and ZES-BMS comparisons. And the remaining 65 genes were down regulated in both the SES-BMS and ZES-BMS comparisons. This strong co-directionality is consistent with the rapamycin-derived origin of both zotarolimus and sirolimus.

A supervised (ANOVA p-value < 0.05) differential expression analysis and hierarchical clustering between BMS-, SES- and ZES-exposed artery samples resulted in a distinct separation between all three groups (Figure 3.1). Not only do the artery samples from each stent type group together, the samples from each individual group together, indicating a similar expression profile.

3.3.1 Genes differentially expressed in SES

Gene Set Enrichment Analysis (GSEA) demonstrated that in SES-exposed arteries compared to BMS-exposed arteries there was up regulation in gene sets for

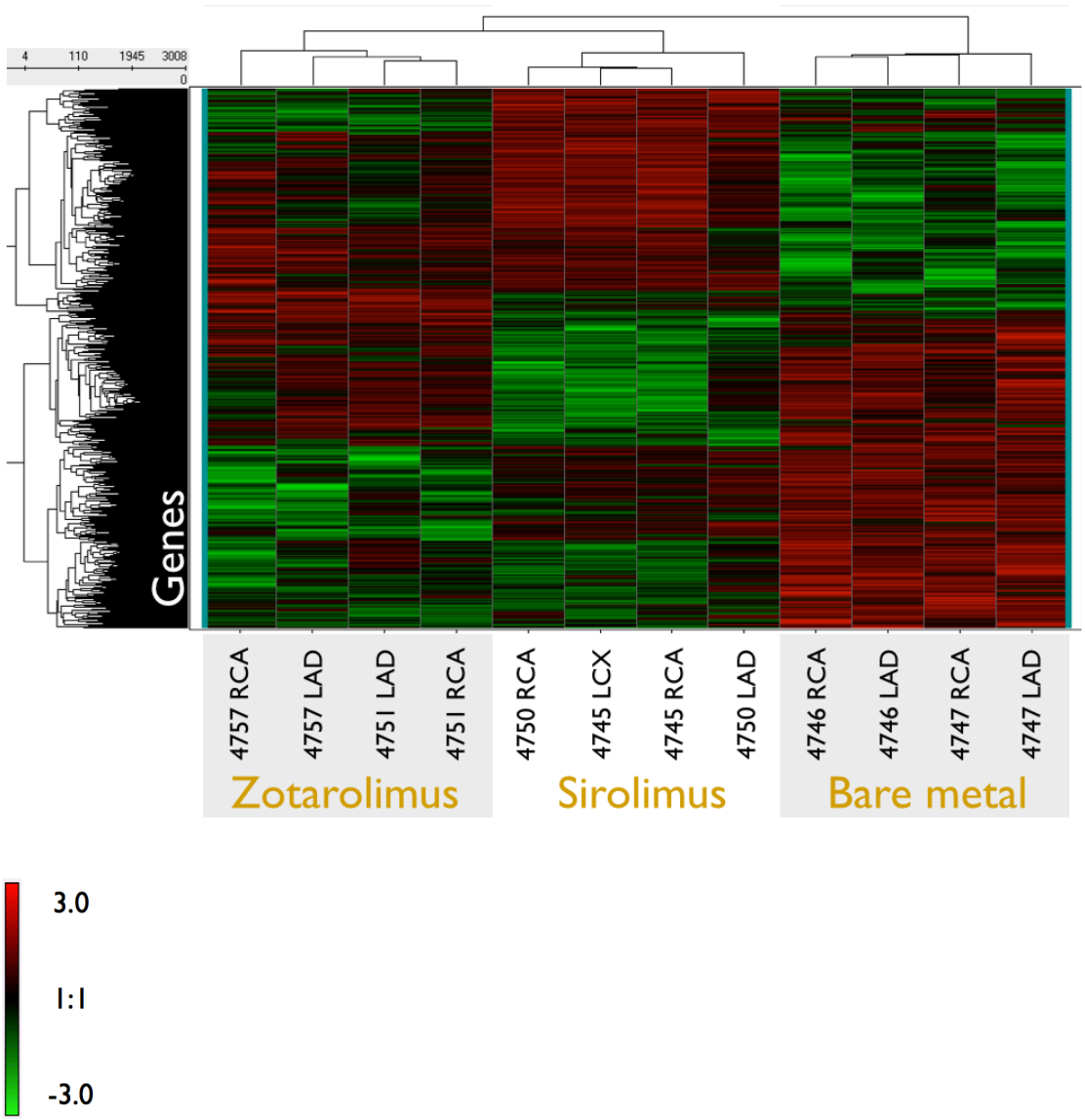

Figure 3.1. *Hierarchical clustering of 3008 genes differentially expressed among arterial tissue exposed to bare metal, sirolimus-eluting, and zotarolimus-eluting stents.* This heat map was generated by Z-score normalization of log2 expression values from Affymetrix GeneChip Porcine Genome arrays. Displayed are the relative expression levels of genes (rows) differentially expressed (red = relatively over-expressed compared to BMS-exposed tissues; green = relatively under-expressed compared to BMS-exposed tissues) in 4 arteries exposed to bare metal stents, 4 arteries exposed to sirolimus-eluting stents, and 4 arteries exposed to zotarolimus-eluting stents.

chemokine activity and inflammatory response and down regulation in gene sets having to do with potassium transport and channels, as well as muscle activity (Mootha et al. 2003; Subramanian et al. 2005).

3.3.1.1 Extracellular matrix activity associated with SES

In the integrated model of in-stent restenosis, vascular smooth muscle cell migration from the tunica media to the tunica intima occurs concurrently with the infiltration of leukocytes (Welt and Rogers 2002). Thus in order to migrate, vascular smooth muscle cells (VSMC) must degrade and breach the extracellular matrix (ECM) layers of the media, in a three step process of phenotypic change from contractile state into synthetic state, proteolytic dissolution of ECM, and migration through the digested matrix (Kuzuya and Iguchi 2003).

Matrix metalloproteinases are involved in the turnover of ECM in the normal physiological life of connective tissue, morphogenesis, and wound healing by cleaving collagens (Kuzuya and Iguchi 2003). In our samples (Table 3.3), matrix metalloproteinases 1,3, and 9 (*MMP1*, *MMP3*, *MMP9*) are all over-expressed in SES-exposed arteries relative to arteries exposed to BMS (p-value = 0.005, log2 fold change = 3.69 ; p-value = 0.002, log2 fold change = 3.13; p-value = 0.002 log2 fold change = 2.46, respectively). MMP-1 is a collagenase, able to cleave interstitial collagens I, II, and III at a specific site, as well as digesting other ECM components (Will et al. 1996). MMP3, also known as stromelysin 1, digests ECM components, including basement membrane, and also cleaves proMMP1 to form fully activated MMP1 (Suzuki et al. 1990). MMP1-mediated cleavage is also associated with cell

Table 3.3. *Extracellular matrix process genes.*

Significant up regulation of metalloproteinase genes involved in the breakdown of ECM when comparing arterial tissue exposed to sirolimus-eluting stents and bare metal stents. This breakdown is essential to the migration of vascular smooth muscle cells during the middle stages of restenosis. This table lists the log2 fold change difference comparing sirolimus-eluting, and bare metal stents, as well as t-test p-values for tests of differences in average expression levels between the two. Displayed are fold change differences and p-values for all genes grouped under the gene ontology listing for extracellular matrix part, basement matrix, proteinaceous extracellular matrix, and extracellular matrix. Genes with a p-value less than the multiple testing adjusted value of 0.046 are bolded.

Gene Symbol	SES-BMS log2 fold change		SES-BMS t-test p-value	Gene title
AEBP1	-3.67	± 1.71	**0.006573346**	AE binding protein
ANXA2	0.5	± 0.08	**0.001576484**	annexin A2
APP	-0.99	± 0.55	**0.012302513**	amyloid beta (A4) precursor protein
ATP7A	-3.51	± 1.44	**0.00684966**	ATPase Cu++ transporting alpha polypeptide
BGLAP	-2.62	± 1.32	0.021518431	bone gamma carboxyglutamate (gla) protein
BGN	-1.18	± 0.88	0.039634364	biglycan
CLU	1.37	± 0.39	**0.000948126**	clusterin
COL1A1	-2.82	± 0.84	**0.015206919**	collagen type I alpha 1
COL2A1	-2.02	± 0.89	**0.010637478**	collagen type II alpha 1
COL3A1	-0.69	± 0.34	0.023999384	collagen type III alpha 1
COL5A3	2.07	± 0.13	**0.004183389**	Collagen type V alpha 3
CST3	-1.37	± 0.45	0.020747497	Cystatin C
CTSD	-1.54	± 1.01	0.028342424	cathepsin D
DPP4	2.54	± 0.38	**0.000318554**	dipeptidyl peptidase 4
FN1	1.86	± 0.24	**0.000292543**	fibronectin
IGFBP7	-1.5	± 0.84	0.033975975	insulin like growth factor binding protein 7
LAMB1	-1.42	± 0.79	0.02463023	laminin beta 1
LGALS1	-1.54	± 0.48	**0.001043365**	lectin galactoside binding soluble 1
LMCD1	-1.6	± 1	0.037627101	LIM and cysteine rich domains 1
LPL	1.65	± 0.5	**0.014813832**	lipoprotein lipase
MGP	-1.11	± 0.46	**0.011740611**	matrix Gla protein
MMP1	3.69	± 0.98	**0.005682639**	matrix metallopeptidase 1 (interstitial collagenase)
MMP3	3.13	± 0.48	**0.002120225**	matrix metallopeptidase 3 (stromelysin 1 progelatinase)
MMP9	2.46	± 0.71	**0.001878166**	Matrix metallopeptidase 9 (gelatinase B 92kDa gelatinase 92kDa type IV collagenase)

Table 3.3 (continued)

MMP13	-6.69	± 0.38	**0.030576684**	Matrix metallopeptidase 13
PLAT	2.3	± 0.43	**0.00237602**	plasminogen activator tissue
RPSA	-0.5	± 0.22	0.036423376	ribosomal protein SA
SOD1	-0.36	± 0.22	0.029389833	superoxide dismutase 1 soluble
SPARC	-2.18	± 0.5	**0.000145088**	Secreted protein acidic cysteine rich (osteonectin)
SPARC	-0.88	± 0.31	0.0364355	Secreted protein acidic cysteine rich (osteonectin)
SPARCL1	-3.26	± 1.8	0.01767792	SPARC like 1 (hevin)
TIMP1	1.37	± 0.28	**0.000589379**	TIMP metallopeptidase inhibitor 1
TNC	-3.25	± 2.1	0.035336136	tenascin C
VCAN	-3.09	± 2.23	0.041221801	Versican
VEGFA	2.55	± 0.47	**0.000532369**	vascular endothelial growth factor A
VTN	-4.25	± 2.03	**0.007115448**	vitronectin

migration, platelet aggregation, and inflammation. MMP3-mediated cleavage is associated with cell migration, angiostatin-like fragment generation, enhanced collagen affinity, and inflammation (Visse and Nagase 2003). MMP9 digests the denatured collagens, known as gelatins. Elevated serum levels of MMP9 have been noted in humans post-stent implantation in association with restenosis (Ge et al. 2006; Katsaros et al. 2010).

Tissue inhibitors of metalloproteinases (TIMP) are endogenous inhibitors of MMPs that bind one to one. TIMPs inhibit all MMPs, although TIMP1 does not inhibit MT1-MMP (Visse and Nagase 2003). TIMP1 is up regulated in SES-exposed arteries (p-value = 0.00058, log2 fold change = 1.37). TIMP1 expression is known to be largely constitutive (Dollery et al. 1995).

In our experiments, extracellular matrix gene expression is significantly differentially expressed in SES-exposed arteries compared to BMS-exposed arteries. We do not observe this differential expression in ZES-exposed arteries (data not shown). The ECM genes that are differentially expressed in SES-exposed arteries are largely involved in collagen cleavage mediated by matrix metalloproteinase (*MMP1*, *MMP3*, *MMP9*, *MMP13*) and the regulation of collagen cleavage (*TIMP1* and *TIMP2*). This is consistent with previous experimental evidence showing that matrix metalloproteinases are correlated with smooth muscle cell migration into the intima (Wu et al. 2008).

Up-regulation of MMP1 (collagenase) has been observed in *in vivo* studies immediately following stent implantation (Wu et al. 2008), and its expression has

also been induced by mechanical injury in cultured vascular smooth muscle cells as well as by rapamycin in fibroblasts (James et al. 1993). Up-regulation of *MMP3* (stromelysin 1) and *MMP9* (collagenase) has been detected in the plasma of in-stent restenosis cases (compared to restenosis-free individuals) at the 1-year mark post-bare metal stent implantation (Jones et al. 2009). Up-regulation of *MMP9* in artery tissue has been observed in *in vivo* studies immediately following angioplasty and vessel damage (Godin et al. 2000; Feldman et al. 2001). Moreover, *MMP3* expression in arteries is a known activator of MMP9-mediated vascular smooth muscle cell migration and neointimal formation (Johnson et al. 2011).

Our results show that SES-exposed arteries have elevated levels of *MMP1*, *MMP3*, and *MMP9* expression (Table 3.3), even prior to measurable luminal narrowing. This suggests that the collagen remodeling associated with middle-stage restenosis is occurring in individuals implanted with the SES. Expression levels for genes associated with the extracellular matrix appeared elevated in ZES-exposed arteries compared to BMS-exposed arteries, but were not significantly differentially expressed. Because ECM gene expression in ZES-exposed arteries generally lies between that observed in SES-exposed arteries and BMS-exposed arteries, most ECM genes are not significantly differentially expressed when comparing ZES-exposed and SES-exposed arteries (see also Section 3.2.1).

3.3.1.2 Ion channel activity associated with SES

When comparing SES-exposed arteries to BMS-exposed arteries, gene sets related to ion channels and muscle components are down regulated. The ion channel gene sets

include those involved in potassium channel activity, potassium ion transport, and ion channel activity (Table 3.4). Among the genes that contribute to these gene sets are L-type voltage-dependent calcium channel alpha 1C subunits (*CACNA1C*, also known as $Ca_V1.2$), and alpha 1S subunits (*CACNA1S*, also known as $Ca_V1.1$), both primary components of different L-type calcium channels. Also contributing is calcium-activated large potassium channel sub-family M beta member 1 subunit (*KCNMB1*, also known as $K_{Ca}1.1$), a modulatory component of large calcium-activated potassium channels. Contractile vascular smooth muscle cells (VSMC) strongly express $K_{Ca}1.1$, which provides negative feedback against depolarization (Beech 2007). These potassium channels thus limit Ca^{2+} flow through $Ca_V1.2$. When VSMC switch to the proliferating phenotype there is a noted down-regulation of $Ca_V1.2$ observed in cultured rat VSMC, as well as following balloon injury in rat arteries (Richard et al. 1992; Quignard et al. 2001; Ihara et al. 2002). Normal contractile VSMC also predominantly express $K_{Ca}1.1$, and studies in cultured rat aortic cells show that in response to injury their expression is down regulated (Neylon et al. 1999; Si et al. 2006). The down-regulation of both of these ion channels is indicative of the phenotypic changes that accompany a shift from contractile to proliferative function in VSMCs.

3.3.2 Genes differentially expressed in ZES

3.3.2.1 Extracellular matrix, basement membrane, and proteinaceous extracellular matrix genes up-regulated in ZES compared to SES

Table 3.4. *Potassium ion channel activity and ion channel activity genes differentially expressed in SES compared to BMS*

Significant down regulation of ion channel activity genes characteristic of vascular smooth muscle cells (VSMCs) switching from a sessile to proliferative phenotype. This switch occurs during the migration of VSMCs from the tunica media to the tunica intima as a part of the middle stages of in-stent restenosis. This table lists the log2 fold change difference comparing sirolimus-eluting, and bare metal stents, as well as t-test p-values for tests of differences in average expression levels between the two. Displayed are fold change differences and p-values for all genes grouped under the gene ontology listing for potassium ion channel activity and ion channel activity. Genes with a p-value less than the multiple testing adjusted value of 0.046 are bolded.

Gene symbol	Gene title	SES-BMS log2 fold change			SES-BMS t-test p-value
CACNA1B	calcium channel, voltage-dependent, beta 1 subunit	-1.83	±	1.89	0.1053
CACNA1C	calcium channel, voltage-dependent, L type, alpha 1C subunit	-5.47	±	6.8	0.0597
CACNA1E	calcium channel, voltage-dependent, alpha 1E subunit	-1.5	±	1.56	0.2509
CACNA1S	calcium channel, voltage-dependent, L type, alpha 1S subunit	-2.42	±	3.5	0.2806
CACNB2	calcium channel, voltage-dependent, beta 2 subunit	-3.85	±	5	0.0632
CACNB3	calcium channel, voltage-dependent, beta 3 subunit	-1.42	±	0.37	0.1859
CLCN2	chloride channel 2	-1.92	±	3.51	0.3828
CLCN2	chloride channel 2	-2.39	±	0.26	**0.0048**
CLCN4	chloride channel 4	-2.9	±	3.95	0.2391
KCNH2	potassium voltage-gated channel, subfamily H (eag-related), member 2	-3.03	±	4.38	0.226
KCNH3	potassium voltage-gated channel, subfamily H (eag-related), member 3	-3.35	±	16.96	0.1927
KCNH4	potassium voltage-gated channel, subfamily H (eag-related), member 4	-2.22	±	2.02	0.1232
KCNMB1	potassium large conductance calcium-activated channel, subfamily M, beta member 1	-7.73	±	9.38	**0.0202**
KCNMB1	potassium large conductance calcium-activated channel, subfamily M, beta member 1	-2.99	±	2.3	0.2285
NMUR2	neuromedin U receptor 2	-1.88	±	2.31	0.2096
RYR3	ryanodine receptor 3	-1.74	±	8.81	0.6811
RYR3	ryanodine receptor 3	-6.47	±	5.94	0.062
SCN1B	sodium channel, voltage-gated, type I, beta	-2.17	±	0.78	0.2813
TRPC1	transient receptor potential cation channel, subfamily C, member 4	-2.3	±	1.17	0.1525
TRPV6	transient receptor potential cation channel, subfamily V, member 6	-2.8	±	8.55	0.3805

We used GSEA to find those gene sets whose member genes do not individually show large fold-changes, but may be acting in concert to generate a biologically significant effect. The gene sets significantly up-regulated in ZES-exposed arteries compared to SES-exposed arteries as determined by GSEA can be grouped into two categories; extracellular matrix genes and muscle component genes.

Of the extracellular matrix gene sets, the terms basement membrane and extracellular matrix have FDR q-values of 0.18 and 0.24, respectively. The genes that contribute to the up regulation of the entire process are related to collagen synthesis and non-collagen components associated with the basement membrane. The collagen elements include collagen type IV alpha 2, collagen type IV alpha 5, and collagen type VII alpha 1 (Table 3.5). The type IV collagens found in basement membranes are known to be genetically distinct from the Type I – III fibrillar collagens found in neointimal growth. Collagen type VII alpha 1 is specifically found in basement membranes, anchoring the external endothelia to the underlying stroma. The non-collagen elements include laminin alpha 2, laminin alpha 3, laminin alpha 4, laminin beta 1, laminin beta 2, laminin gamma 1, as well as sarcoglycan delta, sarcoglycan epsilon syntrophin gamma 1, and sarcospan. Laminins are the principle multiadhesive matrix protein found in basement membranes and the most abundant non-collagenous protein in basement membranes.

Denudation of the endothelial layer and damage to the supporting basement membrane occur during angioplasty (Welt and Rogers 2002). At 30 days, the luminal surfaces of stented porcine arteries have fully re-endothelialized, and are in

Table 3.5. *Extracellular matrix genes and basement membrane genes differentially expressed in ZES compared to SES*

Significant up regulation of extracellular matrix genes consistent with newly replaced endothelial cells synthesizing and depositing new basement membrane following denudation of the endothelial layer. Re-deposit of this basement membrane layer follows re-endotheialization at 30 days post-stent implantation. This table lists the log2 fold change difference comparing sirolimus-eluting, and zotarolimus-eluting stents, as well as t-test p-values for tests of differences in average expression levels between the two. Displayed are fold change differences and p-values for all genes grouped under the gene ontology listing for extracellular matrix genes and basement membrane genes. Genes with a p-value less than the multiple testing adjusted value of 0.046 are bolded.

Gene Symbol	Gene Title	ZES-SES log2 fold-change	ZES-SES t-test p-value
LAMA3	laminin, alpha 3	4.44 ± 2.37	**0.028**
LAMB2	laminin, beta 2 (laminin S)	4.91 ± 1.28	**0.008**
SGCD	sarcoglycan, delta (35kDa dystrophin-associated glycoprotein)	3.02 ± 1.61	0.053
COL9A2	collagen, type IX, alpha 2	2.67 ± 1.37	0.265
COL18A1	collagen, type XVIII, alpha 1	2.89 ± 1.29	0.120
SNTG1	syntrophin, gamma 1	3.54 ± 6.59	0.299
COL4A2	collagen, type IV, alpha 2	5.11 ± 2.53	**0.004**
COL7A1	collagen, type VII, alpha 1 (epidermolysis bullosa, dystrophic, dominant and recessive)	2.51 ± 5.00	0.197
COL4A5	collagen, type IV, alpha 5 (Alport syndrome)	2.81 ± 0.86	**0.012**
EFEMP2	EGF-containing fibulin-like extracellular matrix protein 2	2.15 ± 0.27	0.051
LAMC1	laminin, gamma 1 (formerly LAMB2)	2.48 ± 1.51	0.057
COL16A1	collagen, type XVI, alpha 1	1.99 ± 2.44	0.134
SGCE	sarcoglycan, epsilon	1.84 ± 0.80	0.141
APLP1	amyloid beta (A4) precursor-like protein 1	1.63 ± 0.52	0.142
LAMB1	laminin, beta 1	1.94 ± 0.78	0.100
LAMA4	laminin, alpha 4	1.55 ± 0.13	**0.013**
NID2	nidogen 2 (osteonidogen)	1.16 ± 1.76	0.605
COL8A1	collagen, type VIII, alpha 1	1.62 ± 0.74	0.263
SSPN	sarcospan (Kras oncogene-associated gene)	1.64 ± 0.37	0.063
LAMA2	laminin, alpha 2 (merosin, congenital muscular dystrophy)	1.68 ± 0.47	**0.011**

the process of re-depositing the basement membrane matrix (Virmani et al.). Our observed up-regulation of key basement membrane component genes in our GSEA analysis is consistent with the newly replaced endothelial cells synthesizing and depositing a new basement membrane. That we observe no significant regulatory differences in basement membrane or extracellular matrix gene sets when comparing ZES-exposed arteries to BMS-exposed arteries is consistent with ZES having already exhausted its drug-elution and leaving the arteries in the early phases of neointima formation.

Of the muscle component gene sets, the terms contractile fiber, contractile fiber part, myofibril, and structural constituent of muscle have FDR q-values of 0.21, 0.22, and 0.22, respectively. The genes that contribute to the myofibril, contractile fiber and contractile fiber part term include supervillin, desmin, troponin I type 3, nebuline, titin, myomesin 1, and myosin light chain 9 (Table 3.6). The genes that contribute to the structural constituent of muscle term are nebulin, titin, smoothelin, myomesin 1, myosin heavy chain 11, actinin alpha 2, actin alpha, sorbin, myomesin 2, myosin light chain 2, telethonin, tropomyosin, nebulette, and myosin binding protein H.

Smoothelin (*SMTN*) and desmin (*DES*) are well-established VSMC differentiation markers in porcine coronary arteries after stent implantation (Christen et al. 1999). In our samples smoothelin was up-expressed at a log2 fold change of 2.74±0.69 (t-test p-value 0.0227), while desmin was up-expressed at a log2 fold change of 1.44±0.66 (t-test p-value of 0.041). Smoothelin is a cytoskeletal protein specifically

Table 3.6. *Muscle component gene set genes differentially expressed in ZES compared to SES*

Gene symbol	Gene title	ZES-SES log2 fold-change	ZES-SES t-test p-value
SVIL	supervillin	3.70 ± 3.05	0.094
DES	desmin	6.73 ± 4.02	**0.023**
TNNI3	troponin I type 3 (cardiac)	5.21 ± 2.03	0.216
NEB	nebulin	2.58 ± 1.15	**0.017**
TTN	titin	-6.54 ± 6.11	0.048
MYOM1	myomesin 1 (skelemin) 185kDa	4.67 ± 3.98	0.198
MYL9	myosin, light chain 9, regulatory	3.91 ± 2.65	0.093

Table 3.7. *Inflammatory process genes differentially expressed in SES compared to BMS and ZES compared to BMS*

Gene Symbol	SES-BMS log2 fold-change	ZES-BMS log2 fold-change	SES-BMS t-test p-value	ZES-BMS t-test p-value	Gene Title
CCL2	4.18 ± 0.03	1.57 ± 0.05	0.0012	0.1864	chemokine (C-C motif) ligand 2
CCL5	10.26 ± 0.09	1.85 ± 0.09	0.0007	0.1575	chemokine (C-C motif) ligand 5
ICAM-2	-1.02 ± 0.11	2.56 ± 0.06	0.9617	0.0091	intercellular adhesion molecule 2
ICAM-1	7.29 ± 0.07	4.20 ± 0.11	0.0001	0.0048	intercellular adhesion molecule 1
IL1B	71.60 ± 0.44	10.39 ± 0.41	0.0091	0.0793	interleukin 1 beta
IL1A	10.46 ± 0.20	4.77 ± 0.16	0.0145	0.0557	interleukin-1-alpha
SELE	1.48 ± 0.74	1.83 ± 0.55	0.6866	0.4753	selectin-E
SYK	3.11 ± 0.05	1.83 ± 0.06	0.0443	0.2262	spleen-tyrosine-kinase

expressed in differentiated contractile smooth muscle cells and appears later in VSMC development than other differentiation markers like desmin (van der Loop et al. 1996). Desmin is an intermediate filament protein of both smooth and striated muscles known to be a VSMC differentiation marker. Both smoothelin and desmin have been found to be up-expressed in neointima induced by bare metal stent implantation in porcine arteries at 7, 15, and 30 days (Christen et al. 2001). This supports our extracellular matrix expression results suggesting that restenosis has progressed to neointima formation by VSMC proliferation in our ZES-exposed artery samples.

3.3.3 Inflammation in both ZES and SES exposed arteries

When comparing ZES-exposed to BMS-exposed arteries expression of gene sets related to the inflammatory response are up regulated (FDR q-value = 0.18). We also see up-regulation in this gene set when comparing SES-exposed to BMS-exposed arteries (FDR q-value = 0.050). A number of components of the inflammatory response gene set are known to be involved in the restenotic process (Table 3.7).

3.3.3.1 Intercellular adhesion molecule 1 (ICAM-1)

Intercellular adhesion molecule 1 is an Ig-like adhesion molecule expressed by endothelial cells and leukocytes both, mediating the binding of integrins that result in adhesion between leukocytes and endothelial cells. This reversible adhesion with leukocytes, slows their progress and causes them to roll on the endothelial surface. This is the first step in recruiting neutrophils to adhere to the blood vessel wall and

enter the inflammatory site. In our samples, ICAM-1 is significantly up-regulated both in SES-exposed arteries compared to BMS-exposed arteries, as well was in ZES-exposed arteries compared to BMS-exposed arteries.

3.3.3.2 Chemokine (C-C motif) ligand 5 (CCL5)

The chemokine CCL5 activate leukocyte integrins to more strongly bind to intracellular adhesion molecules (ICAM), leading to tighter adhesion between free blood-borne leukocytes and endothelial cells prior to extravasation. This chemokine gradient directs the migration of leukocytes into the subendothelial space, where the leukocytes can then release growth factors that drive the proliferation and migration of smooth muscle cells in the neointima (Gomes et al. 2005). The formation of neointima then causes restenosis. In our samples, CCL5 was significantly up-regulated in SES-exposed artery samples as compared to bare metal stent exposed arteries (fold change = 10.26, p-value = 0.0007)

3.3.3.3 Interleukin 1A

IL-1A (IL1A) is a pro-inflammatory cytokine. It is an important mediator of the inflammatory response, and is involved in a variety of cellular activities, including cell proliferation, differentiation, and apoptosis. IL-1A is significantly elevated in SES-exposed arteries compared to bare metal stented arteries, while ZES-exposed arteries are up regulated, but not significantly so relative to BMS-exposed arteries.

3.4. DISCUSSION

While a number of gene expression-profiling studies have been conducted to characterize post-angioplasty and stented arteries, none to date have focused on the molecular response of arteries to drug-eluting stents (Zohlnhofer et al. 2001; Li et al. 2007; Muldowney et al. 2007). We conducted gene expression analyses of porcine arteries exposed to BMS, SES and ZES at 28 days post-implantation. In general, our results indicate that the rapamycin family eluting stents, SES and ZES, delay the inflammatory response and proliferative processes associated with restenosis for as long as the stents elute the drug.

At 28 days, BMS-exposed arteries have been shown to transition from proliferative smooth muscle cell-based neointimal growth to mature extracellular matrix-based neointimal growth (Finn et al. 2002). Since 80% of the sirolimus is reported to be eluted from SES within 30 days (Acharya and Park 2006) following implantation, at 28 days, SES-exposed arteries might be expected to be just entering restenosis where the process of leukocyte recruitment and smooth muscle cell migration and proliferation begins (Virmani et al.). Consistent with this expectation, SES-exposed arteries displayed a gene expression pattern indicative of leukocyte infiltration and SMC migration characteristic of early stages of in-stent restenosis-a process that is typically observed after BMS-stent implantation after only 1-3 days (Costa and Simon 2005). In contrast, ZES have been reported to release 90% of their drug payload within 14 days of implantation (Kandzari and Leon 2006). Thus at 28 days post-implantation, ZES exposed arteries might be expected to be at the same stage of restenotic progression as a 14 day old BMS-exposed artery, where neointimal formation transitions from SMC migration to a more mature SMC proliferation-

driven state (Welt and Rogers 2002). Consistent with this expectation, we found that at 28 days post-implantation, ZES-exposed arteries displayed gene expression patterns indicative of extracellular matrix formation, muscle cell growth and basement membrane formation, all emblematic of a transition from migratory VSMC to proliferative SMC and a restored endothelial layer. Thus, the molecular profiles are consistent with a model of delayed restenosis due to the drug-induced suppression of inflammatory responses and proliferative processes associated with drug eluting stents.

3.5. CONCLUSION

Our results suggest that the reported differences between SES and ZES stents in delaying restenosis is mostly due to a differential delay in the onset of the response due to differences in the drug elution rates associated with the two stents and less to a qualitative difference in the responses of arteries to the stents. In addition to providing insight into the detailed molecular responses of arterial tissues to the implantation of SES and ZES, our results indicate that biomarkers of restenosis are clearly apparent on the molecular level well before the process manifests itself at the macroscopic level. Thus, molecular profiling may be useful in evaluating early arterial responses to implants and may serve as an asset in the future design and evaluation of drug eluting stents.

3.6. REFERENCES

Acharya G, Park K. 2006. Mechanisms of controlled drug release from drug-eluting stents. *Advanced Drug Delivery Reviews* **58**(3): 387-401.

Beech DJ. 2007. Ion channel switching and activation in smooth-muscle cells of occlusive vascular diseases. *Biochem Soc Trans* **35**(Pt 5): 890-894.

Braun-Dullaeus RC, Mann MJ, Dzau VJ. 1998. Cell Cycle Progression : New Therapeutic Target for Vascular Proliferative Disease. *Circulation* **98**(1): 82-89.

Burke SE, Kuntz RE, Schwartz LB. 2006. Zotarolimus (ABT-578) eluting stents. *Advanced Drug Delivery Reviews* **58**(3): 437-446.

Cheol Whan L, Duk-Woo P, Seung-Hwan L, Young-Hak K, Myeong-Ki H, Jae-Joong K, Seong-Wook P, Sung-Cheol Y, In-Whan S, Jae-Hwan L et al. 2009. Comparison of the Efficacy and Safety of Zotarolimus-, Sirolimus-, and Paclitaxel-Eluting Stents in Patients With ST-Elevation Myocardial Infarction. *The American Journal of Cardiology* **104**(10): 1370-1376.

Christen T, Bochaton-Piallat M-L, Neuville P, Rensen S, Redard M, van Eys G, Gabbiani G. 1999. Cultured Porcine Coronary Artery Smooth Muscle Cells : A New Model With Advanced Differentiation. *Circulation Research* **85**(1): 99-107.

Christen T, Verin V, Bochaton-Piallat M-L, Popowski Y, Ramaekers F, Debruyne P, Camenzind E, van Eys G, Gabbiani G. 2001. Mechanisms of Neointima Formation and Remodeling in the Porcine Coronary Artery. *Circulation* **103**(6): 882-888.

Coombes KR. 2010. ClassComparison: Classes and methods for "class comparison" problems on microarrays.

Costa MA, Simon DI. 2005. Molecular Basis of Restenosis and Drug-Eluting Stents. *Circulation* **111**(17): 2257-2273.

Dollery CM, McEwan JR, Henney AM. 1995. Matrix Metalloproteinases and Cardiovascular Disease. *Circ Res* **77**(5): 863-868.

Feldman LJ, Mazighi M, Scheuble A, Deux J-Fß, De Benedetti E, Badier-Commander Cc, Brambilla E, Henin D, Steg PG, Jacob M-P. 2001. Differential Expression of Matrix Metalloproteinases After Stent Implantation and Balloon Angioplasty in the Hypercholesterolemic Rabbit. *Circulation* **103**(25): 3117-3122.

Finn AV, Gold HK, Tang A, Weber DK, Wight TN, Clermont A, Virmani R, Kolodgie FD. 2002. A Novel Rat Model of Carotid Artery Stenting for the Understanding of Restenosis in Metabolic Diseases. *Journal of Vascular Research* **39**(5): 414-425.

Fischman DL, Leon MB, Baim DS, Schatz RA, Savage MP, Penn I, Detre K, Veltri L, Ricci D, Nobuyoshi M et al. 1994. A Randomized Comparison of Coronary-Stent Placement and Balloon Angioplasty in the Treatment of Coronary Artery Disease. *New England Journal of Medicine* **331**(8): 496-501.

Ge J, Shen C, Liang C, Chen L, Qian J, Chen H. 2006. Elevated matrix metalloproteinase expression after stent implantation is associated with restenosis. *International Journal of Cardiology* **112**(1): 85-90.

Godin D, Ivan E, Johnson C, Magid R, Galis ZS. 2000. Remodeling of Carotid Artery Is Associated With Increased Expression of Matrix Metalloproteinases in Mouse Blood Flow Cessation Model. *Circulation* **102**(23): 2861-2866.

Gomes WJ, Giannotti-Filho O, Hossne NA, Jr, Catani R, Buffolo E. 2005. Inflammatory Reaction After Sirolimus-Eluting Stent Implant. *Ann Thorac Surg* **80**(5): 1903-1904.

Grüntzig AR, Senning Å, Siegenthaler WE. 1979. Nonoperative Dilatation of Coronary-Artery Stenosis. *New England Journal of Medicine* **301**(2): 61-68.

Ihara E, Hirano K, Hirano M, Nishimura J, Nawata H, Kanaide H. 2002. Mechanism of down-regulation of L-type Ca2+ channel in the proliferating smooth muscle cells of rat aorta. *Journal of Cellular Biochemistry* **87**(2): 242-251.

James TW, Wagner R, White LA, Zwolak RM, Brinckerhoff CE. 1993. Induction of collagenase and stromelysin gene expression by mechanical injury in a vascular smooth muscle-derived cell line. *J Cell Physiol* **157**(2): 426-437.

Johnson JL, Dwivedi A, Somerville M, George SJ, Newby AC. 2011. Matrix Metalloproteinase (MMP)-3 Activates MMP-9 Mediated Vascular Smooth Muscle Cell Migration and Neointima Formation in Mice. *Arteriosclerosis, Thrombosis, and Vascular Biology* **31**(9): e35-e44.

Jones GT, Tarr GP, Phillips LV, Wilkins GT, van Rij AM, Williams MJA. 2009. Active matrix metalloproteinases 3 and 9 are independently associated with coronary artery in-stent restenosis *Atherosclerosis* **207**(2): 5.

Kandzari DE, Leon MB. 2006. Overview of Pharmacology and Clinical Trials Program with the Zotarolimus-Eluting Endeavor Stent. *Journal of Interventional Cardiology* **19**(5): 405-413.

Katsaros KM, Kastl SP, Zorn G, Maurer G, Wojta J, Huber K, Christ G, Speidl WS. 2010. Increased Restenosis Rate After Implantation of Drug-Eluting Stents in Patients With Elevated Serum Activity of Matrix Metalloproteinase-2 and -9. *J Am Coll Cardiol Intv* **3**(1): 90-97.

Kuzuya M, Iguchi A. 2003. Role of Matrix Metalloproteinases in Vascular Remodeling. *Journal of Atherosclerosis and Thrombosis* **10**(5): 275-282.

Lewis AL, Stratford PW. 2002. Phosphorylcholine-Coated Stents. *Journal of Long-Term Effects of Medical Implants* **12**(4): 20.

Li J-m, Zhang X, Nelson PR, Odgren PR, Nelson JD, Vasiliu C, Park J, Morris M, Lian J, Cutler BS et al. 2007. Temporal evolution of gene expression in rat carotid artery following balloon angioplasty. *Journal of Cellular Biochemistry* **101**(2): 399-410.

Marx SO, Marks AR. 2001. Bench to Bedside: The Development of Rapamycin and Its Application to Stent Restenosis. *Circulation* **104**(8): 852-855.

Mootha VK, Lindgren CM, Eriksson KF, Subramanian A, Sihag S, Lehar J, Puigserver P, Carlsson E, Ridderstrale M, Laurila E et al. 2003. PGC-1alpha-responsive genes involved in oxidative phosphorylation are coordinately downregulated in human diabetes. *Nat Genet* **34**(3): 267-273.

Muldowney JAS, III, Stringham JR, Levy SE, Gleaves LA, Eren M, Piana RN, Vaughan DE. 2007. Antiproliferative Agents Alter Vascular Plasminogen Activator Inhibitor-1 Expression: A Potential Prothrombotic Mechanism of Drug-Eluting Stents. *Arterioscler Thromb Vasc Biol* **27**(2): 400-406.

Neylon CB, Lang RJ, Fu Y, Bobik A, Reinhart PH. 1999. Molecular Cloning and Characterization of the Intermediate-Conductance Ca2+-Activated K+

Channel in Vascular Smooth Muscle : Relationship Between KCa Channel Diversity and Smooth Muscle Cell Function. *Circulation Research* **85**(9): e33-e43.

Pendyala L, Jabara R, Shinke T, Chronos N, Robinson K, Li J, Hou D. 2008. Drug-Eluting Stents: Present and Future. *Cardiovascular & Hematological Agents in Medicinal Chemistry* **6**: 105-115.

Quignard J-Fß, Harricane M-Cc, M√©nard C, Lory P, Nargeot Jl, Capron LØ, Mornet D, Richard S. 2001. Transient down-regulation of L-type Ca2+ channel and dystrophin expression after balloon injury in rat aortic cells. *Cardiovascular Research* **49**(1): 177-188.

Rasmussen K, Maeng M, Kaltoft A, Thayssen P, Kelbæk H, Tilsted HH, Abildgaard U, Christiansen EH, Engstrøm T, Krusell LR et al. 2010. Efficacy and safety of zotarolimus-eluting and sirolimus-eluting coronary stents in routine clinical care (SORT OUT III): a randomised controlled superiority trial. *The Lancet* **375**(9720): 1090-1099.

Richard S, Neveu D, Carnac G, Bodin P, Travo P, Nargeot J. 1992. Differential expression of voltage-gated Ca2+-currents in cultivated aortic myocytes. *Biochimica et Biophysica Acta (BBA) - Protein Structure and Molecular Enzymology* **1160**(1): 95-104.

Serruys PW, de Jaegere P, Kiemeneij F, Macaya C, Rutsch W, Heyndrickx G, Emanuelsson H, Marco J, Legrand V, Materne P et al. 1994. A Comparison of Balloon-Expandable-Stent Implantation with Balloon Angioplasty in Patients with Coronary Artery Disease. *New England Journal of Medicine* **331**(8): 489-495.

Si H, Grgic I, Heyken W-T, Maier T, Hoyer J, Reusch H-P, Köhler R. 2006. Mitogenic modulation of Ca2+-activated K+ channels in proliferating A7r5 vascular smooth muscle cells. *British Journal of Pharmacology* **148**(7): 909-917.

Sigwart U, Puel J, Mirkovitch V, Joffre F, Kappenberger L. 1987. Intravascular Stents to Prevent Occlusion and Re-Stenosis after Transluminal Angioplasty. *New England Journal of Medicine* **316**(12): 701-706.

Subramanian A, Tamayo P, Mootha VK, Mukherjee S, Ebert BL, Gillette MA, Paulovich A, Pomeroy SL, Golub TR, Lander ES et al. 2005. Gene set enrichment

analysis: A knowledge-based approach for interpreting genome-wide expression profiles. *Proceedings of the National Academy of Sciences of the United States of America* **102**(43): 15545-15550.

Suzuki K, Enghild JJ, Morodomi T, Salvesen G, Nagase H. 1990. Mechanisms of activation of tissue procollagenase by matrix metalloproteinase 3 (stromelysin). *Biochemistry* **29**(44): 10261-10270.

van der Loop FT, Schaart G, Timmer ED, Ramaekers FC, van Eys GJ. 1996. Smoothelin, a novel cytoskeletal protein specific for smooth muscle cells. *The Journal of Cell Biology* **134**(2): 401-411.

Virmani R, Kolodgie FD, Finn AV, Gold HK. Pathological Anatomy of Restenosis. 47-58.

Visse R, Nagase H. 2003. Matrix Metalloproteinases and Tissue Inhibitors of Metalloproteinases: Structure, Function, and Biochemistry. *Circ Res* **92**(8): 827-839.

Welt FGP, Rogers C. 2002. Inflammation and Restenosis in the Stent Era. *Arterioscler Thromb Vasc Biol* **22**(11): 1769-1776.

Will H, Atkinson SJ, Butler GS, Smith B, Murphy G. 1996. The Soluble Catalytic Domain of Membrane Type 1 Matrix Metalloproteinase Cleaves the Propeptide of Progelatinase A and Initiates Autoproteolytic Activation. *Journal of Biological Chemistry* **271**(29): 17119-17123.

Wu Y-W, Yang W-S, Chen M-F, Lee B-C, Hung C-S, Liu Y-C, Jeng J-S, Huang P-J, Kao H-L. 2008. High Serum Level of Matrix Metalloproteinase-1 and Its Rapid Surge After Intervention in Patients with Significant Carotid Atherosclerosis. *Journal of the Formosan Medical Association* **107**(1): 6.

Zohlnhofer D, Klein CA, Richter T, Brandl R, Murr A, Nuhrenberg T, Schomig A, Baeuerle PA, Neumann F-J. 2001. Gene Expression Profiling of Human Stent-Induced Neointima by cDNA Array Analysis of Microscopic Specimens Retrieved by Helix Cutter Atherectomy : Detection of FK506-Binding Protein 12 Upregulation. *Circulation* **103**(10): 1396-1402.

CHAPTER 4

REVERSIBLE EXPRESSION OF EPITHELIAL CELL MARKERS AND PHENOTYPES IN OVARIAN CANCER CELLS TREATED WITH MIR-429

4.1. Introduction

Ovarian cancer is the eighth most common cancer and fifth most common cause of cancer deaths among women in the USA with an annual incidence rate of 12.2 per 100,000 and annual death rate of 8 per 100,000 in 2007 (Group 2012). Although the overall 5-year relative survival rate is 43.2%, mortality is high because 70% of ovarian cancers are diagnosed after metastatic spread of the tumor (Cho and Shih Ie 2009; Howlader et al. 2012). In the US in 2009, an estimated 1 in 72 women would develop ovarian cancer in their lifetime (Howlader et al. 2012). Globally, ovarian cancer is the sixth most common cancer in women, and more than 90% of primary malignant ovarian tumors are epithelial in origin (Sankaranarayanan and Ferlay 2006).

Unlike other solid tumors that go through multiple steps of extravasation before metastasizing through the blood circulatory system, ovarian cancer cells typically metastasize by direct contact with adjacent organs or by detaching from the primary tumor (Gupta and Massague 2006). Detached tumor cells can then travel in peritoneal fluids throughout the abdominal cavity. In this manner,

carcinoma can attach to reproductive organs, the omentum, or the sigmoid colon. Additionally, metastasized carcinoma can also be transported via the lymph node system (Eisenkop and Spirtos 2001).

The epithelial-mesenchymal transition (EMT) of ovarian surface epithelium (OSE) is thought to normally be involved in postovulatory repair, where the transition to a mesenchymal phenotype provides the motility and proliferation necessary for extracellular matrix remodeling (Salamanca et al. 2004). The transition is typical of cellular transformations crucial in embryogenesis, such as mesoderm formation, neural crest development, and secondary palate formation, as well as in organogenesis. EMT is also the first step in the epithelial-mesenchymal-epithelial transitions during ovarian carcinoma metastasis, beginning with the disruption of E-cadherin-mediated cell-cell interactions (Ahmed et al. 2007). This permits epithelial cells to detach from the basement membrane and loosens connections between carcinoma cells. Once detached these cells can now enter the peritoneal fluid, and be passively moved into the coelomic space. The cancer cells also acquire a mesenchymal phenotype becoming spindle-like, and more motile.

The reverse process, known as the mesenchymal-epithelial transition (MET) is involved in reverting the motile mesenchymal-like ovarian cancer cells created via EMT to a more epithelial-like phenotype at the secondary tumor site. E-cadherin, known to induce the MET pathway, is expressed in both primary and metastatic ovarian carcinomas, but not normal ovarian surface epithelium (Veatch et al. 1994; Darai et al. 1997; Maines-Bandiera and Auersperg 1997; Davies et al. 1998). E-cadherin expression in human ovarian surface epithelium induces the localization of

E-cadherin, catenins, and f-actin to the locations of cell-cell contact, gaining epithelial characteristics associated with MET (Auersperg et al. 1999). Consistent with this, work in a human bladder cancer model has shown that MET contributes to the establishment of metastatic deposits, where targeted abrogation of FGF pathways involved in MET both reverses MET and increases survival in TSU-Pr1 tumor cell line inoculated mice (Chaffer et al. 2005; Chaffer et al. 2006). MET occurs naturally during somitogenesis, kidney formation, and coelomic-cavity formation, and work done in these areas has identified important modulators likely to be involved in cancer metastasis (Saga and Takeda 2001; Vainio and Lin 2002). Given the plasticity of the native ovarian surface epithelium, MET is thought to be the molecular reversal of EMT (Wong and Leung 2007).

At the same time, our understanding about the mechanisms involved in MET is incomplete, particularly in its role in cancer progression. E-cadherin is involved in signaling capable of inducing MET in human ovarian surface epithelium (Auersperg 1999). Studies comparing primary ovarian carcinomas to metastases demonstrated lower Snail expression in metastases than in primary carcinomas, higher expression of Twist1 and Zeb1 in metastases, and the regulation of Snail localization by Pak1, leading to E-cadherin re-expression in metastases (Elloul et al. 2010). EMT induced by TGF-β1 signaling through a Smads-dependent pathway in rat and human alveolar epithelial-like cells could be reversed, via the MAPK/ERK kinase pathway, by culturing with FGF-1 for 48 hours, suggesting that EMT and MET might arise from induction of separate pathways rather than reversing the induction of a single pathway (Ramos et al. 2010). These experiments outline the complex signaling

involved in both EMT and MET coordinated by the actions of multiple gene products.

microRNA (miRNA) are an extensive class of small (18-24 nt) endogenous regulatory non-coding RNAs that post-transcriptionally regulate gene expression in plants and animals (Bartel 2004). They were originally discovered as a small RNA, encoded by the lin-4 gene, capable of binding the 3' untranslated region of lin-14 mRNA and inhibiting its translation in *Caenorhabditis elegans* (Wightman et al. 1993). A miRNA begins as a hairpin structure that forms from a larger transcript, called a pri-miRNA (Lee et al. 2004b). This stem-loop structure is then recognized and cut by Drosha/DGCR8, leaving a 60-nucleotide pre-miRNA (Han et al. 2004). Dicer, a RNAse III enzyme, further processes the pre-miRNA into a 21-23 nt double-stranded RNA duplex, of which one strand is incorporated into the RNA-induced silencing complex (RISC), comprised of dicer, TAR (HIV-1) RNA binding protein (TRBP), and argonaute (Lin et al. 2005). miRNAs block the translation of target mRNAs by imperfectly base pairing with specific sequences in the 3' untranslated regions of their target mRNA and inhibiting translation or promoting degradation via the RNA-induced silencing complex. miRNAs are particularly attractive for use as cancer therapies because individual miRNAs can post-transcriptionally regulate tens to hundreds of genes at once (Brennecke et al. 2005; Wu and Belasco 2008).

A regulatory role for microRNAs in metastasis-related EMT and MET has been elucidated from studies examining miRNA abundance in metastatic cancer tissue (Pigati et al. 2010; Guttilla et al. 2012; Moes et al. 2012; Ru et al. 2012). They suggest potential therapies where individual miRNAs or suites of miRNAs may be

used to control the metastatic process. Multiple *in vitro* studies examining miRNA transfections of cancer cell lines highlight a role for miRNAs in the inhibition of EMT in different cancer cell lines via a diverse set of targets and potential pathways. Forced miR-7 expression in breast cancer cells up-regulated E-cadherin and down-regulated vimentin and fibronectin expression, while at the same time suppressing tumor cell proliferation, anchorage independent growth, migration, and invasion in aggressive breast cancer cell lines (Kong et al. 2012). The invasive fronts of primary colorectal cancers showed lower expression of miR-200c and miR-141 than their matched liver metastatic tissue (Hur et al. 2012). Transfection of the primary colorectal cancers suppressed invasion and migration, but also led to cell proliferation, as well as increased E-cadherin and decreased vimentin expression. Over-expression of miR-429 in HEY cells, mesenchymal-like cells derived from papillary cystadenocarcinoma of the ovary, resulted in decreased migration, suppression of anchorage-independent growth, as well as a change in morphology from an elongated, spindle shaped, mesenchymal phenotype to a rounded, epithelial-like phenotype (Chen et al. 2011). This was accompanied by decreases in *ZEB1* and *ZEB2*, known activators of EMT and targets of miR-429, and increases in E-cadherin expression. miR-429 belongs to the miRNA-200 family of microRNAs, identified as important regulators in EMT-associated cancer metastasis (Gregory et al. 2008a; Korpal and Kang 2008; Paterson et al. 2008; Chen et al. 2011; Shahab et al. 2011).

Our study represents the first time course analysis of miR-429-induced MET in ovarian cancer cells. We transfected Hey cells with miR-429 and assayed gene

expression over the course of 144 hours at regular intervals. The cell morphology and gene expression of our transfected cells changed to become more epithelial-like at 24 and 48 hours and then became more mesenchymal-like by 144 hours. By 144 hours the average gene expression levels for 98.6% of our genes were not significantly different from the levels they started from at 0 hours when we adjusted for baseline expression changes observed in our negative control treated cells. We also examine the pathways and genes that are differentially expressed in the 0-48 hour and 48-144 hour time spans.

4.2. Methods

4.2.1 Cell lines and transfection

The HEY cell line was derived from a patient with moderately differentiated papillary cystadenocarcinoma of the ovary (Buick et al. 1985). The HEY cell line was kindly provided by Gordon Mills, Department of Molecular Therapeutics, University of Texas, MD Anderson Cancer Center. HEY cells were cultured in R10 medium: RPMI 1640 medium supplemented with 10% fetal bovine serum (FBS, Atlanta Biologicals, Lawrenceville, GA) and 1% antibiotic-antimycotic solution (Mediatech-Cellgro, Manassas, VA)

Cells were harvested after Trypsin/EDTA treatment, the cell pellet was suspended in growth medium, then counted to determine density before being diluted to $5x10^4$ cells/mL. 10^5 cells per well were seeded into four 6-well plates and allowed to grow for 24 hours. After 24 hours, cells were harvested from one plate as 0 hour samples.

On the remaining three plates, cells in three wells were transfected with 30 nM of miR-429 miRNA oligonucleotides (Life Technologies, Grand Island, NY) and cells in the remaining three wells were transfected with Pre-miR™ miRNA Precursor Negative Control #1 (Life Technologies, Grand Island, NY), using Lipofectamine 2000 reagent (Life technologies, Grand Island, NY). These transfected plates were incubated at 37°C and 5% CO_2 for four hours, whereupon the medium was changed to R10 medium. At 24 hours following transfection, cells were harvested from one plate for the 24-hour timepoint. Then at 48 hours following transfection, cells were harvested from another plate for the 48-hour timepoint. At 72 hours following transfection, cells were split from the remaining plate and allowed to continue to grow. Finally at 144 hours following transfection, cells in the remaining plate were harvested for the 144-hour time point.

4.2.2 RNA Quantification, microarray assays

Total RNA was isolated from harvested cells using the RNeasy Mini RNA isolation kit (QIAGEN, Valencia, CA). The integrity of the RNA was verified using an Agilent 2100 Bioanalyzer (1.8-2.0; Agilent Technologies, Palo Alto, CA). mRNAs were converted to double stranded (ds)-cDNA and amplified using Applause 3'-Amp System (NuGen, San Carlos, CA). This cDNA was fragmented and biotin labeled using the Encode Biotin Module (NuGen), hybridized to Affymetrix HG-U133 Plus 2.0 oligonucleotide arrays and analyzed with a GeneChip Scanner 3000 (Affymetrix, Santa Clara, CA).

4.2.3 Statistical analysis

Robust Microarray Averaging (RMA) was used for normalization of microarray signal and summarization using the Affymetrix Microarray Suite (Affymetrix Inc. Santa Clara, CA) (Irizarry et al. 2003). Statistical analysis of the expression data was carried out using the R statistical programming environment (R Development Core Team 2010). Genes with significant differential expression over the entire time course from 0 to 144 hours were identified using a two regression step approach in the maSigPro R package where individual gene expression across time (0 to 144 hours) is modeled with a global regression model and then genes with significantly different expression models in the miR-429 treated cells compared to the negative control treated cells are identified using a comparison of model coefficients (Conesa et al. 2006). This allows us to ask for each gene if its expression profile in miR-429-treated cells is significantly different from its expression profile in negative-control treated cells across the entire time period (0, 24, 48, and 144 hours). We used a significance level of 0.05 for the global regression model, and false-discovery rate controlled significance level of 0.05 and r-squared cut-off of 0.6 for the step-wise regression used in the variable selection. For the comparisons of only two time points, we used a linear modeling method in the Limma R package where differential expression changes were tested for significance using a moderated F-test (Smyth 2004). Results from both selection methods were further analyzed using GeneGO to perform gene enrichment to determine those pathways that showed larger numbers of differentially expressed constituents than would otherwise be expected by chance (GeneGO Inc., Carlsbad, CA). Significantly enriched GeneGO pathways were chosen for a false discovery rate of 0.05.

4.3. Results

To characterize the transcriptomic effects of miR-429 transfection in HEY cells, we conducted a high-density expression microarray profiling analysis (Affymetrix HG-U133 Plus 2.0) comparing HEY cells treated with miR-429 with negative controls treated with a non-targeted miRNA. We sampled our treatment and control cells at 0 (pre-transfection), 24, 48, and 144 hours post-transfection to examine the expression changes in these cells over time.

4.3.1 Time course analysis (0-144 hours)

Of particular interest are genes that both change significantly over the time course and show a course of expression that is significantly different from that of the negative control. To achieve this, we used a two-step linear regression algorithm that identifies genes with statistically significant changes through time and between different cell treatments (Conesa et al. 2006). Our time course analysis results show that 3635 genes were significantly differentially up or down regulated compared with the negative control over the time course (false discovery rate < 0.05). Mesenchymal markers like *FN1* (fibronectin) were significantly down-regulated, while epithelial markers like *CAV2* (caveolin 2), *CTNND1* (cadherin-associated protein, delta 1), *KRT8* (keratin, type II cytoskeletal 8) and *DSP* (desmoplakin) were significantly up-regulated (Turley et al. 2008) (Table 4.1). Transcription factors associated with metastasis like *ZEB1* (zinc finger E-box-binding homeobox 1), and *ZEB2* (zinc finger E-box-binding homeobox 2) are down-regulated (Davidson et al. 2012). Signaling molecules involved in MET, like *FGF1* (fibroblast growth factor 1

Table 4.1. *Multiple genes associated with EMT or MET are differentially expressed across the 144 hour time course*
These selected genes are those that are known to be involved in EMT or MET processes and are differentially expressed across the time course (0-144 hours) by maSigPro (FDR = 0.05). The fold change values compare the miR-429-treated cells' average expression to the negative control-treated cells' average expression at each time point (24, 48, and 144 hours).

		Fold change in miR-429 treated cells			Time course
Probe ID	Symbol	24 hours	48 hours	144 hours	p-value
220016_at	AHNAK	-0.63	-0.35	0.95	7.05E-10
203323_at	CAV2	2.21	2.21	0.67	9.20E-07
203324_s_at	CAV2	0.69	0.95	0.35	2.88E-09
213426_s_at	CAV2	0.96	1.13	0.28	1.46E-06
203440_at	CDH2	0.27	0.05	-0.14	0.000233764
1556499_s_at	COL1A1	-0.56	-0.80	-0.42	5.60E-09
202310_s_at	COL1A1	-0.04	-0.39	-0.32	2.99E-09
208407_s_at	CTNND1	0.41	0.40	0.08	5.32E-08
200606_at	DSP	1.20	1.49	0.86	3.76E-10
1552721_a_at	FGF1	0.81	0.96	-0.41	2.33E-10
204421_s_at	FGF2	1.29	0.53	0.01	1.92E-08
204422_s_at	FGF2	1.62	1.71	-0.04	6.91E-12
205014_at	FGFBP1	1.94	1.60	2.79	3.36E-07
210495_x_at	FN1	-1.65	-2.70	-0.13	2.53E-06
211719_x_at	FN1	-1.70	-2.66	-0.12	1.31E-06
212464_s_at	FN1	-1.68	-2.76	-0.05	4.03E-06
214702_at	FN1	-0.67	-1.66	-0.33	7.10E-05
216442_x_at	FN1	-1.58	-2.63	-0.11	4.54E-06
204115_at	GNG11	-0.78	-0.49	0.09	0.000205213
1561633_at	HMGA2	-0.92	-0.14	0.00	1.64E-05
208025_s_at	HMGA2	0.17	-0.36	-0.20	8.88E-16
201508_at	IGFBP4	-0.38	-0.15	0.16	0.000128644
209008_x_at	KRT8	0.29	0.90	0.68	9.49E-06
226066_at	MITF	0.19	0.54	-0.33	8.80E-10
200600_at	MSN	-0.66	-0.51	0.28	2.03E-05
205455_at	MST1R	0.49	0.60	0.48	1.44E-05
207924_x_at	PAX8	-0.04	0.09	0.44	8.90E-06
221990_at	PAX8	-0.81	-0.46	0.06	2.06E-07
202627_s_at	SERPINE1	-0.78	0.11	0.99	3.25E-06
203076_s_at	SMAD2	-0.49	-0.59	0.07	3.55E-09
226563_at	SMAD2	-0.28	-0.52	-0.23	0.000342423
204790_at	SMAD7	0.82	-0.14	-0.82	1.61E-07
209875_s_at	SPP1	-0.10	-1.03	-0.38	6.05E-13
205542_at	STEAP1	-0.31	-0.11	0.09	4.29E-05
212385_at	TCF4	0.05	-0.82	-0.73	6.28E-05
213891_s_at	TCF4	-0.48	-0.74	-0.26	1.63E-07

Table 4.1 (continued)					
202011_at	TJP1	1.04	0.89	0.04	0.00108346
218834_s_at	TMEM132A	-1.12	-1.06	0.15	7.68E-05
217979_at	TSPAN13	0.21	0.27	0.33	2.24E-06
204619_s_at	VCAN	0.89	0.92	0.22	4.28E-05
204620_s_at	VCAN	0.95	0.95	0.14	8.69E-05
215646_s_at	VCAN	1.04	0.99	-0.37	0.001017159
221731_x_at	VCAN	0.65	0.97	0.18	5.41E-05
212764_at	ZEB1	-1.29	-1.72	-0.14	1.33E-07
239952_at	ZEB1	-1.17	-1.36	-0.20	1.33E-05
203603_s_at	ZEB2	-0.43	-1.12	-0.33	2.14E-05

(acidic)), and in EMT, like *FGF2* (fibroblast growth factor 2 (basic)), are up-regulated (Thiery 2002).

4.3.1.1 Characteristic expression response to miR-429 is temporary

For those genes that are differentially expressed across the time course, we noted a characteristic gene expression response to the treatment with miR-429. Expression levels for many of these genes reach a maximum or minimum at 24 or 48 hours (Figure 4.1). We also noted that expression levels appeared similar at 0 and 144 hours for many genes, so we asked if the average expression levels in miR-429 treated Hey cells at 0 hour were significantly different from the average level at 144 hours, corrected for the change in expression observed in the negative control-treated cells over the same time interval. By 144 hours, 98.6% (3585 out of 3635) of genes that were differentially expressed across the time course had returned to expression levels that were not significantly different from their expression at 0 hours (FDR = 0.05) (Figure 4.2).

4.3.1.2 Small number of genes do not return to 0 hour expression levels following miR-429 treatment

We were then interested in the function of those 50 genes that showed significantly different average expression at 144 hours compared to their expression at 0 hours (Table 4.2). Of particular interest, for their potential involvement in EMT/MET, were *Wnt7A, IL-1β, SERPINE1*, and *LAMC2* (Figure 4.3). Moreover, *FGD6*, which may activate *CDC42* and play a role in cell cycle signaling, and *DCLK1*, a doublecortin and calmodulin-like kinase that shows expression in human hippocampal and cortical tissue, are targets of miR-429, though both genes show up-regulated expression by

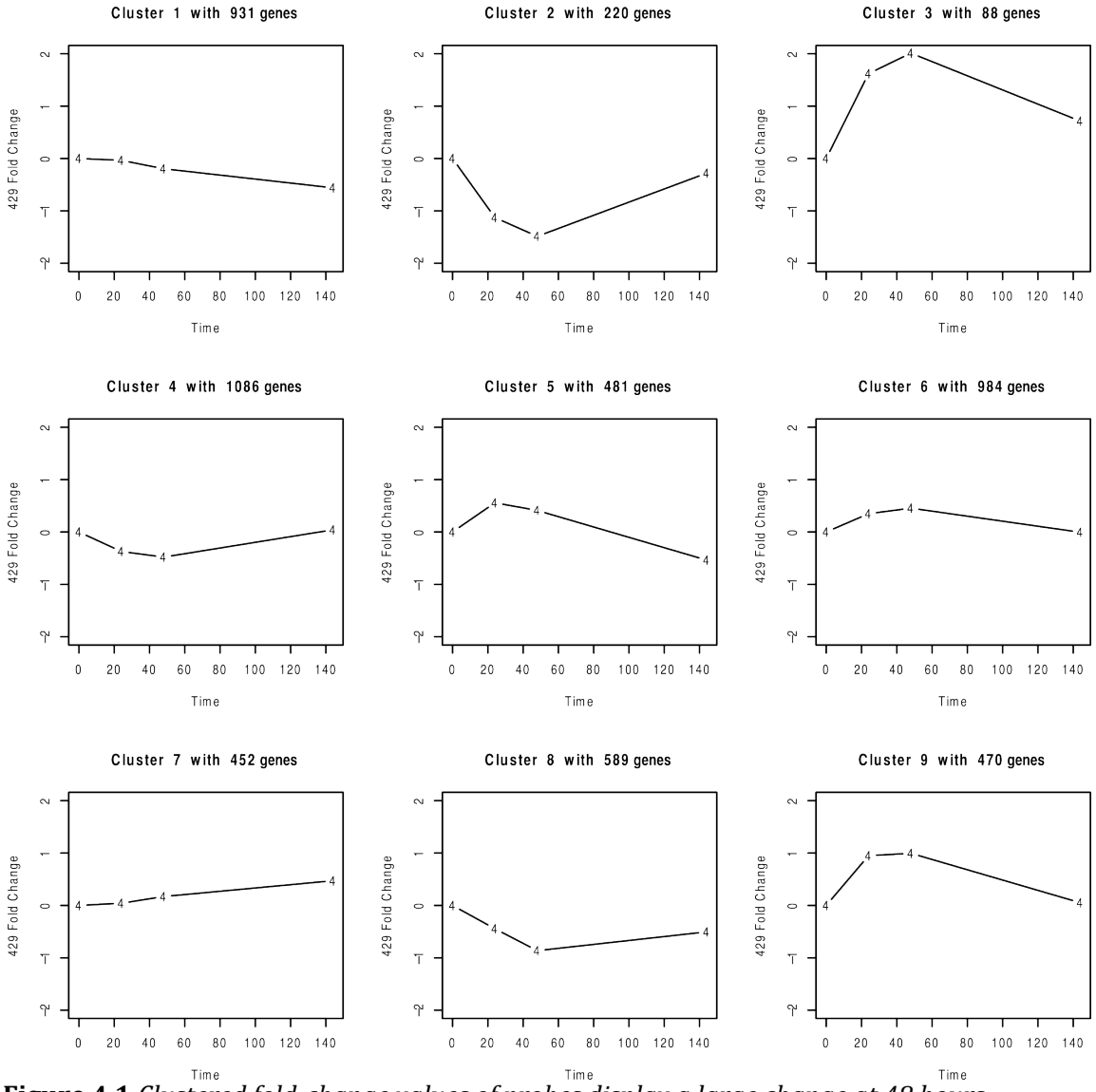

Figure 4.1 *Clustered fold-change values of probes display a large change at 48 hours*
The lines labeled as 4 show overall expression patterns common to our set of genes that are significantly differentially expressed genes over the time course (0-144 hours). Partitioning is performed by k-means clustering on the fold-change values of each gene into 9 groups.

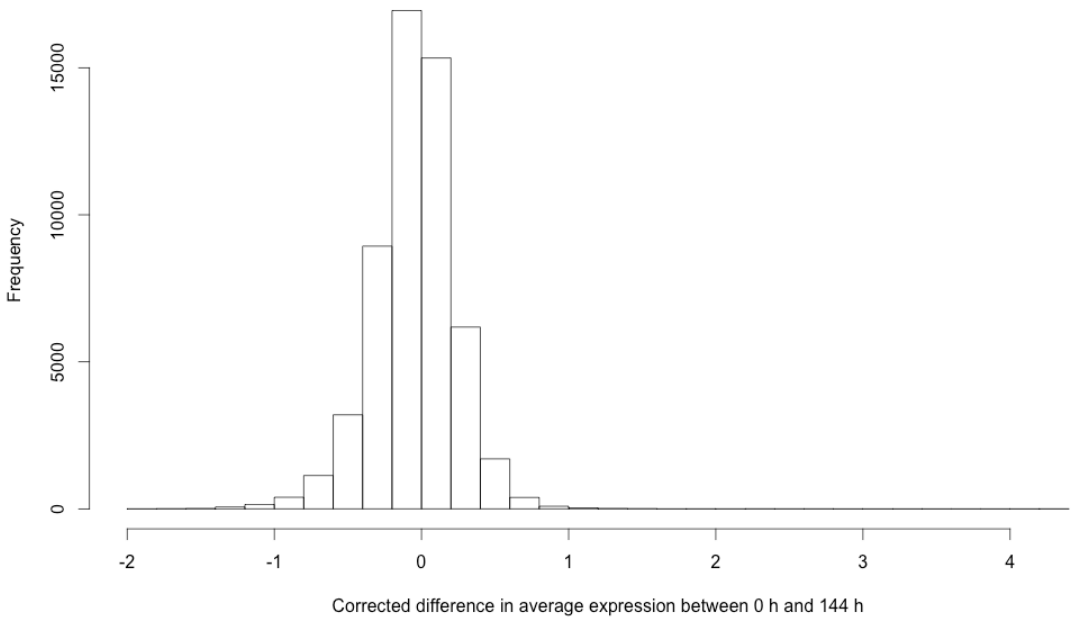

Figure 4.2 *By 144 hours, most genes in miR-429 treated cells have the same average expression as at 0 hours*
Histogram of corrected differences of average expression at 0 hours compared to 144 hours for all genes assayed. To correct for baseline changes, we subtracted the change in average expression for cells treated with the negative control between 0 h and 144 h from the change observed in cells treated with miR-429 during the same time.

Table 4.2 *Genes that do not return to their 0 hour expression levels by 144 hours post-transfection*

These genes showed a significantly large corrected difference of average expression at 0 hours compared to 144 hours out of all genes. To correct for baseline changes, we subtracted the change in average expression for cells treated with the negative control between 0 h and 144 h from the change observed in cells treated with miR-429 during the same time, listed here as the corrected difference.

Probe ID	Symbol	Corrected difference	p-value
222108_at	AMIGO2	-1.08	1.35E-06
230875_s_at	ATP11A	-0.99	5.22E-05
218723_s_at	C13orf15	2.41	2.56E-07
228193_s_at	C13orf15	2.32	3.62E-07
219010_at	C1orf106	-1.00	1.01E-05
230339_at	CCDC138	-1.12	1.18E-05
243864_at	CCDC80	-1.10	4.73E-05
223655_at	CD163L1	-1.20	1.92E-06
226187_at	CDS1	1.54	2.16E-05
1569183_a_at	CHM	-1.30	1.36E-05
233396_s_at	CSRP2BP	-0.99	4.38E-05
226393_at	CYP2U1	-1.32	8.95E-06
205399_at	DCLK1	1.36	6.69E-07
226281_at	DNER	-1.35	3.51E-06
205741_s_at	DTNA	-0.85	4.29E-05
228361_at	E2F2	-1.14	4.33E-05
200878_at	EPAS1	1.51	9.11E-08
213929_at	EXPH5	1.06	1.13E-05
223000_s_at	F11R	0.97	2.91E-05
241456_at	FAM78B	-1.78	3.43E-05
1555137_a_at	FGD6	1.72	2.13E-07
219901_at	FGD6	1.21	4.93E-05
205014_at	FGFBP1	2.79	1.57E-10
204417_at	GALC	1.42	3.32E-05
215243_s_at	GJB3	1.33	2.63E-06
205490_x_at	GJB3	1.50	6.98E-06
214467_at	GPR65	4.33	6.21E-12
218537_at	HCFC1R1	0.92	4.64E-05

Table 4.2 (continued)			
39402_at	IL1B	1.28	1.61E-06
205067_at	IL1B	1.25	3.37E-05
228414_at	KCNMA1	-1.61	2.93E-05
202267_at	LAMC2	1.15	6.43E-07
222561_at	LANCL2	-1.20	5.17E-07
206483_at	LRRC6	-1.13	1.79E-05
204475_at	MMP1	2.08	4.69E-08
206186_at	MPP3	-1.31	5.17E-05
236718_at	MYO10	-1.05	7.81E-06
232317_at	PLXNA4	-1.36	1.68E-06
230015_at	PRCD	1.42	1.40E-06
232532_at	QRICH2	-1.08	3.09E-05
206884_s_at	SCEL	2.36	1.86E-08
232056_at	SCEL	2.40	4.74E-07
202627_s_at	SERPINE1	0.99	2.21E-05
222838_at	SLAMF7	-1.32	9.55E-06
202816_s_at	SS18	-0.92	2.72E-05
235086_at	THBS1	-1.35	6.45E-07
210248_at	WNT7A	1.85	6.40E-06
219836_at	ZBED2	2.67	2.96E-06
222016_s_at	ZNF323	-1.79	4.35E-06

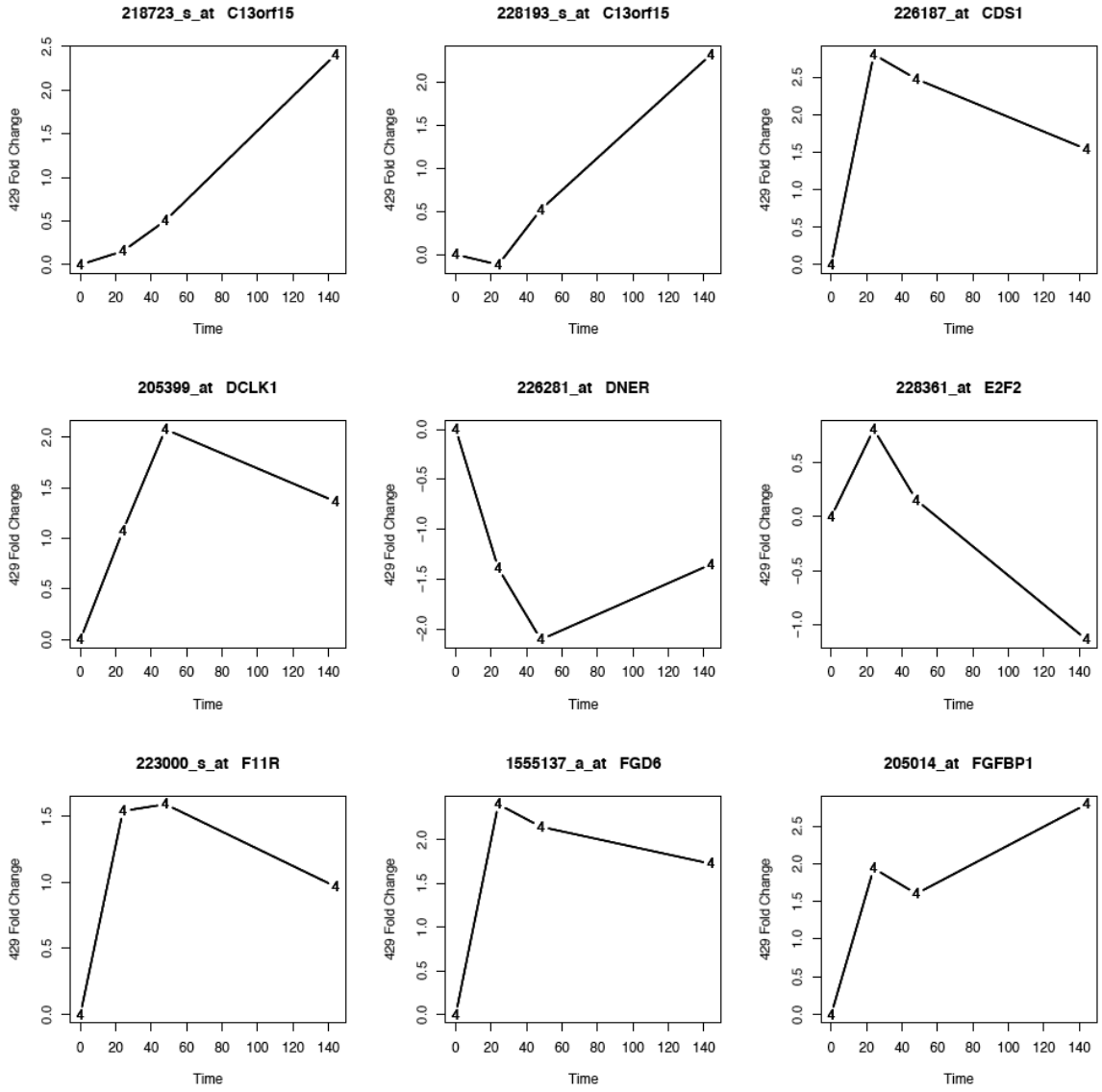

Figure 4.3 *Fold-change over time of selected genes with significantly different expression at 144 hours than at 0 hours*

Expression patterns of genes that are thought to be involved in EMT or MET or otherwise predicted targets of miR-429, depicting fold-change over the experimental time course. The expression across time is indicate by the curve labeled "4".

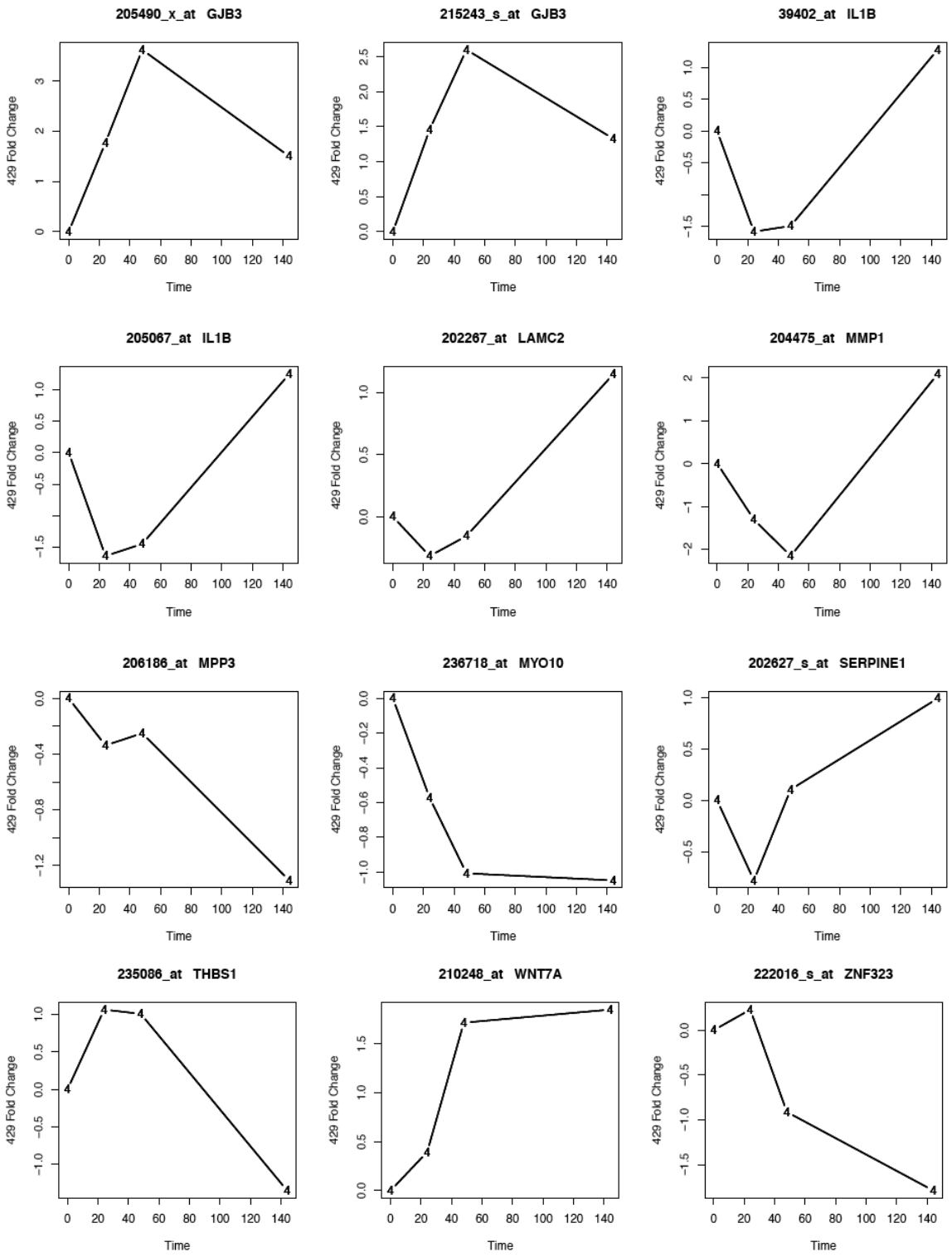

Figure 4.3 (continued)

144 hours in our treated samples (Havik et al. 2012). Response gene to complement 32 (*C13orf15*) is up-regulated through the entire time course, and is known to mediate EMT in human renal proximal cells (Huang et al. 2009). *E2F2* is a transcription factor involved in cell cycle regulation observed to be over-expressed in nonepithelial ovarian cancers compared to normal ovaries, and is down regulated in our miR-429-treated samples (Vui-Kee et al. 2012). Lamin gamma 2 (*LAMC2*), a component of the lamins that are a constituent of basement membranes and were observed to be up-expressed in ovarian metastatic tumors, are also up-regulated in our miR-429 treated cells (Schaner et al. 2005). Also up-regulated in our miR-429 treated cells was wingless-type MMTV integration site family member 7A (*WNT7A*) that has been shown to be abundant in the epithelium of serous ovarian carcinomas, and lacking in benign tumors, normal ovaries, and endometrioid carcinomas (Yoshioka et al. 2012). Wnt signaling is of particular interest because it has been shown to regulate Slug and EMT activity (Wu et al. 2012). Plasminogen activator inhibitor-1 (*SERPINE1*) a marker for EMT linked to metastasis was down-regulated at 24 hours, but was up-regulated at 144 hours in miR-429-treated cells (Bajou et al. 1998). Interleukin 1 beta (*IL-1β*) is a well-characterized inflammatory cytokine that was down regulated at 24 and 48 hours, but up regulated by 144 hours in our treated cells. In peritoneal mesothelial cells, IL-1β was shown to induce down regulation of E-cadherin and cytokeratin, and also induce NF-κB translocation, which is necessary for epithelial-mesenchymal transitions in breast cancer progression (Huber et al. 2004; Strippoli et al. 2008).

4.3.1.3 miR-429 treated cells also return to a mesenchymal-like phenotype at 144 hours

We believe this pattern where expression reaches a maximum at 24 or 48 hours and then returns to the same zero hour expression level by 144 hours represents the direct impact of miR-429 on different transcription targets. This impact attenuates as the miRNA degrades over time and is diluted through successive cell passaging at 48 hours. The response, followed by return to 0 hour levels corresponds closely to our observations of cell phenotypes over time, where the miR-429 transfected cells change from a pre-transfection (0 hour) elongated fibroblast-like morphology to increasingly rounded, cobblestone epithelial-like morphology at 24 and 48 hours and then return to the fibroblast-like morphology at 144 hours (Figure 4.4). The negative control transfected cells did not change from their original mesenchymal-like morphology during the 0-144 hour time course, suggesting that these negative control cells represent a stable baseline.

4.3.1.4 Gene set enrichment and miR-429 predicted targets

Given the large number of differentially expressed genes, we then asked what biological pathways and processes were over-represented among our differentially expressed genes. Gene set enrichment analysis using GeneGO demonstrated that the significantly differentially expressed genes were significantly enriched for gene sets related to cell adhesion, cytoskeletal remodeling, EGFR signaling, apoptosis, and regulation of the epithelial-mesenchymal transition, among others (Figure 4.5). The presence of significantly enriched gene sets suggests that miR-429 is not only

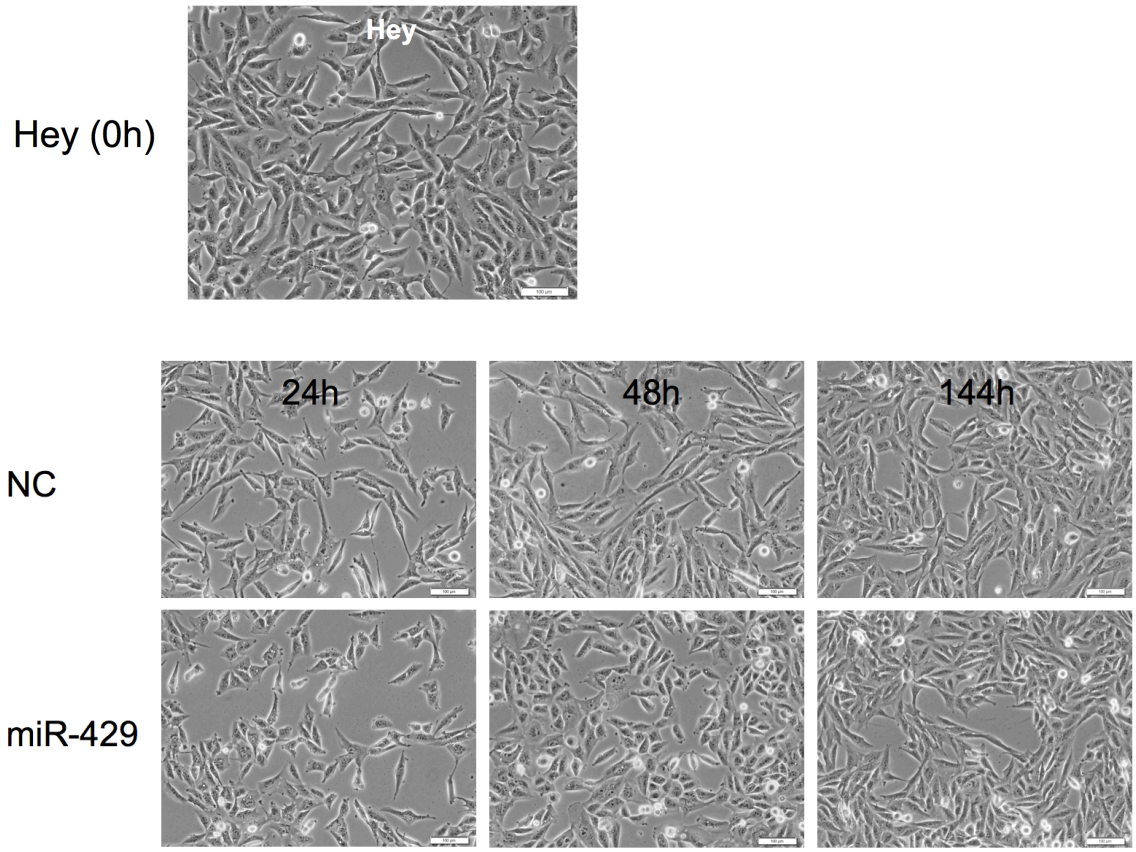

Figure 4.4 *miR-429 transfection in HEY cells induces morphological changes characteristic of MET and then EMT*
Cells transfected with miR-429 displayed a change from the elongated mesenchymal-like morphology (0 h) to a rounded, cobblestone epithelial-like morphology (24, 48 h), which later returned to the mesenchymal-like morphology by 144 hours. No morphological changes were observed in cells transfected with the negative control.

Process Networks

Export | Export to image

#	Networks	-log(pValue)	pValue
1	Cell adhesion_Cell junctions		2.262e-8
2	Development_Regulation of angiogenesis		6.635e-8
3	Signal transduction_NOTCH signaling		1.929e-7
4	Development_EMT_Regulation of epithelial-to-mesenchymal transition		8.860e-7
5	Reproduction_Feeding and Neurohormone signaling		1.376e-5
6	Apoptosis_Anti-Apoptosis mediated by external signals via MAPK and JAK/STAT		1.423e-5
7	Reproduction_FSH-beta signaling pathway		7.501e-5
8	Protein folding_Response to unfolded proteins		8.916e-5
9	Signal Transduction_Cholecystokinin signaling		8.997e-5
10	Cell adhesion_Integrin-mediated cell-matrix adhesion		1.592e-4

Pathway Maps

Export | Export to image

#	Maps	-log(pValue)	pValue
1	Apoptosis and survival_Endoplasmic reticulum stress response pathway		2.491e-10
2	Transport_Clathrin-coated vesicle cycle		3.397e-9
3	Development_A2B receptor: action via G-protein alpha s		8.638e-8
4	Cytoskeleton remodeling_TGF, WNT and cytoskeletal remodeling		1.297e-7
5	Apoptosis and survival_p53-dependent apoptosis		2.198e-7
6	Development_G-CSF signaling		3.087e-7
7	Role of alpha-6/beta-4 integrins in carcinoma progression		3.233e-7
8	Cell adhesion_Chemokines and adhesion		3.444e-7
9	Development_EGFR signaling pathway		4.481e-7
10	Immune response_Gastrin in inflammatory response		7.095e-7

Figure 4.5 *Gene enrichment analysis of genes differentially expressed across the 0-144 hour time course (FDR=0.05)*
Gene set enrichment analysis by GeneGO revealed multiple gene sets belonging to pathway maps and process networks associated with cell adhesion, cytoskeletal remodeling, EGFR signaling, and the regulation of the epithelial-mesenchymal transition. Gene sets with significantly higher numbers of genes differentially expressed across the time course (0-144 hours) are ordered here by their geometric distribution p-values.

causing the differential expression of individual genes, but also altering entire pathways related to the epithelial-mesenchymal transition.

We also asked which genes that are differentially expressed across the time course are also predicted targets of miR-429. Out of the 3635 genes that were differentially expressed over the time course, 261 (7.1%) of these were predicted as targets of miR-429 by miRanda (Table 4.3). Among these known differentially expressed miR-429 targets were transcription factors *ZEB1* and *ZEB2* that were observed to be significantly down regulated. *ZEB1* and *ZEB2* are transcription factors that play a key role in EMT by binding to E-box elements and directly repressing E-cadherin expression and polarity factor genes (Gregory et al. 2008a; Korpal et al. 2008). Among the up-regulated genes was *TSPAN13* (tetraspanin-13) (p-value = 2.24×10^{-6}), an epithelial marker over-expressed in many known subtypes of epithelial ovarian cancer and shown to mediate trans-membrane signaling events (Huang et al. 2007; Martin et al. 2009). The low fraction of differentially expressed genes that are also predicted targets of miR-429 confirms our previous studies showing equally low fractions and implying the majority of molecular and phenotypic changes are indirect effects of miR-429 transfection (Chen et al. 2011; Shahab et al. 2011).

4.3.2 Expression changes before and after the 48-hour mark

We observed that the magnitude of phenotypic and gene expression changes is greatest at the 48 hour mark in our time course, therefore we have split the time course into two time spans to show that statistically significant gene expression

Table 4.3 *Genes targeted by miR-429, as predicted by miRanda, that are differentially expressed over the time course (0-144 hours)*
These genes are differentially expressed across the time course (0-144 hours) by maSigPro (FDR = 0.05), and are predicted targets of miR-429 by miRanda. The fold change values compare the miR-429-treated cells' average expression to the negative control-treated cells' average expression at each time point (24, 48, and 144 hours).

		Fold change in miR-429 treated cells				
Probe ID	Symbol	24 hours	48 hours	144 hours	p-value	R-squared
207819_s_at	ABCB4	-0.42	-0.62	-0.39	2.67E-09	0.90
1552731_at	ABRA	-0.42	-0.44	-0.85	2.20E-04	0.61
218658_s_at	ACTR8	-0.24	-0.40	-0.54	3.15E-07	0.80
1552519_at	ACVR1C	0.08	0.30	0.47	1.99E-04	0.62
202952_s_at	ADAM12	1.02	1.50	-1.34	8.13E-07	0.82
201346_at	ADIPOR2	-0.83	-0.51	-0.13	2.34E-07	0.77
202820_at	AHR	0.62	0.36	-0.05	9.15E-06	0.67
203180_at	ALDH1A3	1.30	1.25	0.38	6.68E-05	0.71
219649_at	ALG6	0.44	0.10	-0.10	4.36E-05	0.67
205621_at	ALKBH1	0.13	-0.12	-0.33	5.43E-08	0.83
205609_at	ANGPT1	-1.24	-0.52	-0.78	5.12E-05	0.61
206385_s_at	ANK3	-0.20	-2.16	-0.05	7.68E-04	0.62
1556361_s_at	ANKRD13C	0.00	-0.09	-0.77	7.21E-07	0.78
218158_s_at	APPL1	1.42	1.04	0.01	5.91E-05	0.71
205239_at	AREG	1.56	2.02	0.52	3.56E-09	0.90
203264_s_at	ARHGEF9	0.98	0.96	0.09	5.51E-10	0.92
221230_s_at	ARID4B	-0.02	-0.36	-0.36	2.34E-09	0.88
202641_at	ARL3	0.00	0.00	0.21	1.72E-05	0.70
217852_s_at	ARL8B	0.91	0.75	-0.09	2.58E-07	0.84
218862_at	ASB13	-1.18	-1.06	0.05	1.91E-09	0.88
201855_s_at	ATMIN	-0.53	-0.82	-0.48	3.29E-06	0.70
203188_at	B3GNT1	-2.13	-1.03	-0.04	9.41E-08	0.79
37549_g_at	BBS9	-0.09	-0.51	-0.13	1.27E-05	0.66
205433_at	BCHE	-0.53	-1.29	-0.08	1.83E-08	0.82
203140_at	BCL6	-0.56	-0.74	-0.21	5.98E-06	0.77
203840_at	BLZF1	0.88	0.89	0.01	1.63E-06	0.80
201849_at	BNIP3	-0.41	-0.16	0.02	7.38E-04	0.62
218024_at	BRP44L	-0.55	-0.48	-0.36	2.45E-05	0.74
205548_s_at	BTG3	1.59	1.14	0.18	1.80E-04	0.67
203944_x_at	BTN2A1	-0.04	-0.44	0.03	1.25E-04	0.69
217905_at	C10orf119	0.36	-0.01	-0.54	2.91E-06	0.75
218867_s_at	C12orf49	-0.56	-0.32	-0.87	3.23E-07	0.76
219099_at	C12orf5	0.25	0.13	0.23	9.96E-09	0.86
1552310_at	C15orf40	0.37	0.29	-0.25	2.58E-05	0.74
219439_at	C1GALT1	0.67	0.85	-0.07	5.35E-07	0.83
220992_s_at	C1orf25	0.64	0.28	-0.01	1.73E-04	0.67
219706_at	C20orf29	-0.61	-0.14	-0.27	1.88E-05	0.70
1552740_at	C2orf15	0.40	0.89	0.06	6.36E-07	0.74

Table 4.3 (continued)						
218646_at	C4orf27	-0.73	-0.60	0.17	2.23E-10	0.88
205500_at	C5	0.05	0.10	-0.69	1.08E-04	0.64
220032_at	C7orf58	-0.33	-0.22	0.19	1.74E-04	0.67
217873_at	CAB39	1.17	0.59	-0.08	8.16E-05	0.70
1552682_a_at	CASC5	0.06	-0.04	-0.76	8.18E-05	0.65
1554785_at	CCDC82	0.66	0.71	-0.63	6.49E-04	0.62
219226_at	CDK12	0.08	0.05	-0.71	1.24E-10	0.91
204604_at	CDK14	1.48	1.51	-0.17	5.43E-05	0.71
204029_at	CELSR2	1.79	1.06	-0.12	6.38E-07	0.82
218566_s_at	CHORDC1	0.17	0.17	-0.34	2.38E-07	0.84
219944_at	CLIP4	0.20	0.14	0.49	1.98E-08	0.85
203291_at	CNOT4	-0.22	-0.23	-0.61	1.24E-04	0.64
1552344_s_at	CNOT7	-0.11	-0.48	-0.63	2.27E-06	0.76
203642_s_at	COBLL1	-0.04	-0.15	-0.34	6.01E-06	0.73
211981_at	COL4A1	0.05	0.26	0.20	5.36E-07	0.79
203551_s_at	COX11	-0.32	-0.02	-0.20	4.53E-08	0.84
201117_s_at	CPE	0.10	-0.84	-0.37	7.38E-09	0.89
201990_s_at	CREBL2	-0.13	-0.28	-0.24	5.07E-06	0.74
205630_at	CRH	0.20	0.60	0.30	2.23E-05	0.64
201380_at	CRTAP	-1.69	-1.64	-0.11	1.92E-11	0.94
220753_s_at	CRYL1	-0.73	-0.64	-0.35	2.42E-05	0.64
221139_s_at	CSAD	0.09	0.50	-0.03	1.00E-03	0.60
201112_s_at	CSE1L	0.13	0.21	-0.04	4.22E-05	0.72
219179_at	DACT1	0.37	-0.41	0.66	5.14E-05	0.67
202250_s_at	DCAF8	0.12	-0.09	0.19	3.49E-10	0.90
205399_at	DCLK1	1.08	2.08	1.36	1.23E-12	0.94
206752_s_at	DFFB	0.96	0.14	-0.31	3.21E-04	0.65
203791_at	DMXL1	0.50	0.23	-0.19	5.71E-04	0.63
213853_at	DNAJC24	-0.88	-0.84	-0.01	2.12E-06	0.80
208499_s_at	DNAJC3	-0.76	-0.28	-0.15	5.79E-10	0.92
205545_x_at	DNAJC8	-1.32	-0.79	-0.15	5.90E-04	0.63
217976_s_at	DYNC1LI1	0.27	0.16	-0.06	3.55E-06	0.79
202023_at	EFNA1	0.31	0.45	0.53	3.45E-06	0.70
208112_x_at	EHD1	-1.18	-1.06	-0.15	1.80E-05	0.65
201632_at	EIF2B1	-0.34	-0.27	-0.07	1.10E-04	0.69
220161_s_at	EPB41L4B	0.47	0.03	0.09	2.91E-06	0.75
206114_at	EPHA4	-0.77	-1.12	-0.81	8.60E-04	0.61
208394_x_at	ESM1	-1.47	-1.23	0.47	6.21E-06	0.68
219121_s_at	ESRP1	0.80	2.68	0.74	6.32E-08	0.79
207981_s_at	ESRRG	-0.48	-0.57	-0.23	1.64E-07	0.85
201574_at	ETF1	1.13	0.65	-0.07	4.23E-04	0.64
1555355_a_at	ETS1	-0.18	-0.29	-0.53	6.66E-08	0.74
1569024_at	FAM13A	0.09	-0.71	-0.68	2.00E-06	0.76
218518_at	FAM13B	0.68	-0.07	-0.71	3.86E-05	0.62
1553749_at	FAM76B	0.62	0.62	0.31	2.69E-04	0.66
203420_at	FAM8A1	-0.95	-0.44	0.42	7.50E-06	0.77

Table 4.3 (continued)						
201911_s_at	FARP1	-1.01	-0.58	-0.08	4.12E-05	0.62
219901_at	FGD6	1.85	2.03	1.21	7.79E-13	0.96
203033_x_at	FH	0.27	0.62	-0.01	3.59E-05	0.73
218530_at	FHOD1	-1.31	-0.64	0.02	2.24E-05	0.74
204359_at	FLRT2	0.06	-0.19	-0.65	8.65E-06	0.67
205935_at	FOXF1	-0.53	-1.46	-0.16	2.40E-04	0.66
206377_at	FOXF2	-0.31	-0.44	-0.38	1.70E-04	0.62
202724_s_at	FOXO1	0.90	0.61	-0.02	3.63E-08	0.87
208475_at	FRMD4A	-0.31	-0.51	0.09	1.51E-06	0.81
201564_s_at	FSCN1	-0.59	-0.10	0.59	6.55E-09	0.87
219683_at	FZD3	0.51	0.52	-0.61	1.25E-05	0.66
203706_s_at	FZD7	1.30	0.41	0.16	6.61E-05	0.60
218885_s_at	GALNT12	-0.38	-1.14	-0.66	2.71E-06	0.79
205848_at	GAS2	0.03	-0.91	-0.77	1.77E-06	0.76
203925_at	GCLM	-0.27	-0.62	-0.66	1.71E-07	0.81
205498_at	GHR	-0.19	-0.12	-0.42	1.72E-05	0.70
219467_at	GIN1	0.27	0.38	0.00	2.91E-06	0.70
201576_s_at	GLB1	-0.47	-0.25	0.19	2.99E-06	0.79
202382_s_at	GNPDA1	-0.65	-0.47	-0.26	2.82E-05	0.73
201057_s_at	GOLGB1	-0.04	0.22	0.21	5.09E-06	0.74
220264_s_at	GPR107	-0.51	-1.99	-0.36	8.23E-06	0.77
220265_at	GPR107	-0.52	-1.68	-0.43	3.85E-05	0.72
205862_at	GREB1	-1.20	-1.55	-0.64	8.91E-07	0.82
205930_at	GTF2E1	-0.77	-1.19	-0.07	3.95E-08	0.80
203138_at	HAT1	0.31	0.15	0.06	7.11E-06	0.77
202815_s_at	HEXIM1	0.56	0.25	-0.30	1.68E-06	0.80
205466_s_at	HS3ST1	0.45	1.50	0.49	2.59E-05	0.63
204569_at	ICK	0.56	0.23	-0.37	2.89E-04	0.66
206693_at	IL7	-0.08	-0.61	-0.33	5.29E-08	0.83
202859_x_at	IL8	-1.14	-3.13	0.28	3.84E-06	0.79
208193_at	IL9	-0.17	-0.19	0.26	8.94E-05	0.70
223681_s_at	INADL	0.81	1.41	0.15	4.21E-07	0.75
1559716_at	INO80C	0.76	0.70	-0.38	1.81E-08	0.88
218905_at	INTS8	-0.36	-0.32	0.13	1.04E-06	0.81
204686_at	IRS1	0.42	0.86	0.02	2.72E-08	0.87
204301_at	KBTBD11	-0.13	-0.97	-0.63	4.28E-06	0.69
219479_at	KDELC1	-1.56	-1.55	-0.09	2.07E-08	0.81
200040_at	KHDRBS1	0.09	0.16	-0.05	3.41E-05	0.73
203288_at	KIAA0355	-0.17	-0.59	-0.14	1.34E-09	0.91
219570_at	KIF16B	1.06	0.33	-0.06	4.48E-05	0.72
219657_s_at	KLF3	0.87	1.42	0.84	3.71E-05	0.62
221221_s_at	KLHL3	0.22	-0.76	-0.75	7.84E-06	0.73
218604_at	LEMD3	0.52	0.49	-0.09	2.82E-07	0.84
202594_at	LEPROTL1	0.04	0.01	-0.32	1.30E-04	0.63
218326_s_at	LGR4	-0.07	0.00	0.28	1.93E-05	0.70
218656_s_at	LHFP	-1.24	-2.09	-0.26	1.44E-11	0.91

Table 4.3 (continued)						
219399_at	LIN7C	0.19	-0.15	-0.47	1.84E-06	0.76
1559433_at	LOC149773	1.03	0.61	-0.64	1.12E-08	0.86
204298_s_at	LOX	-0.80	-0.63	-0.46	5.32E-04	0.63
218577_at	LRRC40	-0.21	-0.68	0.03	4.65E-07	0.75
203804_s_at	LUC7L3	0.08	-0.38	0.07	2.11E-04	0.67
206584_at	LY96	-0.47	-1.39	-0.58	2.78E-08	0.81
207292_s_at	MAPK7	-1.02	-0.60	-0.13	4.48E-04	0.64
206091_at	MATN3	-0.85	-1.45	-0.39	1.24E-04	0.69
220195_at	MBD5	-0.10	-0.96	0.12	9.04E-04	0.61
201930_at	MCM6	0.12	0.17	-0.09	6.89E-05	0.71
223780_s_at	MED13	-0.66	-0.39	-0.55	1.85E-05	0.70
202016_at	MEST	1.20	0.94	0.06	1.03E-06	0.81
1552312_a_at	MFAP3	1.29	1.50	-0.51	3.11E-07	0.84
218259_at	MKL2	0.37	0.26	-0.36	2.72E-08	0.87
217883_at	MMADHC	0.31	0.30	0.09	1.50E-07	0.85
219265_at	MOBKL2B	0.31	0.69	-0.31	2.15E-08	0.88
200600_at	MSN	-0.66	-0.51	0.28	2.03E-05	0.74
216095_x_at	MTMR1	0.05	-0.38	-0.08	6.49E-11	0.93
221250_s_at	MXD3	-0.24	-0.51	0.13	2.26E-06	0.80
201798_s_at	MYOF	0.15	0.17	0.29	2.15E-04	0.61
204823_at	NAV3	-0.11	-1.19	0.02	2.52E-05	0.69
201384_s_at	NBR1	-0.44	-0.43	0.15	3.35E-10	0.92
207760_s_at	NCOR2	-0.51	-0.37	-0.05	1.01E-05	0.67
218266_s_at	NCS1	-0.63	-0.48	-0.16	3.21E-04	0.65
203039_s_at	NDUFS1	0.07	0.11	0.16	4.85E-06	0.74
219031_s_at	NIP7	-0.32	-0.04	-0.43	9.48E-07	0.78
218902_at	NOTCH1	-0.08	-0.42	-0.11	2.09E-04	0.67
202679_at	NPC1	-0.21	-0.41	0.62	3.45E-10	0.92
205440_s_at	NPY1R	0.32	-0.24	-0.84	9.17E-06	0.72
204791_at	NR2C1	0.50	0.47	0.35	1.48E-04	0.68
1560204_at	NT5DC4	0.36	0.73	0.44	3.93E-04	0.64
205729_at	OSMR	-0.28	0.00	-0.37	1.81E-04	0.62
218196_at	OSTM1	-2.09	-2.78	-0.66	9.77E-15	0.97
219160_s_at	PAPOLG	-0.18	0.09	-0.45	2.30E-05	0.69
205534_at	PCDH7	0.38	0.87	-0.21	1.16E-05	0.66
202731_at	PDCD4	0.84	0.35	0.81	1.57E-04	0.63
205078_at	PIGF	0.37	0.46	-0.47	1.62E-06	0.80
204269_at	PIM2	-0.32	-0.73	-0.55	2.52E-08	0.87
205570_at	PIP4K2A	-0.60	-0.32	0.08	2.02E-06	0.80
201081_s_at	PIP4K2B	0.10	0.24	-0.74	2.31E-05	0.74
221027_s_at	PLA2G12A	0.72	0.80	0.38	1.26E-10	0.93
201682_at	PMPCB	0.29	0.54	-0.11	7.81E-06	0.77
205878_at	POU6F1	-0.40	-0.56	0.05	6.31E-07	0.82
219195_at	PPARGC1A	0.48	0.63	-0.23	3.55E-05	0.73
203063_at	PPM1F	-1.72	-1.69	-0.03	6.63E-12	0.91
202166_s_at	PPP1R2	0.71	0.42	0.08	5.25E-07	0.83

Table 4.3 (continued)						
204507_s_at	PPP3R1	0.34	-0.13	-0.39	2.79E-05	0.63
208004_at	PROL1	0.27	0.61	-0.09	5.11E-05	0.61
218040_at	PRPF38B	0.35	-0.37	-0.49	2.55E-05	0.69
201053_s_at	PSMF1	-0.19	-0.50	-0.53	3.22E-06	0.70
219654_at	PTPLA	-0.29	-0.36	-0.31	7.14E-06	0.73
205438_at	PTPN21	-0.41	-0.83	-0.28	2.35E-04	0.61
203884_s_at	RAB11FIP2	-0.75	-0.76	0.03	4.70E-09	0.84
203885_at	RAB21	0.15	-0.38	-0.39	8.24E-06	0.72
219210_s_at	RAB8B	-0.45	-0.58	-0.57	4.22E-07	0.83
218668_s_at	RAP2C	-0.68	-0.95	0.03	2.31E-04	0.66
203097_s_at	RAPGEF2	-0.16	-0.95	-0.27	4.04E-05	0.62
219286_s_at	RBM15	-0.13	-0.29	-0.31	3.18E-05	0.63
205407_at	RECK	-1.66	-1.87	-0.25	1.66E-06	0.72
204365_s_at	REEP1	-0.45	-0.30	-0.93	1.04E-07	0.82
218430_s_at	RFX7	0.07	0.26	-0.43	1.21E-04	0.69
220483_s_at	RNF19A	-0.01	-0.21	-0.33	1.40E-04	0.63
205215_at	RNF2	-0.82	-0.70	-0.46	3.27E-06	0.70
203161_s_at	RNF8	-0.05	0.06	-0.49	1.29E-07	0.82
204208_at	RNGTT	-0.14	-0.33	-0.03	4.50E-13	0.96
1554080_at	RQCD1	-0.34	-0.33	-0.20	1.75E-08	0.88
218370_s_at	S100PBP	-0.43	-0.33	-0.04	1.68E-06	0.80
202797_at	SACM1L	-0.15	-0.23	-0.05	8.12E-06	0.77
218346_s_at	SESN1	-1.03	-0.78	0.15	9.24E-06	0.76
205933_at	SETBP1	-0.40	-0.32	-0.86	5.74E-06	0.62
201811_x_at	SH3BP5	-0.08	0.08	0.66	8.05E-13	0.95
219493_at	SHCBP1	-2.10	-1.96	-0.30	2.79E-08	0.87
219083_at	SHQ1	-0.10	-0.35	-0.45	3.43E-08	0.87
219159_s_at	SLAMF7	-0.34	-0.55	-0.93	1.05E-09	0.89
204404_at	SLC12A2	-0.16	-0.27	-0.55	7.10E-05	0.66
204462_s_at	SLC16A2	-0.90	-1.46	-1.09	5.27E-05	0.61
204587_at	SLC25A14	0.38	0.34	-0.35	1.44E-04	0.68
203306_s_at	SLC35A1	1.18	1.11	0.22	1.51E-08	0.88
207440_at	SLC35A2	-0.96	-0.83	-0.07	1.87E-06	0.80
207678_s_at	SOX30	-0.42	0.00	-0.50	5.19E-09	0.87
220456_at	SPTLC3	0.35	0.34	-0.77	1.51E-06	0.77
206095_s_at	SRSF10	0.17	0.02	-0.35	1.41E-05	0.71
217790_s_at	SSR3	-0.63	-0.49	0.12	1.70E-08	0.82
220979_s_at	ST6GALNAC5	0.93	2.14	0.40	1.84E-10	0.93
234140_s_at	STIM2	0.47	0.40	-0.29	7.69E-04	0.62
214512_s_at	SUB1	0.11	0.21	0.30	4.15E-10	0.90
201838_s_at	SUPT7L	0.98	0.33	-0.35	3.85E-06	0.79
219156_at	SYNJ2BP	0.57	0.82	-0.14	5.85E-05	0.60
200976_s_at	TAX1BP1	0.18	0.39	0.24	2.91E-10	0.92
219682_s_at	TBX3	-0.05	-0.38	-0.59	4.41E-08	0.84
202720_at	TES	0.61	0.37	0.15	7.34E-04	0.62
205016_at	TGFA	1.62	1.67	0.48	9.31E-09	0.89

Table 4.3 (continued)						
201506_at	TGFBI	-0.28	-0.40	-0.66	2.48E-04	0.61
219122_s_at	THG1L	0.14	-0.30	-0.42	9.18E-05	0.65
219950_s_at	TIAM2	0.31	0.71	0.36	2.99E-05	0.73
203046_s_at	TIMELESS	0.03	0.48	-0.25	4.33E-04	0.64
1558487_a_at	TMED4	-0.60	-1.02	-0.57	3.80E-07	0.76
218962_s_at	TMEM168	0.30	0.15	-0.17	3.44E-04	0.65
218113_at	TMEM2	2.08	1.95	0.11	1.46E-07	0.85
217743_s_at	TMEM30A	0.90	0.33	-0.01	9.56E-06	0.67
219449_s_at	TMEM70	0.32	0.12	-0.22	2.47E-09	0.90
205611_at	TNFSF12	-1.08	-1.01	-0.30	9.02E-09	0.89
201519_at	TOMM70A	-0.33	-0.30	-0.16	1.07E-05	0.76
203786_s_at	TPD52L1	0.25	0.44	0.28	4.76E-08	0.87
202478_at	TRIB2	1.66	1.48	-0.32	2.94E-04	0.65
217979_at	TSPAN13	0.21	0.27	0.33	2.24E-06	0.76
203894_at	TUBG2	-0.27	0.35	0.55	1.20E-04	0.64
222989_s_at	UBQLN1	0.18	0.19	-0.17	2.85E-07	0.84
215983_s_at	UBXN8	-0.46	-0.90	-0.47	1.02E-07	0.78
219960_s_at	UCHL5	0.13	0.60	-0.07	1.47E-04	0.68
218257_s_at	UGGT1	-0.37	-0.13	-0.20	3.63E-06	0.75
203583_at	UNC50	-0.26	-0.28	-0.16	4.24E-05	0.72
201672_s_at	USP14	-0.14	-0.22	-0.19	6.19E-05	0.66
1552678_a_at	USP28	-0.21	-0.72	-0.74	1.72E-06	0.76
1562238_at	USPL1	-0.08	0.81	-0.02	7.24E-07	0.82
202829_s_at	VAMP7	-0.21	-0.41	0.01	1.70E-06	0.76
219060_at	WDYHV1	-0.45	-0.40	0.15	1.23E-04	0.69
206067_s_at	WT1	-0.05	-0.27	-0.71	3.82E-09	0.87
206537_at	XIAP	0.02	-0.04	-0.46	2.53E-04	0.61
218753_at	XKR8	-1.35	-1.22	-0.30	6.18E-06	0.68
210813_s_at	XRCC4	0.61	1.36	0.21	6.71E-09	0.89
205340_at	ZBTB24	-0.19	-0.03	-0.50	1.39E-04	0.63
1554470_s_at	ZBTB44	0.61	0.70	0.06	5.19E-04	0.63
221193_s_at	ZCCHC10	0.12	-0.11	-0.29	7.26E-07	0.78
218249_at	ZDHHC6	-0.03	-0.30	-0.17	5.83E-07	0.82
212764_at	ZEB1	-1.29	-1.72	-0.14	1.33E-07	0.78
239952_at	ZEB1	-1.17	-1.36	-0.20	1.33E-05	0.66
203603_s_at	ZEB2	-0.43	-1.12	-0.33	2.14E-05	0.74
1553736_at	ZFC3H1	-0.05	-0.57	-0.53	4.51E-07	0.75
219778_at	ZFPM2	-0.86	-1.09	-0.44	5.71E-08	0.80
207920_x_at	ZFX	0.27	0.24	-0.63	1.92E-05	0.70
207753_at	ZNF304	-0.30	-0.34	-0.12	3.32E-08	0.87
1553718_at	ZNF548	0.30	-0.74	-1.25	3.51E-07	0.80
1553719_s_at	ZNF548	0.15	-0.72	-0.55	1.98E-07	0.81

changes are occurring around this time point even when each span is considered by itself: 0 to 48 hours and 48 to 144 hours. Here we used a linear model time course fitting to determine which genes are differentially expressed, treating each time span as a separate time course and correcting for the gene expression change observed in our negative control-treated cells.

4.3.2.1 Expression changes between 0 to 48 hours

Across the 0 to 48 hour time span, 1339 genes in the miR-429-treated cells were differentially expressed (FDR < 0.1) compared to the negative control-treated cells (Table 4.4). Among these are *FN1*, a mesenchymal marker that was down regulated. *CAV2* and *DSP*, both epithelial markers, were up regulated. *β-catenin*, required for the creation of epithelial cell layers, was also up regulated. *MMP9*, involved in the breakdown of basement membranes in EMT, was down regulated. *SMAD7* is down regulated. *ZEB1* and *ZEB2* were both down regulated. Gene set enrichment analysis showed that the significantly differentially expressed genes across this time span were significantly enriched for gene sets related to the regulation of EMT, extracellular matrix (ECM) remodeling, cell adhesion, TGF-β-dependent induction of EMT via *RhoA*, *PI3K*, and *ILK*, the *EGFR* signaling pathway, and others (Figure 4.6). Out of the total of 1339 differentially expressed genes 118 (8.8%) differentially expressed genes were predicted targets of miR-429 by miRanda. Among these are *ZEB1, ZEB2* and *MSN* (moesin).

4.3.2.2 Expression changes between 48 to 144 hours

Across the 48-144 hour time span, 772 genes in miR-429-treated cells were differentially expressed (FDR = 0.1) compared to the negative control-treated cells

Table 4.4 *Selected genes differentially expressed in the miR-429 treated cells during the 0 to 48 hour time span*

These selected genes are those that are known to be involved in EMT or MET processes, are differentially expressed across the MET-like time span (0-48 hours) by Limma (FDR = 0.1). The fold change values compare the miR-429-treated cells' average expression to the negative control-treated cells' average expression at each time point (24, 48, and 144 hours).

		Fold change in miR-429 treated cells			0-48 hour time span
ID	Symbol	24 hours	48 hours	144 hours	p-value
1552721_a_at	FGF1	0.81	0.96	-0.41	0.001634427
1558683_a_at	HMGA2	-1.20	-0.06	-0.01	0.000131942
1561633_at	HMGA2	-0.92	-0.14	0.00	0.000717811
1568765_at	SERPINE1	-2.48	-0.83	-0.51	0.000303968
200606_at	DSP	1.20	1.49	0.86	1.78E-06
201533_at	CTNNB1	0.90	0.78	-0.01	0.00213969
202011_at	TJP1	1.04	0.89	0.04	2.82E-05
202627_s_at	SERPINE1	-0.78	0.11	0.99	0.000742481
203323_at	CAV2	2.21	2.21	0.67	6.45E-09
203324_s_at	CAV2	0.69	0.95	0.35	0.001389587
203603_s_at	ZEB2	-0.43	-1.12	-0.33	0.001528935
203780_at	MPZL2	-0.14	1.00	0.22	0.001227715
203936_s_at	MMP9	-0.16	-1.08	-0.23	0.002371341
204422_s_at	FGF2	1.62	1.71	-0.04	1.40E-07
204619_s_at	VCAN	0.89	0.92	0.22	0.000139842
204620_s_at	VCAN	0.95	0.95	0.14	0.002186291
204790_at	SMAD7	0.82	-0.14	-0.82	0.000517814
205014_at	FGFBP1	1.94	1.60	2.79	2.93E-07
205122_at	TMEFF1	0.40	-0.80	0.14	0.001217298
209552_at	PAX8	-1.10	-0.04	0.38	0.00327345
209875_s_at	SPP1	-0.10	-1.03	-0.38	0.001039589
210495_x_at	FN1	-1.65	-2.70	-0.13	2.71E-09
211719_x_at	FN1	-1.70	-2.66	-0.12	1.24E-09
212464_s_at	FN1	-1.68	-2.76	-0.05	2.72E-09
212764_at	ZEB1	-1.29	-1.72	-0.14	4.75E-06
213891_s_at	TCF4	-0.48	-0.74	-0.26	0.00195207
214702_at	FN1	-0.67	-1.66	-0.33	0.002989896
216442_x_at	FN1	-1.58	-2.63	-0.11	5.79E-09
221029_s_at	WNT5B	-1.33	-1.14	-0.23	0.001165162
221731_x_at	VCAN	0.65	0.97	0.18	0.001740123
228333_at	ZEB2	-1.21	-0.51	-0.25	0.001361533
239952_at	ZEB1	-1.17	-1.36	-0.20	0.001502772

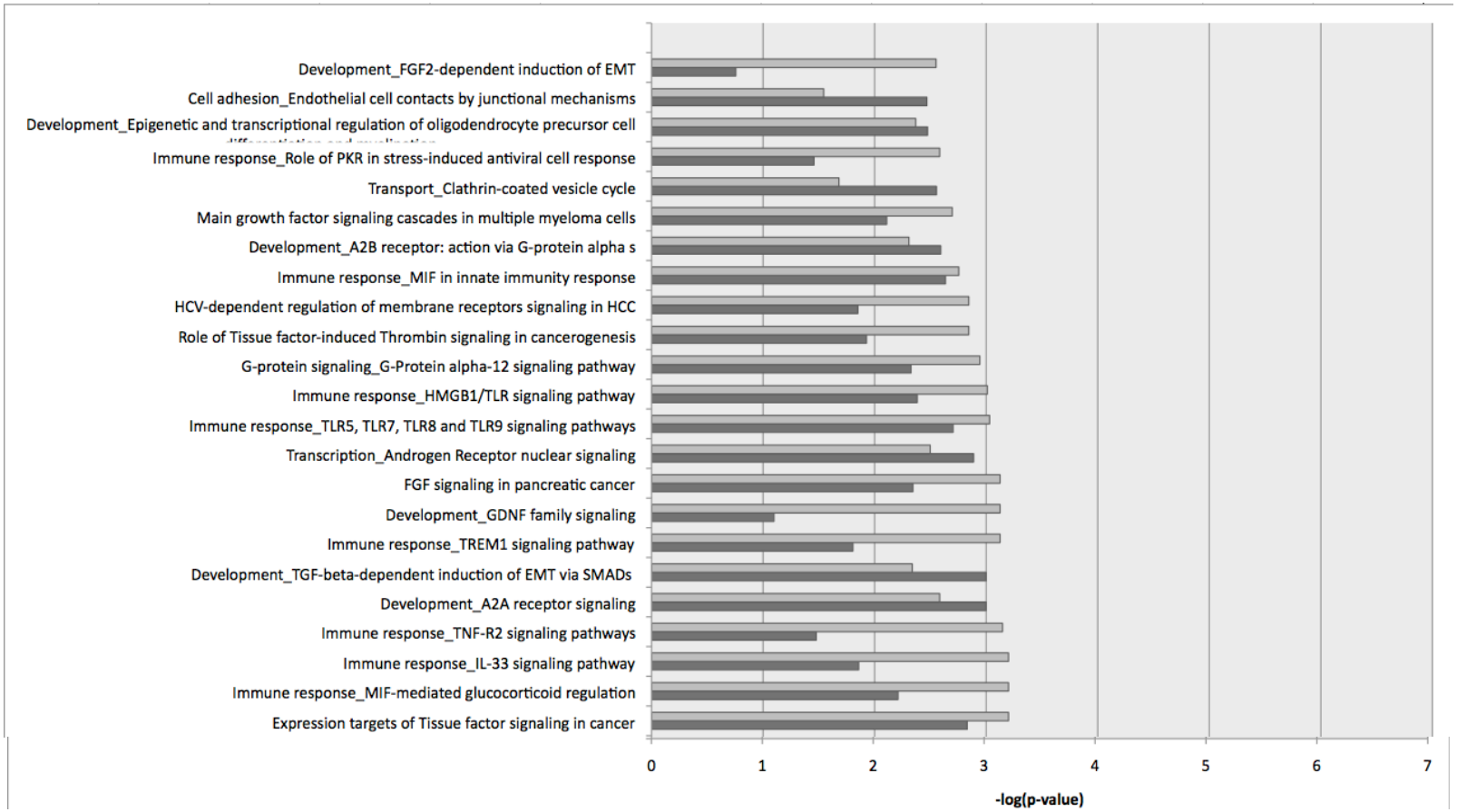

Figure 4.6 *Gene set enrichment of genes differentially expressed in the miR-429 treated cells during the 0 to 48 and 48 to 144 hour time span* Signfiicantly differentially expressed genes from each time span were analyzed for significantly enriched pathways using GeneGO. Gene sets with significantly higher numbers of genes differentially expressed across the 0-48 hour time span (dark grey) and 48-144 hour time span (light grey) are ordered here by their geometric distribution p-values.

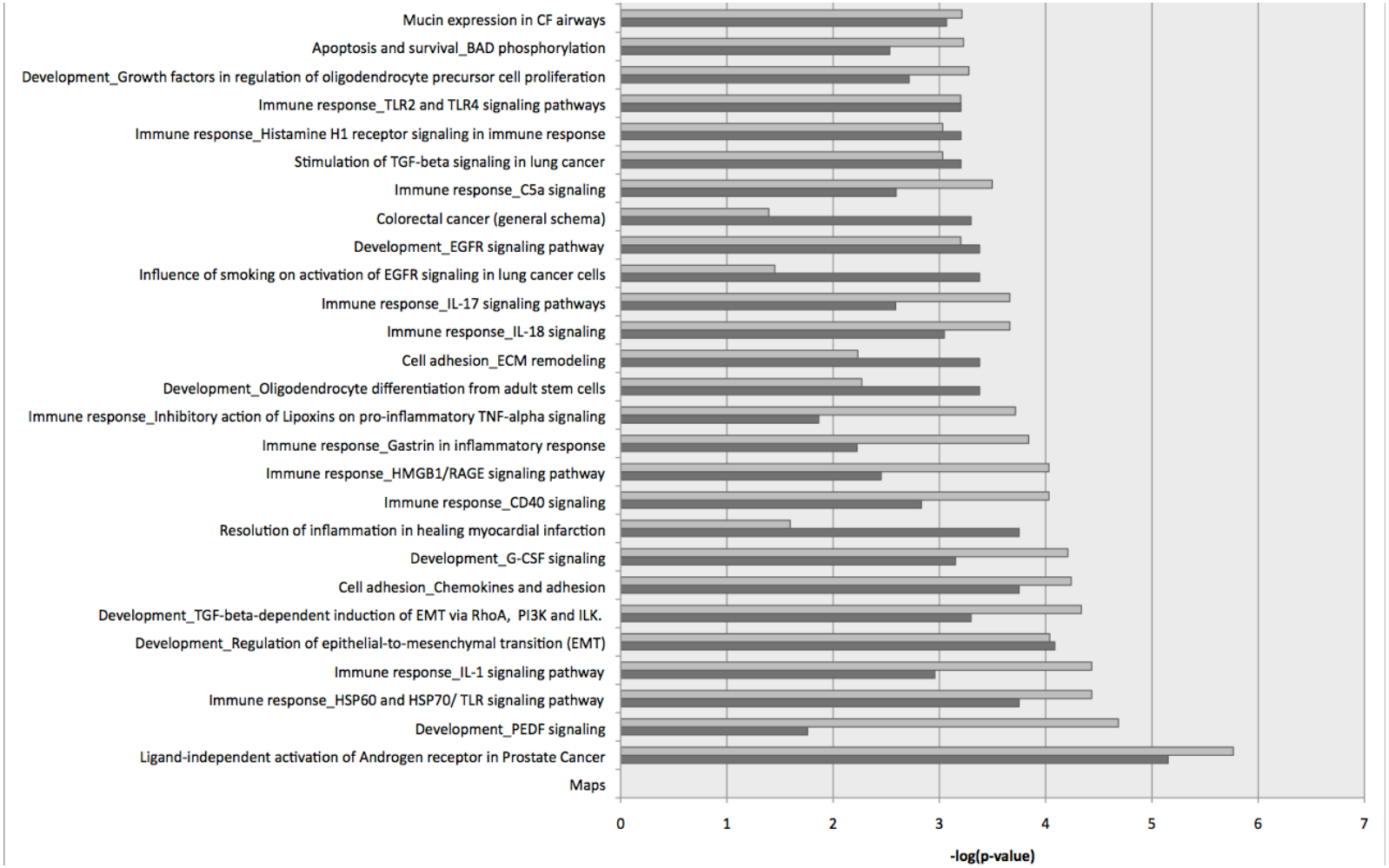

Figure 4.6 (continued)

(Table 4.5). Among these are fibronectin (*FN1*) and *ZEB1* that were up regulated during this time span. *FGF1, FGF2*, and *CAV2* were down regulated. Gene set enrichment analysis showed that the significantly differentially expressed genes across this time span were significantly enriched for gene sets related to the regulation of EMT, TGF-β-dependent induction of EMT via *RhoA*, *PI3K*, and *ILK*, chemokines and adhesion, the *EGFR* signaling pathway, *IL-15* signaling, *IL-1* signaling, *PEDF* signaling, and others (Figure 4.6). Out of the 772 genes that were differentially expressed across the 48-144 time span, 59 (7.6%) differentially expressed genes were predicted targets of miR-429 by miRanda. Among these are *ZEB1* and *MSN* (moesin).

Immune response pathways are strongly represented in the gene set enrichments for both time spans, due in large part to the differential expression of *IL1β*, *IL6*, *IL8*, and *MAPK* proteins that are part of the EMT pathway. The three interleukins are all down regulated by 48 hours and have previously been noted to be potential inducers and maintainers of EMT through autocrine loops (Lee et al. 2004a; Palena et al. 2012; Xie et al. 2012).

4.3.3. Regulation of EMT through TGF-β/Smads/MAPK signaling axis

One of our primary interests in miR-429 is its impact on the regulation of EMT and its potential role in altering the diverse signaling pathways leading to EMT. In our enrichment, we see up-regulation of TGF-β signaling components, as well as up-regulation of downstream elements such as *MAPK*, SMAD family member proteins, and *PI3K* that are important in TGF-β-dependent induction of EMT (Massague 2000;

Table 4.5 *Selected genes differentially expressed in the miR-429 treated cells during the 48 to 144 hour time span*
These selected genes are those that are known to be involved in EMT or MET processes, are differentially expressed across the EMT-like time span (48-144 hours) by Limma (FDR = 0.1). The fold change values compare the miR-429-treated cells' average expression to the negative control-treated cells' average expression at each time point (24, 48, and 144 hours).

		Fold change in miR-429 treated cells			Time span
ID	Symbol	24 hours	48 hours	144 hours	p-value
1552721_a_at	FGF1	0.81	0.96	-0.41	7.98E-05
200600_at	MSN	-0.66	-0.51	0.28	0.00129774
201389_at	ITGA5	-0.63	-0.41	0.45	0.00165984
202011_at	TJP1	1.04	0.89	0.04	0.000560457
202627_s_at	SERPINE1	-0.78	0.11	0.99	0.001365373
203323_at	CAV2	2.21	2.21	0.67	5.79E-06
204422_s_at	FGF2	1.62	1.71	-0.04	4.32E-06
205014_at	FGFBP1	1.94	1.60	2.79	0.001405309
205122_at	TMEFF1	0.40	-0.80	0.14	0.000856437
210495_x_at	FN1	-1.65	-2.70	-0.13	2.04E-08
211719_x_at	FN1	-1.70	-2.66	-0.12	1.95E-08
212464_s_at	FN1	-1.68	-2.76	-0.05	1.08E-08
212758_s_at	ZEB1	-1.54	-1.54	-0.07	0.000615458
212764_at	ZEB1	-1.29	-1.72	-0.14	3.89E-06
216442_x_at	FN1	-1.58	-2.63	-0.11	2.39E-08
220016_at	AHNAK	-0.63	-0.35	0.95	0.000141059
221729_at	COL5A2	0.05	-0.61	0.21	0.000594582

Zavadil and Bottinger 2005; Bierie and Moses 2006). Included in this pathway are epithelial markers *DSP, KRT19*, and *KRT8* that are up-regulated, and mesenchymal markers *COL1A1, FN1,* and *TPM1* that are down-regulated (Table 4.6).

4.3.3.1 TGF-β signaling

The signaling pathways involved in EMT include *TGF-β* and its downstream transcription factors and signaling proteins. Members of the TGF-β family are known major inducers and maintainers of EMT in carcinoma, although in normal cells they suppress cell proliferation and are involved in the induction of apoptosis (Shipley et al. 1985; Derynck et al. 1987; Massague 2008). In our study, *TGF-β2* is up regulated across the time course, as is the transmembrane receptor *TGF-βR1*. Malignant cells are able to circumvent the tumor-suppressive effects of the TGF-β pathway by either inactivating *TGF-β* or its receptor, or altering downstream elements that are responsible for tumor suppression (Massague 2008). Hey cells, despite their derivation from the surface epithelia of human ovarian carcinoma, are known to have functional *TGF-β* and *TGF-β* receptor expression by PCR and affinity radio-labeling (Jindal et al. 1995). Since TGF-β pathway components are unaltered in Hey cells, the up-regulation of *TGF-β* is able to contribute to the induction of the epithelial phenotype.

4.3.3.2 Smads signaling

TGF-β is known to propagate its signal via receptor-regulated SMADs (Mothers against decapentaplegic) family signal transducer proteins. In our miR-429 treated samples, *SMAD2* and *SMAD7* were significantly down-regulated. When TGF-β is bound, the TGF-β II receptor activates the TGF-βI receptor that is capable of

Table 4.6 *Genes associated with regulation of the epithelial-mesenchymal transition that are differentially expressed over the time course (0-144 hours)*
These selected genes are those that are known to be involved in EMT regulation and are differentially expressed across the time course (0-144 hours) by maSigPro (FDR = 0.05). The fold change values compare the miR-429-treated cells' average expression to the negative control-treated cells' average expression at each time point (24, 48, and 144 hours).

	Fold change in miR-429 treated cells			Time course
Symbol	24 hours	48 hours	144 hours	p-value
ACTG1	0.13	0.09	0.25	3.09E-08
ADAM17	0.32	0.47	0.29	9.34E-06
AKT2	-0.52	-0.46	0.01	5.53E-06
AKT3	0.09	0.51	0.34	3.71E-10
BCL2	0.43	0.09	-0.63	9.03E-06
BMP2	-0.36	-0.52	0.27	1.36E-07
CBL	0.10	0.26	-0.67	2.47E-06
CDC42	-0.40	-0.13	0.11	2.93E-06
CDH2	0.27	0.05	-0.14	0.000233764
CFL1	0.95	0.18	0.56	2.56E-05
CFL2	-1.24	-1.03	-0.21	2.93E-06
CFL2	-2.28	-1.91	-0.15	3.46E-11
CFL2	-1.84	-1.54	0.00	4.93E-06
COL1A1	-0.56	-0.80	-0.42	5.60E-09
COL1A1	-0.04	-0.39	-0.32	2.99E-09
DSP	1.20	1.49	0.86	3.76E-10
EGFR	0.03	-0.10	0.47	0.000228239
ETS1	-0.18	-0.29	-0.53	6.66E-08
FGF1	0.81	0.96	-0.41	2.33E-10
FGF2	1.29	0.53	0.01	1.92E-08
FGF2	1.62	1.71	-0.04	6.91E-12
FGFR1	-0.24	-0.26	-0.48	2.84E-05
FGG	-0.40	-0.34	0.03	0.000370961
FN1	-1.65	-2.70	-0.13	2.53E-06
FN1	-1.70	-2.66	-0.12	1.31E-06
FN1	-1.68	-2.76	-0.05	4.03E-06
FN1	-0.67	-1.66	-0.33	7.10E-05
FN1	-1.58	-2.63	-0.11	4.54E-06
FOS	0.98	1.05	0.02	4.08E-05
FOSL2	0.68	0.34	-0.25	0.000753844
FRS2	0.32	0.55	-0.65	5.40E-05
FRS2	0.18	-0.11	-0.81	2.78E-06

Table 4.6 (continued)				
FZD1	0.22	-0.09	-0.33	2.19E-05
FZD3	0.51	0.52	-0.61	1.25E-05
FZD5	1.96	1.44	0.15	3.47E-05
FZD7	1.02	0.47	0.02	8.02E-06
FZD7	1.30	0.41	0.16	6.61E-05
GAB2	-0.18	-0.86	0.22	4.13E-07
GNAI1	0.33	0.35	-0.30	8.71E-06
GNAQ	0.35	0.19	-0.09	0.001023096
GSK3B	0.21	-0.03	-0.35	4.73E-10
HIF1A	0.35	0.33	0.08	2.91E-07
HMGA2	-0.92	-0.14	0.00	1.64E-05
HMGA2	0.17	-0.36	-0.20	8.88E-16
HSD17B2	-0.05	-1.08	-0.22	6.24E-09
IKBKB	-0.49	-0.89	-0.16	1.40E-10
IL1B	-1.65	-1.45	1.25	3.31E-05
IL1B	-1.59	-1.50	1.28	5.90E-06
IL6ST	0.12	-0.25	-0.48	1.55E-11
IL6ST	-0.80	-0.49	0.19	1.22E-06
ITGB1	-0.70	-0.93	-1.13	2.26E-06
ITGB3	-0.63	-0.91	-0.26	6.94E-05
KRT18	0.01	0.71	0.50	7.04E-05
KRT8	0.29	0.90	0.68	9.49E-06
LEF1	0.51	0.14	-0.77	5.79E-08
LIFR	0.31	0.58	0.15	0.000851456
LIMS1	-0.61	-0.42	-0.10	0.000780253
LOX	-0.80	-0.63	-0.46	0.000532485
LOX	-2.09	-2.73	-0.37	1.59E-11
LOXL2	0.43	0.71	0.15	9.26E-12
MAP2K3	0.00	0.22	0.20	0.000112092
MAPK1	-0.01	-0.09	-0.26	5.01E-07
MAPK14	-0.07	0.34	-0.16	0.000186127
MAPK8	0.66	0.55	-0.26	5.76E-07
MAPK8	1.53	1.12	-0.09	5.87E-05
MAPK8	0.64	0.69	-0.28	1.70E-07
MAPK8	0.94	0.99	-0.26	3.34E-07
MAPK9	0.28	0.24	-0.12	2.44E-15
MET	0.39	0.12	0.26	4.75E-05
MKL2	0.37	0.26	-0.36	2.72E-08
NES	-0.57	-0.63	0.26	6.11E-06
NFKBIA	-0.04	-0.86	0.11	6.64E-10
NOG	0.14	0.42	0.05	7.38E-05

Table 4.6 (continued)				
NOTCH1	-0.08	-0.42	-0.11	0.000209242
NOTCH4	-0.27	-0.44	0.06	2.80E-06
NOX4	-0.04	-0.28	-1.04	4.28E-11
NOX4	0.24	-0.29	-0.88	5.91E-06
OSMR	-0.28	0.00	-0.37	0.000181366
PDPK1	0.53	0.78	-0.12	7.44E-05
PIK3CD	-0.36	-0.71	0.31	6.77E-10
PPP3R1	0.34	-0.13	-0.39	2.79E-05
PTEN	-0.19	-0.10	-0.41	6.76E-07
PTEN	0.44	0.29	-0.29	2.02E-06
PTK2	0.17	0.27	0.07	0.000151619
SERPINE1	-0.78	0.11	0.99	3.25E-06
SMAD2	-0.49	-0.59	0.07	3.55E-09
SMAD2	-0.28	-0.52	-0.23	0.000342423
SMAD7	0.82	-0.14	-0.82	1.61E-07
SOS1	-0.06	-0.22	-0.36	1.28E-07
STAT1	0.04	-0.33	-0.17	1.26E-06
STAT3	1.24	1.71	0.46	4.22E-12
TCF3	-0.26	-0.17	-0.15	4.81E-05
TCF3	-0.33	-0.21	-0.19	3.77E-05
TCF3	-0.24	-0.21	-0.21	0.000526648
TGFB1I1	-1.25	-0.76	0.04	6.28E-05
TGFB2	1.31	0.67	-1.39	1.64E-10
TGFB2	1.37	0.99	-0.83	2.32E-07
TGFBR1	0.62	0.33	0.01	0.000396257
TJP1	1.04	0.89	0.04	0.00108346
TPM1	-0.43	-1.82	-0.62	5.55E-05
TPM1	-0.63	-1.04	-0.34	0.000357113
WNT10A	-0.35	-0.48	-0.41	0.000354227
WNT7A	0.39	1.71	1.85	5.34E-08
ZEB1	-1.29	-1.72	-0.14	1.33E-07
ZEB1	-1.17	-1.36	-0.20	1.33E-05
ZEB2	-0.43	-1.12	-0.33	2.14E-05

phosphorylating Smads. Receptor-phosphorylated Smads are then capable of binding partner Smads and freely move into the nucleus where it can interact with gene regulatory sites (Massague 2000). Valcourt et al. examined the key regulatory role of SMADs in TGF-β-dependent EMT using dominant-negative forms of SMADs and a TGF-β I receptor that was incapable of activating SMADs or inducing EMT alone, showing that SMAD signaling has a critical role in activating the signaling network that induces EMT (Valcourt et al. 2005). *SMAD2* may also serve to maintain the epithelial phenotype, as suggested by studies where *SMAD2* knockout mouse hepatocytes spontaneously transition to the mesenchymal phenotype when TGF-β is absent (Zavadil and Bottinger 2005). *SMAD7* acts as an inhibitor of TGF-β signaling, where *SMAD7* down-regulation by miR-106b-25 has been shown to increase TGF-β signaling, inducing EMT in breast cancer cells (Smith et al. 2012; Xia et al. 2013).

4.3.3.3 MAPK signaling

A number of mitogen-activated protein kinases (*MAPKs*) are also differentially up regulated in our miR-429 treated samples, including *ERK2 (MAPK1), JNK1 (MAPK8), MKK3 (MAP2K3)*, and p38-α (*MAPK14*). Although the canonical TGF-β pathway does not involve MAPK, there is strong evidence for signaling crosstalk between TGF-β signaling and the MAPK pathway in the induction of EMT (Yu et al. 2002; Javelaud and Mauviel 2005). Specifically, when *ERK* activity is inhibited in human keratinocytes in the presence of TGF-β, the disassembly of adherens junctions and subsequent cell mobility associated with EMT was also inhibited (Zavadil et al. 2001). Moreover in TGF-β responsive mouse mammary epithelial cells, inhibition of p38 with SB203580 completely blocks EMT, suggesting that TGF-β-activated p38

MAPK is required for EMT (Yu et al. 2002). Likewise in mouse keratinocytes, inhibition of c-Jun N-terminal kinase 1 (*JNK1*) with antisense oligonucleotides or *JNK* inhibitor SP600125 results in the suppression of fibronectin, and vimentin even when exposed to TGF-β1 (Santibanez 2006). Additionally, when normal mouse keratinocytes are exposed to TGF-β 1, E-cadherin is delocalized and lost from cell contacts. This effect no longer occurs when *JNK* antisense oligonucleotides or inhibitor is added, indicating *JNK*'s importance in TGF-β-induced EMT. Our finding of up-regulated *MAPK* in our miR-429 treated sample appears to contradict their role in promoting EMT, as *MAPK* expression peaks at the same time our miR-429 treated cells display the strongest epithelial phenotype. This may be explained by the down-regulation of integrin β1 (*ITGB1*) in our miR-429 treated cells. *ITGB1* signaling is known to be necessary for TGF-β-activation of p38 *MAPK* leading to EMT in mouse mammary epithelial cells (Bhowmick et al. 2001).

4.3.3.4 TGF-β/Smads/MAPK signaling before and after the 48 hour mark

Because of the apparent cyclic nature of expression levels and the change in cell morphology from mesenchymal-like to epithelial-like and back again, we hypothesize that the same pathways we observe being differentially expressed from 0 to 48 hours then return to their original expression levels between 48 to 144 hours. Thus it is not a different set of pathways that are responsible for returning these Hey cells to a mesenchymal-like state. To this end we examined the significantly enriched TGF-β/Smads/*MAPK* pathways and their constituents in each time span.

4.3.3.4.1 TGF-β signaling

We examined the TGF-β pathway because of its strong involvement in both EMT signaling in carcinoma and maintenance of epithelial characteristics in normal cells. In our study, signaling cytokine *TGF-β2* is differentially expressed in both time spans. It is up regulated during the 0-48 hour and down regulated during the 48-144 hour time courses. At 24 hours post-transfection the fold change of expression levels for *TGF-β2* in miR-429 treated cells compared to negative-control-treated cells is at its highest across the entire 144 hour observation period. Additionally TGF-β receptor type II is up regulated in the 0-48 hour span.

4.3.3.4.2 Smads and MAPK signaling

When examining downstream pathways from TGF-β receptor signaling, SMADs were not differentially expressed in either time span, but elements of the *MAPK* pathway for EMT were differentially expressed, including *MAPK1* (*ERK1/2*), *MAPK8* (*JNK*), *MAPK11* (*p38 MAPK*), and *MAP3K7* (*TAK1*). *ERK1/2*, *p38 MAPK*, and *JNK* were significantly up regulated during the 0-48 hour time span, while only *JNK* was significantly down regulated during the 48-144 hour time span. In the case of *JNK*, both the expression values and fold changes appeared to reach a maximum at 24 hours. *TAK1* and *ERK1/2* have peak expression at 48 hours, but have fold change peaks at 24 hours. p38 *MAPK* was significantly down regulated during the 0-48 hour time span. While the up-regulation of *MAPK* elements suggests an increased role in signaling, without information on the phosphorylation status of *MAPK*s its effect on EMT/MET is ambiguous.

4.3.3.4.3 FGF1 and FGF2 signaling

FGF1 (heparin-binding growth factor 1), which was detected at the edge of nephrogenic growth zones where mesenchyme transitioned into epithelium, is thought to promote MET in renal development (Cancilla et al. 1999). In our miR-429 treated cells, *FGF1* was up-expressed during the 0-48 hour time span, and down-expressed during the 48-144 hour time span, and showed a fold change peak at 48 hours. Ramos et al. showed that FGF1 was capable of reversing TGF-β1-induced EMT in alveolar epithelial-like cells (Ramos et al. 2010). Epithelial cells cultured in the presence of TGF-β1 assumed an elongated, spindle shape with fibroblast-like morphology, and displaying the down-regulation of E-cadherin and up-regulation of α-smooth muscle actin that is characteristic of EMT. Once treated with FGF1, the morphology of these cells reverted to a cobblestone-like epithelial shape, and the expression levels of these markers were restored to nearly their untreated levels. Ramos (2010) also showed that FGF1-induced reversion mainly occurred through the MEK/ERK pathway, major components of which are up-expressed in our miR-429 treated samples as detailed above. This signaling through the MEK/ERK pathway eventually inhibits Smad2 phosphorylation, blocking the usual pathway for TGF-β1-induced Smad-mediated EMT. Our observation of increased *FGF1* expression at 48 hours thus suggests an alternative pathway by which MET may have been induced in our miR-429 treated cells even if TGF-β signaling is circumvented.

FGF2 (basic fibroblast growth factor) is known to promote EMT in renal development, inducing cell motility across basement membranes in cultured proximal tubular epithelium while down-regulating E-cadherin and cytokeratins

(Strutz et al. 2002). In our miR-429 treated cells, *FGF2* was up-expressed during the 0-48 hour time span, and down-expressed during the 48-144 hour time span. FGF2-induces EMT by activating PI3K that then mediates a number of small GTPases (Rho, Rac, and Cdc42), leading to actin cytoskeletal remodeling (Lee and Kay 2006). While we would expect up-expression of *FGF2* to result in EMT, *PI3K* (phosphoinositide-3-kinase) is down-expressed in our miR-429 treated samples, possibly acting as a gatekeeper on FGF2's induction of EMT.

4.4. Discussion

Previous studies have established a role for miR-200 family microRNAs and miR-429 in particular in the induction of MET in ovarian cancer cells with differing metastatic potentials (Bendoraite et al. 2010; Chen et al. 2011). These studies relied on assays of gene expression levels taken from a single time point. However gene expression is a temporal process, and EMT and MET are controlled by multiple regulatory and structural elements that are known to change expression levels. Capturing this increased dimensionality demands time course studies, where the strong autocorrelation between successive time points can be used to reveal the full set of involved genes and expression differences that would not otherwise be significant at single time points. We examined the dynamics of the MET process in mesenchymal-like Hey cells initiated by a single miR-429 transfection, assaying gene expression across multiple time points following the transfection.

We observed significant change in cell morphology and molecular profiles in the 24 to 48 hours following transfection with miR-429, confirming the results from

our previous single-time point transfection study (Chen et al. 2011). Mesenchymal markers like fibronectin (*FN1*) are significantly down regulated in this time period, while N-cadherin (*CDH2*) is slightly up and vimentin is not significantly differentially expressed across the time span. Epithelial markers like caveolin 2 (*CAV2*), cytokeratin 8 (*KRT8*), and desmoplakin (*DSP*) are up-regulated during the 24 to 48 hour period and are significantly differentially expressed across the time span. We also note the characteristic down-regulation of *ZEB1* and *ZEB2*, previously noted as an effect of miR-429. And we note gene enrichment among these significantly differentially expressed genes for multiple pathways related to the mechanisms of MET and EMT.

In our miR-429 transfected cells we observed a shift in cell morphology from mesenchymal-like at 0 hours to more epithelial at 24 and 48 hours followed by a return to a mesenchymal-like morphology by 144 hours. We also observed that nearly all genes (98.6%) that show differential expression across the 0 to 144 hour time span, return to an average expression level by 144 hours that is not significantly different from their average expression level at 0 hours. This suggests that most of the changes induced by the miR-429 transfection both in cell morphology and gene expression are reversible and non-permanent. The nature of the genetic reprogramming that stabilizes a mesenchymal-like phenotype in Hey cells is not well understood, but Gregory et al. (2008) propose that a TGF-β autocrine loop indirectly regulated by miR-200 family miRNAs could increase ZEB expression, resulting in the repression of E-cadherin and other polarity genes and

establishing a mesenchymal phenotype in a reversible manner (Gregory et al. 2008b).

We hypothesized that the same pathways we observe being differentially expressed from 0 to 48 hours, then return to their original expression levels between 48 to 144 hours, rather than different pathways being responsible for returning these Hey cells to a mesenchymal-like state. Our observation that 98.6% of genes that show differential expression across the 0 to 144 hour time period return to 0 hour expressions levels at 144 hours reinforces our hypothesis. However, the abundance of differentially expressed genes enriched for pathways involved in both EMT and MET, coupled with a lack of functional data about signaling states or baseline function of specific pathways leaves us unable to eliminate the possibility that a different set of pathways is responsible for the EMT-like process that is observed after 48 hours. Our examination of the TGF-B/Smads signaling pathway, and its potential crosstalk with MEK/ERK pathways and FGF1 leaves open both possibilities. Our findings underscore the challenges facing the therapeutic use of miRNAs: the wide range of pathway expression altered by miR-429, significant temporal dependence of its impact, and need for further functional study.

4.5. References

Agatston AS, Janowitz WR, Hildner FJ, Zusmer NR, Viamonte M, Jr., Detrano R. 1990. Quantification of coronary artery calcium using ultrafast computed tomography. *J Am Coll Cardiol* **15**(4): 827-832.

Ahmed N, Thompson EW, Quinn MA. 2007. Epithelial-mesenchymal interconversions in normal ovarian surface epithelium and ovarian carcinomas: an exception to the norm. *J Cell Physiol* **213**(3): 581-588.

Auersperg N, Pan J, Grove BD, Peterson T, Fisher J, Maines-Bandiera S, Somasiri A, Roskelley CD. 1999. E-cadherin induces mesenchymal-to-epithelial transition in human ovarian surface epithelium. *Proceedings of the National Academy of Sciences* **96**(11): 6249-6254.

Bajou K, Noel A, Gerard RD, Masson V, Brunner N, Holst-Hansen C, Skobe M, Fusenig NE, Carmeliet P, Collen D et al. 1998. Absence of host plasminogen activator inhibitor 1 prevents cancer invasion and vascularization. *Nature medicine* **4**(8): 923-928.

Bartel DP. 2004. MicroRNAs: genomics, biogenesis, mechanism, and function. *Cell* **116**(2): 281-297.

Bendoraite A, Knouf EC, Garg KS, Parkin RK, Kroh EM, O'Briant KC, Ventura AP, Godwin AK, Karlan BY, Drescher CW et al. 2010. Regulation of miR-200 family microRNAs and ZEB transcription factors in ovarian cancer: Evidence supporting a mesothelial-to-epithelial transition. *Gynecologic Oncology* **116**(1): 117-125.

Bhowmick NA, Zent R, Ghiassi M, McDonnell M, Moses HL. 2001. Integrin beta 1 signaling is necessary for transforming growth factor-beta activation of p38MAPK and epithelial plasticity. *J Biol Chem* **276**(50): 46707-46713.

Bierie B, Moses HL. 2006. TGF-beta and cancer. *Cytokine Growth Factor Rev* **17**(1-2): 29-40.

Brennecke J, Stark A, Russell RB, Cohen SM. 2005. Principles of microRNA-target recognition. *PLoS Biol* **3**(3): e85.

Buick RN, Pullano R, Trent JM. 1985. Comparative properties of five human ovarian adenocarcinoma cell lines. *Cancer Res* **45**(8): 3668-3676.

Cancilla B, Ford-Perriss MD, Bertram JF. 1999. Expression and localization of fibroblast growth factors and fibroblast growth factor receptors in the developing rat kidney. *Kidney Int* **56**(6): 2025-2039.

Chaffer CL, Brennan JP, Slavin JL, Blick T, Thompson EW, Williams ED. 2006. Mesenchymal-to-epithelial transition facilitates bladder cancer metastasis: role of fibroblast growth factor receptor-2. *Cancer Res* **66**(23): 11271-11278.

Chaffer CL, Dopheide B, McCulloch DR, Lee AB, Moseley JM, Thompson EW, Williams ED. 2005. Upregulated MT1-MMP/TIMP-2 axis in the TSU-Pr1-B1/B2 model of metastatic progression in transitional cell carcinoma of the bladder. *Clin Exp Metastasis* **22**(2): 115-125.

Chen J, Wang L, Matyunina L, Hill C, McDonald J. 2011. Overexpression of miR-429 induces mesenchymal-to-epithelial transition (MET) in metastatic ovarian cancer cells. *Gynecologic Oncology* **121**(1): 200-205.

Cho KR, Shih Ie M. 2009. Ovarian cancer. *Annu Rev Pathol* **4**: 287-313.

Conesa A, Nueda MJ, Ferrer A, Talon M. 2006. maSigPro: a method to identify significantly differential expression profiles in time-course microarray experiments. *Bioinformatics* **22**(9): 1096-1102.

Darai E, Scoazec JY, Walker-Combrouze F, Mlika-Cabanne N, Feldmann G, Madelenat P, Potet F. 1997. Expression of cadherins in benign, borderline, and malignant ovarian epithelial tumors: a clinicopathologic study of 60 cases. *Hum Pathol* **28**(8): 922-928.

Davidson B, Trope CG, Reich R. 2012. Epithelial-mesenchymal transition in ovarian carcinoma. *Front Oncol* **2**: 33.

Davies BR, Worsley SD, Ponder BA. 1998. Expression of E-cadherin, alpha-catenin and beta-catenin in normal ovarian surface epithelium and epithelial ovarian cancers. *Histopathology* **32**(1): 69-80.

Derynck R, Goeddel DV, Ullrich A, Gutterman JU, Williams RD, Bringman TS, Berger WH. 1987. Synthesis of messenger RNAs for transforming growth factors alpha and beta and the epidermal growth factor receptor by human tumors. *Cancer Res* **47**(3): 707-712.

Eisenkop SM, Spirtos NM. 2001. The Clinical Significance of Occult Macroscopically Positive Retroperitoneal Nodes in Patients with Epithelial Ovarian Cancer. *Gynecologic Oncology* **82**(1): 143-149.

Elloul S, Vaksman O, Stavnes HT, Trope CG, Davidson B, Reich R. 2010. Mesenchymal-to-epithelial transition determinants as characteristics of ovarian carcinoma effusions. *Clin Exp Metastasis* **27**(3): 161-172.

Gregory PA, Bert AG, Paterson EL, Barry SC, Tsykin A, Farshid G, Vadas MA, Khew-Goodall Y, Goodall GJ. 2008a. The miR-200 family and miR-205 regulate epithelial to mesenchymal transition by targeting ZEB1 and SIP1. *Nat Cell Biol* **10**(5): 593-601.

Gregory PA, Bracken CP, Bert AG, Goodall GJ. 2008b. MicroRNAs as regulators of epithelial-mesenchymal transition. *Cell Cycle* **7**(20): 3112-3118.

Group USCSW. 2012. United States Cancer Statistics: 1999–2008 Incidence and Mortality Web-based Report. U.S. Department of Health and Human Services, Centers for Disease Control and Prevention and National Cancer Institute, Atlanta.

Gupta GP, Massague J. 2006. Cancer Metastasis: Building a Framework. *Cell* **127**(4): 679-695.

Guttilla IK, Adams BD, White BA. 2012. ER±, microRNAs, and the epithelial mesenchymal transition in breast cancer. *Trends in endocrinology and metabolism: TEM* **23**(2): 73-82.

Han J, Lee Y, Yeom K-H, Kim Y-K, Jin H, Kim VN. 2004. The Drosha-DGCR8 complex in primary microRNA processing. *Genes & Development* **18**(24): 3016-3027.

Havik B, Degenhardt FA, Johansson S, Fernandes CPD, Hinney A, Scherag A, Lyb√¶k H, Djurovic S, Christoforou A, Ersland KM et al. 2012. DCLK1 Variants Are Associated across Schizophrenia and Attention Deficit/Hyperactivity Disorder. *PLoS ONE* **7**(4): e35424.

Howlader N, Noone A, Krapcho M, Neyman N, Aminou R, Waldron W, Altekruse SF, Kosary CL, Ruhl J, Tatalovich Z et al. 2012. SEER Cancer Statistics Review, 1975-2009 (Vintage 2009 Populations). National Cancer Institute, Bethesda, MD.

Huang H, Sossey-Alaoui K, Beachy SH, Geradts J. 2007. The tetraspanin superfamily member NET-6 is a new tumor suppressor gene. *J Cancer Res Clin Oncol* **133**(10): 761-769.

Huang W-Y, Li Z-G, Rus H, Wang X, Jose PA, Chen S-Y. 2009. RGC-32 Mediates Transforming Growth Factor-Œ≤-induced Epithelial-Mesenchymal

Transition in Human Renal Proximal Tubular Cells. *Journal of Biological Chemistry* **284**(14): 9426-9432.

Huber MA, Azoitei N, Baumann B, Gr, xFc, nert S, Sommer A, Pehamberger H, Kraut N, Beug H et al. 2004. NF-κB is essential for epithelial-mesenchymal transition and metastasis in a model of breast cancer progression. *The Journal of Clinical Investigation* **114**(4): 569-581.

Hur K, Toiyama Y, Takahashi M, Balaguer F, Nagasaka T, Koike J, Hemmi H, Koi M, Boland CR, Goel A. 2012. MicroRNA-200c modulates epithelial-to-mesenchymal transition (EMT) in human colorectal cancer metastasis. *Gut*.

Irizarry RA, Bolstad BM, Collin F, Cope LM, Hobbs B, Speed TP. 2003. Summaries of Affymetrix GeneChip probe level data. *Nucleic Acids Res* **31**(4): e15.

Javelaud D, Mauviel A. 2005. Crosstalk mechanisms between the mitogen-activated protein kinase pathways and Smad signaling downstream of TGF-beta: implications for carcinogenesis. *Oncogene* **24**(37): 5742-5750.

Jindal SK, Ishii E, Letarte M, Vera S, Teerds KJ, Dorrington JH. 1995. Regulation of transforming growth factor alpha gene expression in an ovarian surface epithelial cell line derived from a human carcinoma. *Biol Reprod* **52**(5): 1027-1037.

Kong X, Li G, Yuan Y, He Y, Wu X, Zhang W, Wu Z, Chen T, Wu W, Lobie PE et al. 2012. MicroRNA-7 Inhibits Epithelial-to-Mesenchymal Transition and Metastasis of Breast Cancer Cells via Targeting FAK Expression. *PLoS ONE* **7**(8): e41523.

Korpal M, Kang Y. 2008. The emerging role of miR-200 family of microRNAs in epithelial-mesenchymal transition and cancer metastasis. *RNA Biol* **5**(3): 115-119.

Korpal M, Lee ES, Hu G, Kang Y. 2008. The miR-200 family inhibits epithelial-mesenchymal transition and cancer cell migration by direct targeting of E-cadherin transcriptional repressors ZEB1 and ZEB2. *J Biol Chem* **283**(22): 14910-14914.

Lee HT, Lee JG, Na M, Kay EP. 2004a. FGF-2 induced by interleukin-1 beta through the action of phosphatidylinositol 3-kinase mediates endothelial

mesenchymal transformation in corneal endothelial cells. *J Biol Chem* **279**(31): 32325-32332.

Lee JG, Kay EP. 2006. FGF-2-mediated signal transduction during endothelial mesenchymal transformation in corneal endothelial cells. *Exp Eye Res* **83**(6): 1309-1316.

Lee Y, Kim M, Han J, Yeom K-H, Lee S, Baek SH, Kim VN. 2004b. MicroRNA genes are transcribed by RNA polymerase II. *EMBO J* **23**(20): 4051-4060.

Lin S-L, Chang D, Ying S-Y. 2005. Asymmetry of intronic pre-miRNA structures in functional RISC assembly. *Gene* **356**(0): 32-38.

Maines-Bandiera SL, Auersperg N. 1997. Increased E-cadherin expression in ovarian surface epithelium: an early step in metaplasia and dysplasia? *Int J Gynecol Pathol* **16**(3): 250-255.

Martin S, Bonnin A, Furio V, Coronado PJ, Vidart JA, Arencibia JM. 2009. Tspan13 expression in epithelial ovarian cancer. *European Journal of Cancer Supplements* **7**(2): 454-455.

Massague J. 2000. How cells read TGF-beta signals. *Nat Rev Mol Cell Biol* **1**(3): 169-178.

-. 2008. TGFbeta in Cancer. *Cell* **134**(2): 215-230.

Moes M, Le Behec A, Crespo I, Laurini C, Halavatyi A, Vetter G, del Sol A, Friederich E. 2012. A Novel Network Integrating a miRNA-203/SNAI1 Feedback Loop which Regulates Epithelial to Mesenchymal Transition. *PLoS ONE* **7**(4): e35440.

Palena C, Hamilton DH, Fernando RI. 2012. Influence of IL-8 on the epithelial-mesenchymal transition and the tumor microenvironment. *Future Oncol* **8**(6): 713-722.

Paterson EL, Kolesnikoff N, Gregory PA, Bert AG, Khew-Goodall Y, Goodall GJ. 2008. The microRNA-200 family regulates epithelial to mesenchymal transition. *ScientificWorldJournal* **8**: 901-904.

Pigati L, Yaddanapudi SCS, Iyengar R, Kim D-J, Hearn SA, Danforth D, Hastings ML, Duelli DM. 2010. Selective Release of MicroRNA Species from Normal and Malignant Mammary Epithelial Cells. *PLoS ONE* **5**(10): e13515.

R Development Core Team. 2010. R: A language and environment for statistical computing. R Foundation for Statistical Computing, Vienna, Austria.

Ramos C, Becerril C, Montano M, Garcia-De-Alba C, Ramirez R, Checa M, Pardo A, Selman Ms. 2010. FGF-1 reverts epithelial-mesenchymal transition induced by TGF-B1 through MAPK/ERK kinase pathway. *American Journal of Physiology - Lung Cellular and Molecular Physiology* **299**(2): L222-L231.

Ru P, Steele R, Newhall P, Phillips NJ, Toth K, Ray RB. 2012. MicroRNA-29b Suppresses Prostate Cancer Metastasis by Regulating Epithelial-Mesenchymal Transition Signaling. *Molecular Cancer Therapeutics*.

Saga Y, Takeda H. 2001. The making of the somite: molecular events in vertebrate segmentation. *Nat Rev Genet* **2**(11): 835-845.

Salamanca CM, Maines-Bandiera SL, Leung PCK, Hu Y-L, Auersperg N. 2004. Effects of Epidermal Growth Factor/Hydrocortisone on the Growth and Differentiation of Human Ovarian Surface Epithelium. *Journal of the Society for Gynecologic Investigation* **11**(4): 241-251.

Sankaranarayanan R, Ferlay J. 2006. Worldwide burden of gynaecological cancer: the size of the problem. *Best Pract Res Clin Obstet Gynaecol* **20**(2): 207-225.

Santibanez JF. 2006. JNK mediates TGF-B1-induced epithelial mesenchymal transdifferentiation of mouse transformed keratinocytes. *FEBS Letters* **580**(22): 5385-5391.

Schaner ME, Davidson B, Skrede M, Reich R, Florenes VA, Risberg B, Berner A, Goldberg I, Givant-Horwitz V, Trope CG et al. 2005. Variation in gene expression patterns in effusions and primary tumors from serous ovarian cancer patients. *Mol Cancer* **4**: 26.

Shahab SW, Matyunina LV, Mezencev R, Walker LD, Bowen NJ, Benigno BB, McDonald JF. 2011. Evidence for the Complexity of MicroRNA-Mediated Regulation in Ovarian Cancer: A Systems Approach. *PLoS ONE* **6**(7): e22508.

Shipley GD, Tucker RF, Moses HL. 1985. Type beta transforming growth factor/growth inhibitor stimulates entry of monolayer cultures of AKR-2B cells into S phase after a prolonged prereplicative interval. *Proc Natl Acad Sci U S A* **82**(12): 4147-4151.

Smith AL, Iwanaga R, Drasin DJ, Micalizzi DS, Vartuli RL, Tan AC, Ford HL. 2012. The miR-106b-25 cluster targets Smad7, activates TGF-beta signaling, and induces EMT and tumor initiating cell characteristics downstream of Six1 in human breast cancer. *Oncogene* **31**(50): 5162-5171.

Smyth GK. 2004. Linear models and empirical bayes methods for assessing differential expression in microarray experiments. *Stat Appl Genet Mol Biol* **3**: Article3.

Strippoli R, Benedicto I, Pérez Lozano ML, Cerezo A, López-Cabrera M, del Pozo MA. 2008. Epithelial-to-mesenchymal transition of peritoneal mesothelial cells is regulated by an ERK/NF-κB/Snail1 pathway. *Disease Models & Mechanisms* **1**(4-5): 264-274.

Strutz F, Zeisberg M, Ziyadeh FN, Yang CQ, Kalluri R, Muller GA, Neilson EG. 2002. Role of basic fibroblast growth factor-2 in epithelial-mesenchymal transformation. *Kidney Int* **61**(5): 1714-1728.

Thiery JP. 2002. Epithelial-mesenchymal transitions in tumour progression. *Nat Rev Cancer* **2**(6): 442-454.

Turley EA, Veiseh M, Radisky DC, Bissell MJ. 2008. Mechanisms of disease: epithelial-mesenchymal transition--does cellular plasticity fuel neoplastic progression? *Nat Clin Pract Oncol* **5**(5): 280-290.

Vainio S, Lin Y. 2002. Coordinating early kidney development: lessons from gene targeting. *Nat Rev Genet* **3**(7): 533-543.

Valcourt U, Kowanetz M, Niimi H, Heldin C-H, Moustakas A. 2005. TGF-Œ≤ and the Smad Signaling Pathway Support Transcriptomic Reprogramming during Epithelial-Mesenchymal Cell Transition. *Molecular Biology of the Cell* **16**(4): 1987-2002.

Veatch AL, Carson LF, Ramakrishnan S. 1994. Differential expression of the cell-cell adhesion molecule E-cadherin in ascites and solid human ovarian tumor cells. *International Journal of Cancer* **58**(3): 393-399.

Vui-Kee K, Mohd Dali AZ, Mohamed Rose I, Ghazali R, Jamal R, Mokhtar NM. 2012. Molecular markers associated with nonepithelial ovarian cancer in formalin-fixed, paraffin-embedded specimens by genome wide expression profiling. *Kaohsiung J Med Sci* **28**(5): 243-250.

Wightman B, Ha I, Ruvkun G. 1993. Posttranscriptional regulation of the heterochronic gene lin-14 by lin-4 mediates temporal pattern formation in C. elegans. *Cell* **75**(5): 855-862.

Wong AS, Leung PC. 2007. Role of endocrine and growth factors on the ovarian surface epithelium. *J Obstet Gynaecol Res* **33**(1): 3-16.

Wu L, Belasco JG. 2008. Let me count the ways: mechanisms of gene regulation by miRNAs and siRNAs. *Mol Cell* **29**(1): 1-7.

Wu Z-Q, Li X-Y, Hu CY, Ford M, Kleer CG, Weiss SJ. 2012. Canonical Wnt signaling regulates Slug activity and links epithelial–mesenchymal transition with epigenetic Breast Cancer 1, Early Onset (BRCA1) repression. *Proceedings of the National Academy of Sciences* **109**(41): 16654-16659.

Xia H, Ooi LL, Hui KM. 2013. MicroRNA-216a/217-induced epithelial-mesenchymal transition targets PTEN and SMAD7 to promote drug resistance and recurrence of liver cancer. *Hepatology (Baltimore, Md)* **58**(2): 629-641.

Xie G, Yao Q, Liu Y, Du S, Liu A, Guo Z, Sun A, Ruan J, Chen L, Ye C et al. 2012. IL-6-induced epithelial-mesenchymal transition promotes the generation of breast cancer stem-like cells analogous to mammosphere cultures. *Int J Oncol* **40**(4): 1171-1179.

Yoshioka S, King ML, Ran S, Okuda H, MacLean JA, 2nd, McAsey ME, Sugino N, Brard L, Watabe K, Hayashi K. 2012. WNT7A regulates tumor growth and progression in ovarian cancer through the WNT/beta-catenin pathway. *Molecular cancer research : MCR* **10**(3): 469-482.

Yu L, Hebert MC, Zhang YE. 2002. TGF-beta receptor-activated p38 MAP kinase mediates Smad-independent TGF-beta responses. *EMBO J* **21**(14): 3749-3759.

Zavadil J, Bitzer M, Liang D, Yang YC, Massimi A, Kneitz S, Piek E, Bottinger EP. 2001. Genetic programs of epithelial cell plasticity directed by transforming growth factor-beta. *Proc Natl Acad Sci U S A* **98**(12): 6686-6691.

Zavadil J, Bottinger EP. 2005. TGF-beta and epithelial-to-mesenchymal transitions. *Oncogene* **24**(37): 5764-5774.

CHAPTER 5

CONCLUSION

5.1. Firefighter coronary risk factor study

In this study, we asked if changes in common accepted thresholds for assessing coronary artery disease (Framingham Risk Scores) could be brought into better concordance with well-established non-invasive measures of atherosclerosis. Individuals with clinically significant amounts of coronary calcification (CAC) and carotid intima-medial thickening (CIMT) are known to have elevated risk of major adverse cardiac events (Nambi et al. 2010; Baldassarre et al. 2012; Budoff et al. 2013). By comparing non-invasive measurements with calculated risk scores in 190 asymptomatic firefighters, we were able to identify a significant sub-population of individuals who had high atherosclerotic burden or significant thickening of carotid arteries despite having low to medium Framingham Risk Scores (<20%). Receiver operator characteristic (ROC) analysis suggested thresholds of 7% for calcification and 9% for intima-medial thickness, which improved the sensitivity of FRS from 17% to 58% and 40% to 67%, respectively. We then asked if adding an age-based smoking adjustment for all individuals, regardless of smoking status, to reflect particulate exposure over time could also improve the sensitivity of FRS. Combined with threshold optimization using ROC, prediction by an FRS threshold of 12% yielded a sensitivity improvement to 43% for CAC and 75% for CIMT. Our

optimizations of FRS thresholds using ROC show that the sensitivity of traditional measures can be improved to capture those at-risk individuals who would otherwise be scored as negative. It is of particular interest to us that those individuals with CAC scores and CIMT in the highest quartile fall into the low to middle risk categories by Framingham Risk Scores. Although much criticized, the recommendations of the Adult Treatment Panel III Committee are still widely used. Given that even with our improved thresholds a number of affected individuals are still called as negative, we suggest that firefighting as a profession may be viewed as a risk equivalent in the Framingham risk assessment on the same level as a family history of coronary disease or diabetes.

As a follow-up to our study, we would recommend increasing the number of sampled individuals, as well as sampling a non-firefighter age and disease-state matched population. This would enable us to more clearly distinguish risk factors specific to firefighters. Moreover, a five and ten year follow-up survey of assayed individuals would enable us to link risk factors more directly to the incidence of major adverse coronary events, as tracked by the Framingham Study. The current suite of non-invasive measures provides a soft demarcation when describing affected and unaffected individuals. Moreover, the combination of long term event data and more sampled individuals would permit us to develop a novel total risk score for this subpopulation.

5.2. Drug eluting stent gene expression study

In this study we asked if coronary stents eluting rapamycin-derived compounds actually stopped the progress of restenosis resulting from stent implantation following angioplasty, or if it only delayed the onset of in-stent restenosis as suggested by a number of clinical reports (Dangas et al. 2010; Garg and Serruys 2010; Kuriyama et al. 2011). We compared the arteries of pigs implanted with traditional bare metal stents with the arteries of pigs implanted with sirolimus and zotarolimus-eluting stents using high-density microarray gene expression assays. Arterial tissue samples surrounding the implanted stents were harvested at 28 days post-implantation. Zotarolimus-eluting stents (ZES) exhaust 90% of their payload by 14 days, while sirolimus-eluting stents (SES) reach that point by 28 days. In our studies, we looked at genes differentially expressed in SES, in ZES, and both SES and ZES. Among those genes significantly differentially expressed in SES we observed up regulation of genes associated with extracellular matrix degradation, specifically matrix metalloproteases, and a down regulation of genes for ion channels that has been previously observed in vascular smooth muscle cells shifting from the contractile to proliferative state. While among the genes significantly differentially expressed in ZES, we observed an up regulation of genes associated with basement membrane growth and structural markers known to accompany the contractile state in vascular smooth muscle cells and neointimal growth. For both SES and ZES, there were significantly differentially expressed inflammatory response genes that are known players in the extravasation that occurs at the restenotic wound site. When taken together with the timeline for restenosis that has been well characterized in histological and molecular assays, this is consistent with

a timeline where SES and ZES have delayed restenosis in their respective arteries up until drug payload exhaustion, whereupon the process resumes. Alternatively, the data we observed may also be consistent with a timeline where SES and ZES stalls the restenotic process in the smooth muscle cell migration and proliferation phase.

Our analysis of the gene expression data relied solely on statistical tests, abandoning prior reliance on fold change as an arbitrary threshold for determining significant differential expression. When analyzing a large number of data points, be they tens of thousands of genes or hundreds of gene sets, multiple testing correction is critical to minimize false positive results. To correct the Student's t-test we used to compare individual gene expression levels between groups, we used a beta-uniform mixed modeling approach (BUM) designed to correct high dimensionality data sets like gene expression microarrays (Allison et al. 2002; Pounds and Morris 2003). BUM models the observed p-value distribution as a mixture of a uniform distribution corresponding to true null values, and a beta distribution corresponding to false null values. This model can then be used to adjust the p-value threshold for significance to generate different false positive and false negative rates. For normalized enrichment scores (NES) calculated by Gene Set Enrichment Analysis (GSEA), false discovery rate (FDR) estimates are calculated for each gene set. For a given observed NES, the probability of that observed NES being a false positive is calculated by permuting phenotype labels to generate a null distribution (Subramanian et al. 2005). We are then able to choose a threshold for an acceptable level of false positives based on these estimates. Both the BUM and FDR approach provide false positive and false negative rate estimates that allow us to adjust

significance thresholds for different data sets. Particularly in these cases where we expect the total number of positives to be small, this enables investigators to weigh changes in the rate of false positives against gains in statistical power and discovery.

Our study has its greatest limitation in the single time point when arterial samples were harvested. To improve resolution of the time course and drug effects over time would require additional time points over a longer time frame and more animals per time point. Adding an angioplasty-only animal series would also allow us to establish a clear base line response for bare metal stent implantation at a high-density microarray resolution. Finally, measuring drug concentration directly in tissue using a pharmacological assay would permit us to adjust for differential effects due to local drug delivery.

5.3. miR-429 treatment of ovarian cancer cell study

In this study, we asked how ovarian cancer cells with a mesenchymal metastatic cell phenotype reacted at the molecular level to a single treatment with microRNA, miR-429. miR-429 previously had been characterized as a member of the miR-200 family that was capable of inducing decreased migration, suppression of anchorage-independent growth, as well as morphological changes when over-expressed in HEY cells. To further characterize the effect of miR-429 in Hey cells, we treated these cells with miR-429 and took molecular "snapshots" at 24, 48, and 144 hours, a time interval over which we had previously observed significant morphological changes. By utilizing a time course analysis approach, we were able to not only capture significant time point-to-time point changes, but also more

subtle changes that occurred across the entire time course while compensating for changes observed in our negative control.

Consistent with prior studies, we observed morphological changes in miR-429-treated Hey cells, where cells changed from a pre-transfection (0 hour) elongated fibroblast-like state to a rounded, cobblestone epithelial-like state by 24 and 48 hours, eventually returning to a fibroblast-like state by 144 hours. Negative control-treated cells showed no morphological changes at any time point. Across this time course, 3635 genes displayed significantly differential expression across the entire time course when compared to the negative control treated Hey cells. Mesenchymal markers like fibronectin were down regulated, while epithelial markers like caveolin 2, catenin, keratin, and desmoplaking were up regulated across the time course. Transition of cancer cells from the drug-resistant mesenchymal phenotype to drug-sensitive epithelial phenotype may permit miR-429 to be used as a co-therapeutic in chemotherapy (Chen et al. 2011).

The return of morphological features to their 0-hour state at 144 hours led us to ask if individual gene expression levels followed the same pattern. We determined that 98% of differentially expressed genes did not have significantly different average expression levels at 144 hours than they did at 0 hours, corrected for the change in expression observed in negative control-treated cells across the same time interval. Out of the 2% that did show significantly different average expression levels at 144 hours, we noted genes that were associated with EMT/MET, such as *Wnt7A*, *Serpine1* and *LAMC2*. This plasticity may prove to be a double-edged sword when translating miR-429's potential as a co-therapeutic. The

brevity of response may necessitate more treatments to develop a sustained effect, but it may also allow patients to escape unwanted side effects more quickly once therapy has been delivered. More testing on other cell types may be necessary to gauge miR-429's long-term effects.

Finally, out of the 3635 genes that were differentially expressed following miR-429 treatment, only 261 genes are predicted targets of miR-429 by miRANDA. This highlights the previously described highly indirect nature of the miR-200 family in affecting gene expression. While the 261 predicted gene targets are in fact enriched for genes having to do with EMT and MET processes, the non-predicted genes are part of the wider secondary effects from miR-429 treatment, highlighting the need for network analysis of highly inter-connected genes. This may also represent a shortcoming in miRANDA's ability to correctly predict targeting by this microRNA. Our ability to research miR-429 and other microRNAs as therapeutics may be greatly improved by further work in system biological approaches to studying microRNA activity and microRNA targeting prediction.

Additional downstream studies to improve our understanding of this plastic response include expanding the sampling time points beyond 144 hours to see if genes that did not return to 0-day expression levels in this study do return on a longer time scale (as well as confirming the long term stability of those genes that appear to return to their 0-day levels). We may also desire to investigate cell migration and other phenotypic response at all time points to determine if the plastic response in gene expression levels and morphology are also reflected in the cells functional responses.

5.4. References

Allison DB, Gadbury GL, Heo M, Fernendez JR, Lee C-K, Prolla TA, Weindruch R. 2002. A mixture model approach for the analysis of microarray gene expression data. *Computational Statistics & Data Analysis* **39**(1): 1-20.

Baldassarre D, Hamsten A, Veglia F, de Faire U, Humphries SE, Smit AJ, Giral P, Kurl S, Rauramaa R, Mannarino E et al. 2012. Measurements of carotid intima-media thickness and of interadventitia common carotid diameter improve prediction of cardiovascular events: results of the IMPROVE (Carotid Intima Media Thickness [IMT] and IMT-Progression as Predictors of Vascular Events in a High Risk European Population) study. *J Am Coll Cardiol* **60**(16): 1489-1499.

Budoff MJ, Young R, Lopez VA, Kronmal RA, Nasir K, Blumenthal RS, Detrano RC, Bild DE, Guerci AD, Liu K et al. 2013. Progression of Coronary Calcium and Incident Coronary Heart Disease EventsMESA (Multi-Ethnic Study of Atherosclerosis). *Journal of the American College of Cardiology* **61**(12): 1231-1239.

Chen J, Wang L, Matyunina LV, Hill CG, McDonald JF. 2011. Overexpression of miR-429 induces mesenchymal-to-epithelial transition (MET) in metastatic ovarian cancer cells. *Gynecologic Oncology* **121**(1): 200-205.

Dangas GD, Claessen BE, Caixeta A, Sanidas EA, Mintz GS, Mehran R. 2010. In-Stent Restenosis in the Drug-Eluting Stent Era. *Journal of the American College of Cardiology* **56**(23): 1897-1907.

Garg S, Serruys PW. 2010. Coronary stents: current status. *J Am Coll Cardiol* **56**(10 Suppl): S1-42.

Kuriyama N, Kobayashi Y, Nakama T, Mine D, Nishihira K, Shimomura M, Nomura K, Ashikaga K, Matsuyama A, Shibata Y. 2011. Late Restenosis Following Sirolimus-Eluting Stent Implantation. *JACC: Cardiovascular Interventions* **4**(1): 123-128.

Nambi V, Chambless L, Folsom AR, He M, Hu Y, Mosley T, Volcik K, Boerwinkle E, Ballantyne CM. 2010. Carotid intima-media thickness and presence or absence of plaque improves prediction of coronary heart disease risk: the ARIC (Atherosclerosis Risk In Communities) study. *J Am Coll Cardiol* **55**(15): 1600-1607.

Pounds S, Morris SW. 2003. Estimating the occurrence of false positives and false negatives in microarray studies by approximating and partitioning the empirical distribution of p-values. *Bioinformatics* **19**(10): 1236-1242.

Subramanian A, Tamayo P, Mootha VK, Mukherjee S, Ebert BL, Gillette MA, Paulovich A, Pomeroy SL, Golub TR, Lander ES et al. 2005. Gene set enrichment analysis: A knowledge-based approach for interpreting genome-wide expression profiles. *Proceedings of the National Academy of Sciences of the United States of America* **102**(43): 15545-15550.

VITA

Andrew D. Huang

HUANG was born in Hoboken, New Jersey. He grew up in Los Angeles, California, received a B.A. in Microbiology from Cornell University, and an M.S. in Bioinformatics from the University of the Sciences in Philadelphia before coming to Georgia Tech to pursue a doctorate. He also previously worked at the Children's Hospital Philadelphia in the Division of Human Genetics and Molecular Biology. Mr. Huang now works with the Enteric Diseases Laboratory Branch at the Centers for Disease Control and Prevention as a consultant with Booz Allen Hamilton.